NASA/TM-20250005284

Mechanics of Preloaded Bolt Tensile Loading With Focus on Load Introduction Factor

John K. Ramsey
Glenn Research Center, Cleveland, Ohio

May 2025

NASA STI Program Report Series

Since its founding, NASA has been dedicated to the advancement of aeronautics and space science. The NASA scientific and technical information (STI) program plays a key part in helping NASA maintain this important role.

The NASA STI program operates under the auspices of the Agency Chief Information Officer. It collects, organizes, provides for archiving, and disseminates NASA's STI. The NASA STI program provides access to the NTRS Registered and its public interface, the NASA Technical Reports Server, thus providing one of the largest collections of aeronautical and space science STI in the world. Results are published in both non-NASA channels and by NASA in the NASA STI Report Series, which includes the following report types:

- TECHNICAL PUBLICATION.
  Reports of completed research or a major significant phase of research that present the results of NASA programs and include extensive data or theoretical analysis. Includes compilations of significant scientific and technical data and information deemed to be of continuing reference value. NASA counterpart of peer-reviewed formal professional papers but has less stringent limitations on manuscript length and extent of graphic presentations.

- TECHNICAL MEMORANDUM.
  Scientific and technical findings that are preliminary or of specialized interest, e.g., quick release reports, working papers, and bibliographies that contain minimal annotation. Does not contain extensive analysis.

- CONTRACTOR REPORT.
  Scientific and technical findings by NASA-sponsored contractors and grantees.

- CONFERENCE PUBLICATION.
  Collected papers from scientific and technical conferences, symposia, seminars, or other meetings sponsored or cosponsored by NASA.

- SPECIAL PUBLICATION.
  Scientific, technical, or historical information from NASA programs, projects, and missions, often concerned with subjects having substantial public interest.

- TECHNICAL TRANSLATION.
  English-language translations of foreign scientific and technical material pertinent to NASA's mission.

Specialized services also include organizing and publishing research results, distributing specialized research announcements and feeds, providing information desk and personal search support, and enabling data exchange services.

For more information about the NASA STI program, see the following:

- Access the NASA STI program home page at http://www.sti.nasa.gov

NASA/TM-20250005284

Mechanics of Preloaded Bolt Tensile Loading With Focus on Load Introduction Factor

John K. Ramsey
Glenn Research Center, Cleveland, Ohio

National Aeronautics and
Space Administration

Glenn Research Center
Cleveland, Ohio 44135

May 2025

Acknowledgments

The author wishes to express his deep appreciation to David "Dutch" Myers/GRC, Ronald Platz/Northrop Grumman Corporation, Dawn Phillips Price/MSFC, Dr. James Smith/JSC, and Robert Wingate/MSFC who have reviewed this work and have contributed material and/or suggestions that have been incorporated into this work. A special thanks to the Orion Program for providing funding to translate the referenced dissertation of Dr. Boenick from German to English. Also, Laura Becker (MORI Associates), editor of this work; Terence Condrich (Abacus Technology Corporation), who illustrated some of the images in the figures; and Lorie Passe (MORI Associates), who created the figures and compiled the final report, have significantly improved the usefulness and quality of this report, and their contributions are very much appreciated.

Level of Review: This material has been technically reviewed by technical management.

This report is available in electronic form at https://www.sti.nasa.gov/ and https://ntrs.nasa.gov/

NASA STI Program/Mail Stop 050
NASA Langley Research Center
Hampton, VA 23681-2199

Contents

Summary 1
1.0 Introduction 1
2.0 Derivation of Traditional Bolt Tensile Load Equation 2
2.1 Stiffness-Based Load Introduction Factor (SBLIF) 14
2.2 Including Bolt Thermal Load 15
3.0 Bolt Rupture Load 16
4.0 Separation Load 16
5.0 Derivation of Fundamental Bolt Tensile Load Equation 17
6.0 Analytical Approximation of Stiffness-Based Load Introduction Factor 19
7.0 Comparison of Geometric and Stiffness-Based Load Introduction Factors 20
7.1 Relative Position of Relieving Load Path 22
7.2 Clearance Hole and Clamped-Member Thickness 22
7.3 Comparison With Finite Element Analysis 26
7.4 Relative Conservatism Between SBLIF and GLIF 28
7.5 Comparison With Experiment 30
8.0 Effect of SBLIF on Graphical Aids 32
8.1 Joint Diagram 32
8.2 $n\phi$ Diagram 34
9.0 Conclusions 37
Appendix A.—Nomenclature 39
A.1 Symbols 39
A.2 Acronyms 41
A.3 Definitions 41
Appendix B.—Using K_c in Place of K_a 45
Appendix C.—Calculating Stiffness-Based and Geometric Load Introduction Factors 49
C.1 Stiffness-Based LIF 49
C.2 Geometric LIF 55
Appendix D.—Location of Maximum Diameter of Nonsymmetric Back-to-Back Frusta 57
Appendix E.—Bolt Thermal Load 59
Appendix F.—Derivation of Axial Stiffness of Frustum Element 63
Appendix G.—Finite Element Prediction of $n\phi$ for Pure Tension Joint Biased Towards Cylindrical Compression Zone 69
Appendix H.—Comparing Analytical Load Introduction Factors With Finite Element Analysis for Tension Joint of Appendix G 73
H.1 Joint Stiffness 74
H.2 Geometric LIF 79
H.3 Comparison of n, n_G, and n_{FEA}, Excluding Bolt Head and Nut Flexibility 80
H.4 Comparison of n, n_G, and n_{FEA} Including Bolt Head and Nut Flexibility 81
Appendix I.—Calculated SBLIF for Comparison With Experiment 85
Appendix J.—Detailed Derivation of Joint Diagram 89
J.1 Preload Phase 89
J.2 Tensile Load Application After Preload 91
J.3 Formulas for Key Features of Joint Diagram 98
References 103

Mechanics of Preloaded Bolt Tensile Loading With Focus on Load Introduction Factor

John K. Ramsey
National Aeronautics and Space Administration
Glenn Research Center
Cleveland, Ohio 44135

Summary

The bolt tensile and joint separation loads are directly influenced by the locations at which the external loads enter the clamped members of a preloaded bolted joint (PBJ) and the associated load paths through the joint. This physical load introduction mechanism affecting the bolt tensile loading is typically represented in the bolt tensile load equation, in part, by a load introduction factor (LIF), which was shown by H.M. Lee of Marshall Space Flight Center to be a natural product of the bolt tensile load equation using a linear spring stiffness model. This LIF, being a function of load-path stiffness, has subsequently been denoted as the stiffness-based LIF (SBLIF), providing a framework to calculate the LIF using whatever load-path stiffness approximations are appropriate.

Expanding upon the work of Lee, it is shown that the SBLIF and the joint stiffness factor are functions of the stiffnesses of the same load paths and regions within a PBJ, and thus they should not be treated as independent variables. Mathematical expressions for the SBLIF are presented.

Comparisons are shown between the analytically calculated SBLIF, the analytically calculated geometric LIF (GLIF), which is a simple clamped-member thickness ratio, the experimentally derived LIF, and the LIF determined by finite element analysis (FEA). Using experiment and FEA as a benchmark, the SBLIF, using traditional load-path stiffness approximations, enables a more accurate prediction of bolt tensile loading than the GLIF, although it can be unconservative near joint separation. The GLIF generally attributes more of the externally applied tensile load to the bolt than does the SBLIF, potentially resulting in heavier and/or more costly bolted joints. Mathematical relationships between the SBLIF and the GLIF are developed.

Supplemental material is provided in the appendixes where the historical practice of using the joint compressive stiffness in place of the joint tensile stiffness is evaluated. The appendixes include step-by-step examples demonstrating the calculation of the SBLIF using traditional stiffness approximations and conclude with the development of the joint diagram in terms of the SBLIF, culminating into formulas for the key features of a joint diagram, which is useful for programming.

1.0 Introduction

It is known that the bolt tensile and joint separation loads are directly influenced by the locations at which the external loads enter the clamped members of a preloaded bolted joint (PBJ) and, consequently, by the associated load paths through the joint. This physical system affecting the bolt tensile loading, herein denoted as load introduction mechanism, is typically represented in the bolt tensile load equation by a load introduction factor (LIF), known synonymously as the loading-plane factor.

It was shown in Reference 1, using a linear spring stiffness model, that the LIF is a function of the stiffness of the load paths within a PBJ and is a natural product of the bolt tensile load equation. Because this LIF is a function of load-path stiffness, it has subsequently been denoted as the stiffness-based LIF (SBLIF) (Ref. 2). The SBLIF provides a framework to use whatever load-path stiffness approximations are appropriate in characterizing the load introduction mechanism.

Expanding upon the work of Reference 1, additional insight into the mechanics of bolt tensile loading is obtained. Starting with Hooke's Law, the traditional bolt tensile load equation is developed in a systematic fashion, illustrating the load introduction mechanism and characterized as the SBLIF. Alternatively, the bolt tensile load equation is also derived in its fundamental form, still naturally accounting for the load introduction mechanism, but without an explicit LIF; rather, it is accounted for through the various load-path stiffnesses. It is shown that the SBLIF and the joint stiffness factor are functions of the stiffnesses of the same load paths and region within a PBJ and thus should not be treated as independent variables.

In the linear realm, the SBLIF can be used to characterize the bolt tensile load from preload to either joint separation or bolt failure. In the nonlinear realm, the SBLIF may be determined as a point quantity, lending itself to be used in a piecewise fashion to characterize the bolt tensile load.

Mathematical expressions for the SBLIF are presented. The accuracy of the SBLIF is only limited by the degree to which the stiffnesses of the load paths and associated regions of a PBJ can be determined. As such, the SBLIF is better suited to represent the load introduction mechanism as opposed to the traditional geometric LIF (GLIF) (Ref. 2). The GLIF is a simple thickness ratio, theoretically restricted to constant stiffness distributions through the thickness of the clamped members. The GLIF also does not account for the relative position of the load paths within the PBJ. The SBLIF, however, does account for the relative position of the load paths within the PBJ. Mathematical relationships between the SBLIF and the GLIF are developed.

Comparisons between the analytically calculated SBLIF, analytically calculated GLIF, experimentally derived LIF, and finite-element-analysis- (FEA-) derived LIF are presented. Appendix A lists definitions of symbols and terms used in this report.

Supplemental material is provided in the appendixes of this work. Appendix B addresses the historical use of the compression stiffness of the clamped members in lieu of their tensile stiffness to determine bolt tensile load. This historical practice is likely due to the tractability of calculating the compression stiffness as opposed to the tensile stiffness. Appendix C provides step-by-step examples demonstrating the calculation of the SBLIF and the GLIF. The appendixes conclude with the derivation of the load-displacement relationships governing the various load paths within a PBJ, culminating in the creation of the bolted-joint diagram. Also provided are formulas for the key coordinates of the joint diagram in terms of the SBLIF, with or without a thermal load, which are useful for programming.

2.0 Derivation of Traditional Bolt Tensile Load Equation

Consider a common PBJ configuration consisting of clamped members preloaded in compression using a bolt, washer(s), and an internally threaded component, whether it be a nut, clamped member, or insert, as shown in Figure 1.

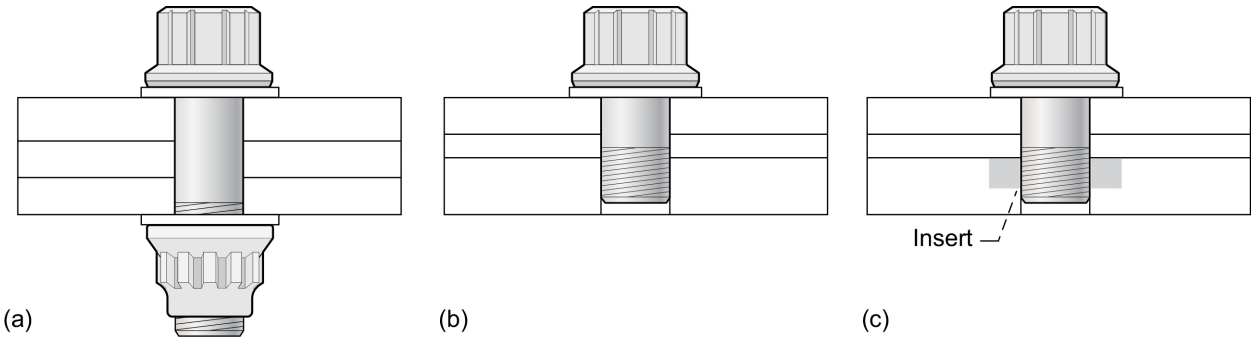

Figure 1.—Typical bolted joints. (a) Through-bolted connection. (b) Threaded connection. (c) Insert connection.

When the assembly is preloaded, a zone of compressed material exists between the bolt head and internally threaded component. This zone of compressed material, known as the compression zone is usually of varying cross section from bolt head to internal threaded component. If the clamped material sufficiently extends radially beyond the bolt head and internally threaded component, the outer boundary of the compression zone typically develops into the shape of a prolate spheroid (Ref. 3); that is, barrel shaped, prior to application of the external tensile load, as shown schematically in Figure 2(a), and computationally from FEA in Figure 2(b). The compression zone may be restricted to certain geometries, such as the situation shown in Figure 2(c), where the compression zone of a tension joint consisting of a bushing is characterized by a combination of tapered and cylindrical geometries.

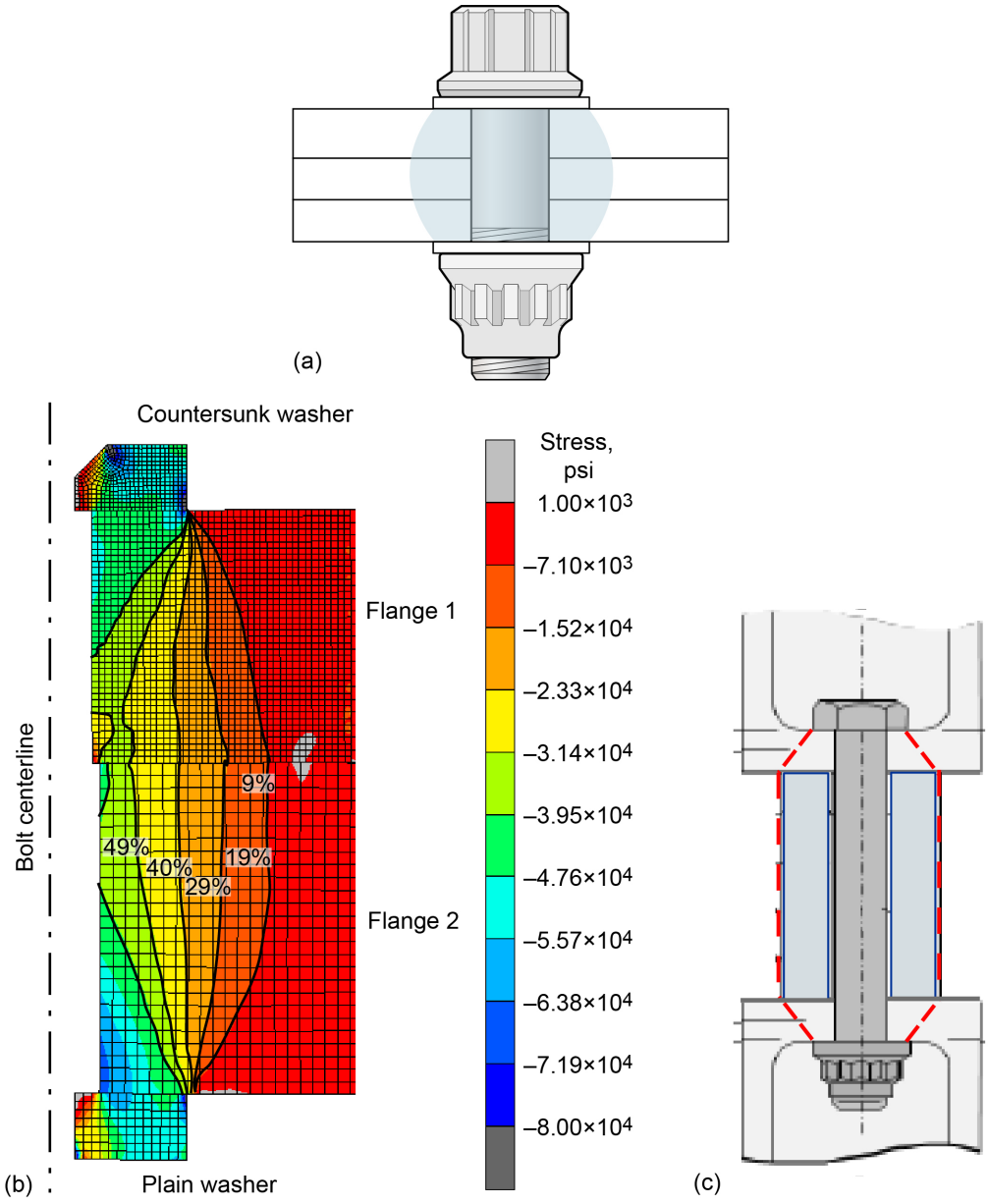

Figure 2.—Compression zone of bolted joint. (a) Typical spheroid-shaped compression zone. (b) FEA model (Ref. 4). Fringe plot of stress field in direction of bolt shank. Contours indicate percent of maximum compressive stress in direction of bolt shank. Bolt and nut not shown. (c) Tapered compression zone transitioned to cylindrical compression zone.

Generally, the compressive stress within the compression zone varies both radially from the bolt clearance hole outward and axially from the bolt head to the internally threaded component as shown in Figure 2(b). Depending upon the joint features, the compressive stress within the compression zone may also vary circumferentially.

As the PBJ reacts to external tension loads applied concentrically or off axis to a bolt, as well as possible shear loads and bending moments, the clamped members undergo displacements typically first in the far field nearer to the location of load application, and the displacements increase near the bolt as the loads increase. This results in a change in stress distribution in the clamped members between the bolt head and internally threaded component. This can be seen from the change from the preload stress distribution of the finite element model of Figure 2(b) now under concentric tensile load in Figure 3. This indicates that the stiffness of the load path under external loading is different than the stiffness of the load path (i.e., compression zone) solely under preload as shown in Figure 2(b).

However, despite the difference in stiffness between the compression zone and that of the load path under external tensile loading, the stiffness of the compression zone has traditionally been used to characterize the PBJ stiffness under external tensile loading. This is not physically correct but is acknowledged as an approximation and is addressed in Appendix B. In the figures that follow, the PBJ load paths under external tensile loading will be notionally depicted with prolate spheroid geometries.

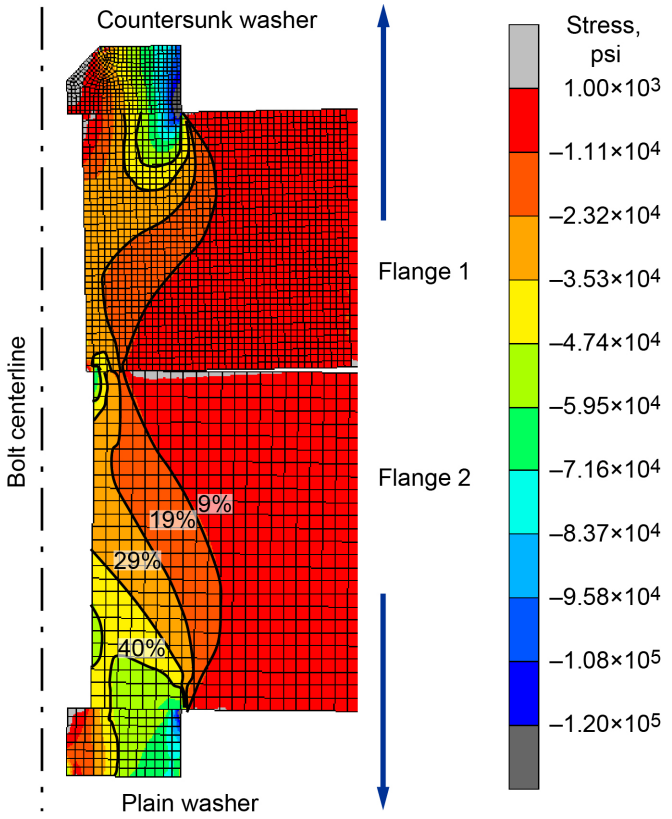

Figure 3.—FEA of PBJ of Figure 2(b) under external tensile load (Ref. 4). Tensile load path is hour-glass shape as revealed by stress contours. Fringe plot of stress field in direction of bolt shank. Stress contours indicate percent of maximum compressive stress in direction of bolt shank. Bolt and nut not shown.

At a point in time, regardless of the physical shape and qualities of the compression zone, its stiffness in the axial direction K_c (collinear with the bolt shank), can be represented as a system of stiffnesses (springs). Likewise, regardless of the physical shape and qualities of the clamped- member's tension load path, its stiffness in the axial direction K_a (collinear with the bolt shank), can also be represented as a system of stiffnesses (springs). In addition, a tensile load P_{ext} can be resolved from any combination of external loads. Thus, the following theoretical developments, assuming known values of K_c, K_a, and P_{ext} at a point in time, apply to all types of bolted joints. The equations developed in this work may be applied in a piecewise or load-step fashion to accommodate nonlinear effects.

As previously mentioned, the mechanical tensile joint load is assumed to be resolved from a general combined loading of tension, shear, and moments.

The load entering the clamped members likely occurs as a traction force or forces distributed over a cross-sectional area or areas of the clamped members. These external tension loads are approximated as a uniform or nonuniform stress distribution on two loading planes as shown in Figure 4. These loading planes are assumed to be perpendicular to the bolt shank and located where the external load is idealized (by engineering judgment) to act on the compression zone.

The distance between the loading planes is equal to the thickness of the relieving load path. The relieving load path consists of members of whole or partial thickness being relieved of some of their preload compression by the external tensile load, and thereby increasing in their thicknesses.

The external tensile load is reacted by two load paths in a PBJ: the relieving load path and the clamping load path. The clamping load path comprises the bolt and the compressed region. The compressed region, which may include a portion of the internal threaded component such as a nut, insert, or clamped member, is compressed above its preload state from the application of external load. These two load paths and associated regions are idealized in Figure 5.

It should be mentioned at this point that the equations leading up to the development of the SBLIF are based on the existence of two loading planes. However, the SBLIF is not limited as such because it can be developed using more than two loading planes for PBJs that have more than two load introduction regions. Even though a SBLIF can be developed for situations involving more than two loading planes, in these cases it is likely more expedient to use FEA to determine the PBJ characteristics. The procedure of how to obtain the PBJ characteristics using FEA is explained in Section 8.2, "$n\phi$ Diagram."

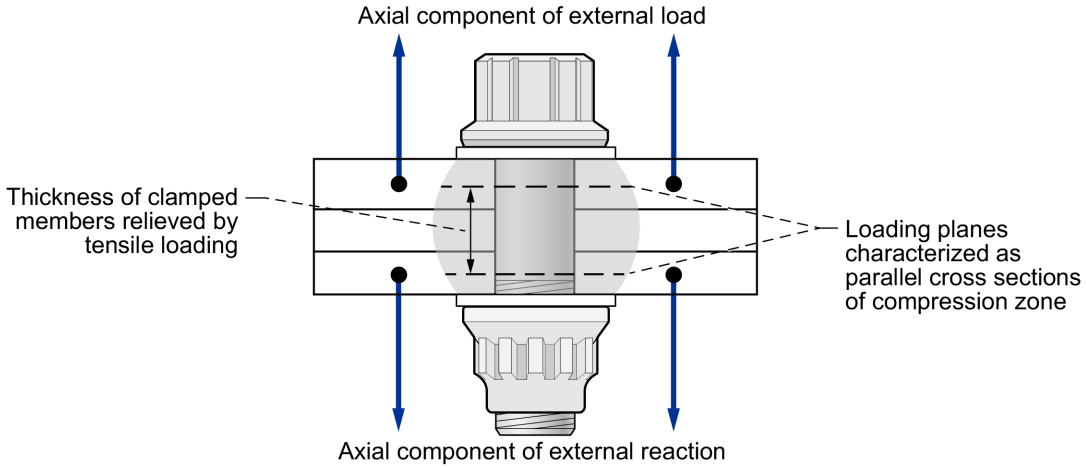

Figure 4.—Typical compression zone of PBJ, showing loading plane idealization of load introduction locations in outer clamped members. There is no direct load introduction to middle clamped member here.

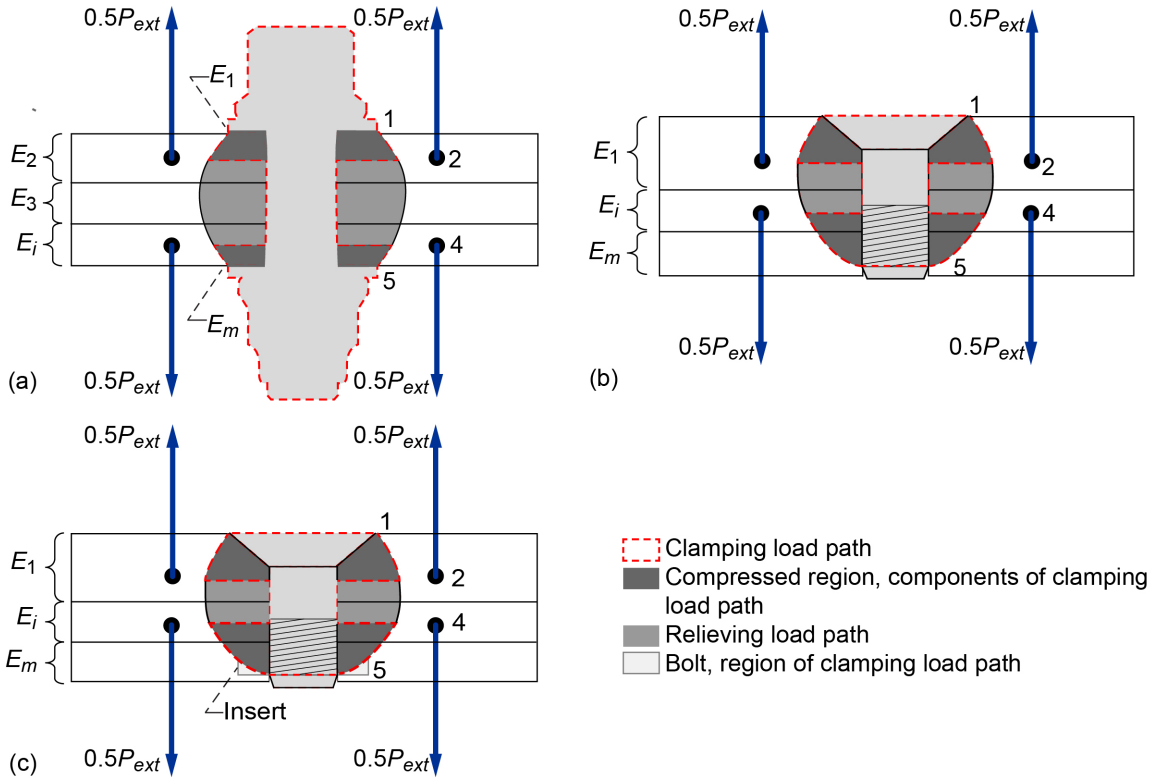

Figure 5.—Clamping and relieving load paths of PBJ under external tension loading. Locations 1 to 5 correspond to points 1 to 5 in Figure 8. E_i = modulus of elasticity of clamped member i where $1 < i < m$. (a) Through-bolted connection. (b) Threaded connection. (c) Insert connection.

During the preload process, prior to the application of the external tension load, it is convenient to consider two load paths as well: the bolt tension load path, consisting of the bolt represented by stiffness K_b, and the compression load path, consisting of all members of whole or partial thickness within the compression zone and represented by stiffness K_c. These load paths for two examples are shown in Figure 6(a) and (b) and also in terms of a system of stiffnesses (springs) in Figure 7.

The PBJs under external load as characterized by Figure 5 can be idealized by the following system of stiffnesses (springs), as shown in Figure 8(a) to (c). For the general nonsymmetric PBJ as shown in Figures 6 and 7 of Reference 1, the clamped members are idealized into four regions, being demarcated by five points (locations), as shown here in Figure 8(a). Point 3 denotes an arbitrary reference plane. Points 2 and 4 denote the loading planes, the discrete locations at which the external tensile load is idealized to act on the joint (using engineering judgment). Point 1 represents the faying surface between the bolt head and the washer or flange (if no washer is used). Point 5 represents the interface between the internal threaded component and the mating load path (compression zone under preload, or clamped-member tension load path under external load). These four regions, in the most general case, will exhibit different stiffness values due to different load-path stiffnesses within each region as shown in Figure 5, and correspondingly represented as springs in Figure 8(a). The stiffness values of these different regions are represented by the product of the clamped-member tensile stiffness K_a, and stiffness coefficients A, B, C, and D, as shown in Figure 8(a).

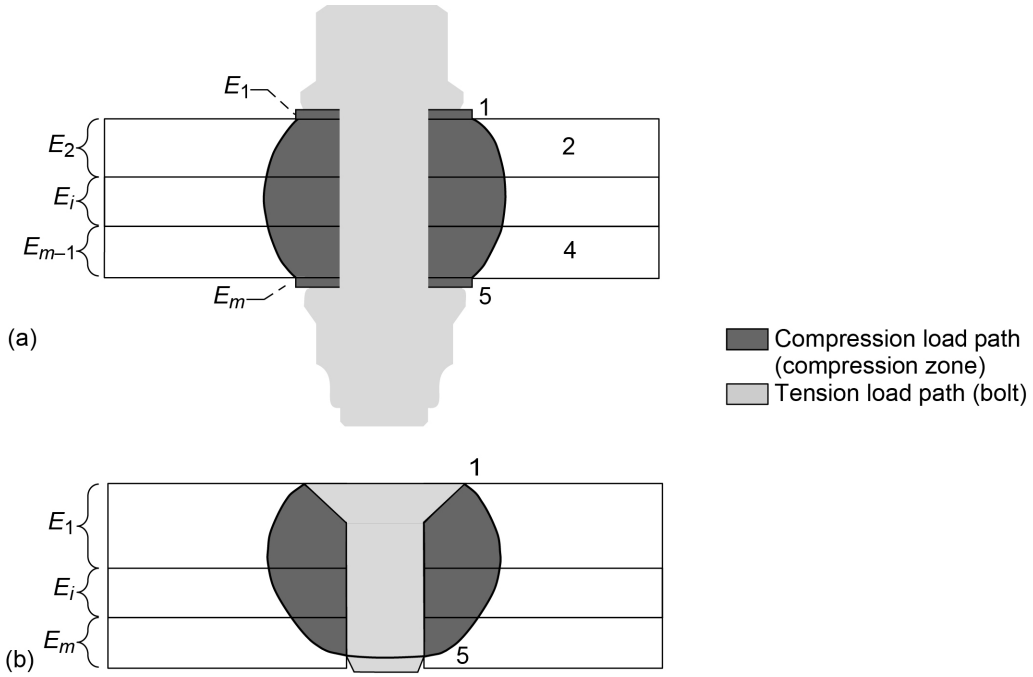

Figure 6.—Two load paths of PBJ, solely reacting preload. (a) Fastener with protruding head in through-bolted connection. (b) Countersunk fastener in threaded connection.

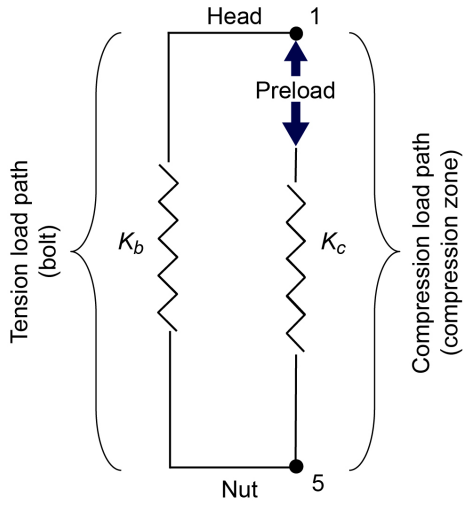

Figure 7.—PBJ solely under preload represented by two springs in parallel.

Because the joint is preloaded, and there is no gapping of faying surfaces, the two stiffnesses BK_a and CK_a, representing the relieving load path between points 2 and 4 of Figure 8(a), act in series.[1] These stiffnesses may be combined into one equivalent stiffness RK_a as shown in Figure 8(b), where

[1]The flexibility of a system of springs in series $1/K$, is equal to the sum of the flexibilities of the individual spring elements comprising the system, as

$$\frac{1}{K} = \frac{1}{K_1} + \frac{1}{K_2} + \frac{1}{K_3} + \cdots$$

$$\frac{1}{RK_a} = \frac{1}{BK_a} + \frac{1}{CK_a} \tag{1}$$

Multiplying Equation (1) by K_a gives the following relationship between the stiffness coefficients:

$$\frac{1}{R} = \frac{1}{B} + \frac{1}{C} = \frac{B+C}{BC} \tag{2}$$

Again, because there is no gapping of the faying surfaces in the joint, the two stiffnesses AK_a and DK_a representing the compressed region between points 1 and 2, and points 4 and 5, respectively, of Figure 8(a) and (b), act in series with the bolt, and therefore with each other, and may be combined into one equivalent stiffness QK_a as shown in Figure 8(c), where

$$\frac{1}{QK_a} = \frac{1}{AK_a} + \frac{1}{DK_a} \tag{3}$$

Multiplying Equation (3) by K_a gives the following relationship between the stiffness coefficients:

$$\frac{1}{Q} = \frac{1}{A} + \frac{1}{D} = \frac{A+D}{AD} \tag{4}$$

Consider the flexibility of the tensile load path, $1/K_a$, of Figure 8(c), which is equal to the sum of the flexibilities of the compressed region and relieving load path:

$$\frac{1}{K_a} = \frac{1}{QK_a} + \frac{1}{RK_a} \tag{5}$$

Multiplying Equation (5) by K_a yields the following relationships between the stiffness coefficients of the relieving load path and compressed regions:

$$1 = \frac{1}{R} + \frac{1}{Q} \tag{6}$$

$$\frac{1}{R} = 1 - \frac{1}{Q} \tag{7}$$

$$\frac{1}{Q} = 1 - \frac{1}{R} \tag{8}$$

The reader is cautioned not to confuse the number of clamped members in any given joint with the number of regions, or equivalently the number of stiffness coefficients, between points 1 and 5 of Figure 8(a) to (c). Any number of clamped members can be represented by the stiffness coefficients of the regions between points 1 and 5, as shown in Figure 8(a) to (c), using the relationships between stiffnesses in series and the known stiffness[2] of the tensile load path K_a.

[2]In practice, K_a is taken as the stiffness of the compression zone, K_c, which is not strictly correct but is more tractable than other approaches or methods. See Appendix B.

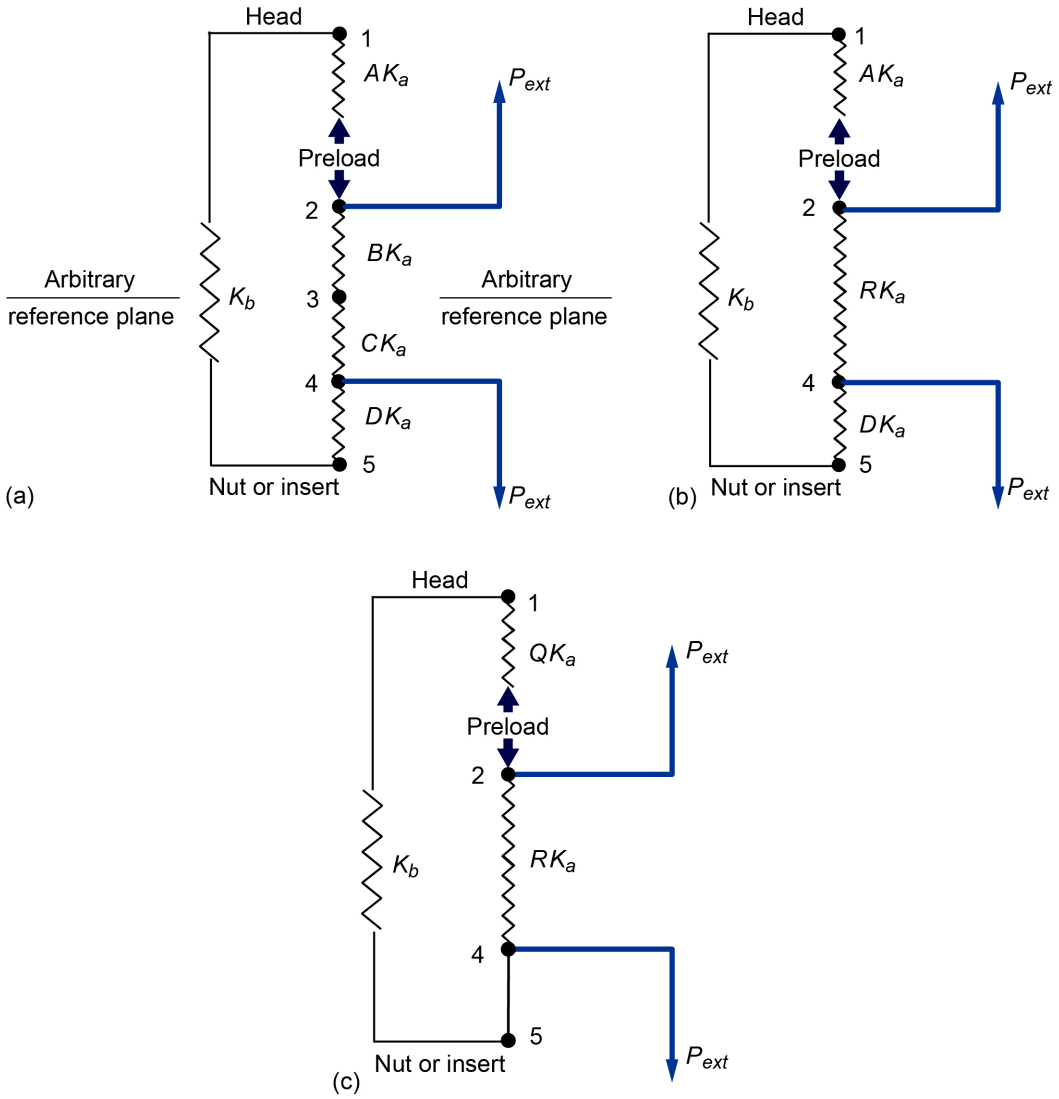

Figure 8.—Spring representation of PBJ with external tension load. (a) As modeled in Figure 6 of Reference 1 with added preload representation. (b) Intermediate representation used for derivation description. (c) As modeled herein.

For example, the following stiffness relationship is written for S clamped members (in whole or in partial thickness), each of stiffness K_i, between points 2 and 4 of Figure 8(b):

$$\sum_{i=1}^{S} \frac{1}{K_i} = \frac{1}{RK_a} \tag{9}$$

Solving Equation (9) for the stiffness coefficient R,

$$R = \frac{1}{\left(\sum_{i=1}^{S} \frac{1}{K_i} \right) K_a} \tag{10}$$

where the tensile load-path stiffness K_a is assumed to be known, having been calculated beforehand by knowing the individual stiffnesses of all clamped members (see example in Appendix C). Therefore, the coefficient R represents any quantity S of clamped members within its associated region or load path. Similar equations to that of Equation (10) may be written for the regions between points 1 and 2 and between points 4 and 5 of Figure 8(b), or between points 1 and 2 of Figure 8(c). Therefore, the configurations shown in Figure 8(a) to (c), and in particular the stiffness coefficients R and Q, represent any number of clamped members. There is no advantage in using the four stiffness coefficients A, B, C, and D, which are only included in this work for continuity with Reference 1. Only the two stiffness coefficients R and Q are required to characterize the PBJ stiffness.

Consider the relieving load path shown in Figure 5, that increases in thickness upon application of the external tensile load P_{ext}. The stiffness of the relieving load path is denoted as $K_{2\text{–}4}$, in keeping with the notation of Reference 1, and is expressed in terms of the stiffness coefficient R and the tensile load-path stiffness K_a of Figure 8(c):

$$K_{2\text{–}4} = RK_a \tag{11}$$

Consider the clamping load path of Figure 5—consisting of the whole and partial thicknesses of the clamped members in the compressed region along with the bolt that is elongated—upon application of the external tensile load P_{ext}. This clamping load path is represented in Figure 8(c) by stiffness QK_a representing the compressed region and by the stiffness K_b representing the bolt. Because the joint is preloaded, there is no gapping of faying surfaces, and these stiffnesses act in series. The combined stiffness is denoted as $K_{1\text{–}2,4\text{–}5}$, in keeping with the notation of Reference 1, and can be determined by

$$\frac{1}{K_{1\text{–}2,4\text{–}5}} = \frac{1}{QK_a} + \frac{1}{K_b} = \frac{K_b + QK_a}{QK_aK_b} \tag{12}$$

Inverting Equation (12), the stiffness of the clamping load path is obtained:

$$K_{1\text{–}2,4\text{–}5} = \frac{QK_aK_b}{QK_a + K_b} \tag{13}$$

The joint idealization shown in Figure 8(c) can be further simplified using the two stiffnesses $K_{2\text{–}4}$ and $K_{1\text{–}2,4\text{–}5}$, corresponding to the relieving and clamping load paths, respectively, that are reacting the external load, as shown in Figure 9.

The stiffnesses shown in Figure 9 act in parallel. This can be more clearly visualized by the slight adjustment of Figure 9, as shown in Figure 10.

The effective stiffness of this entire system shown in Figure 10 can be represented by one effective stiffness denoted as K_{eff}. Since stiffnesses $K_{2\text{–}4}$ and $K_{1\text{–}2,4\text{–}5}$ act in parallel,

$$K_{eff} = K_{2\text{–}4} + K_{1\text{–}2,4\text{–}5} = RK_a + \frac{QK_aK_b}{QK_a + K_b} \tag{14}$$

where Equations (11) and (13) have been employed.

Referring to Figure 10, $\delta_{2\text{–}4}$, which is the relative displacement of points 2 and 4 of the relieving load path after joint equilibrium at preload, can be written in terms of the external tensile load P_{ext} using Hooke's Law as shown:

$$\delta_{2\text{–}4} = \frac{P_{ext}}{K_{eff}} \tag{15}$$

This displacement is due to mechanical loads only. The displacements due to thermal loads will be addressed later.

In like manner, δ_{2-4} can also be expressed in terms of the amount of external load reacted in the clamping load path of Figure 9 or Figure 10 and, equivalently, Figure 8(c). Consider the free-body diagram of the clamping load path of Figure 8(c) as shown in Figure 11.

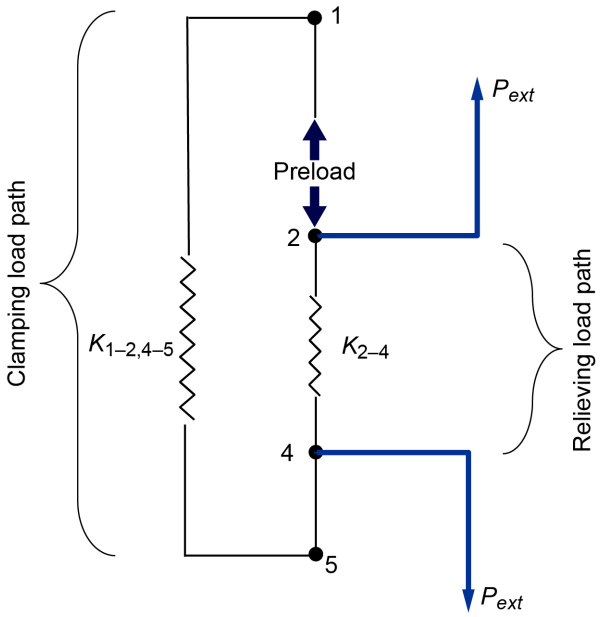

Figure 9.—Preloaded joint represented by two springs in parallel.

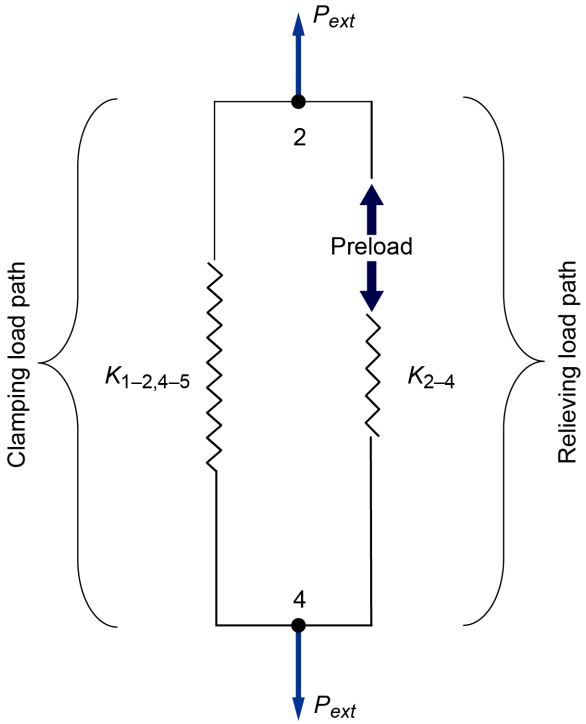

Figure 10.—Preloaded joint represented by two springs in parallel (Figure 8 rearranged for clarity).

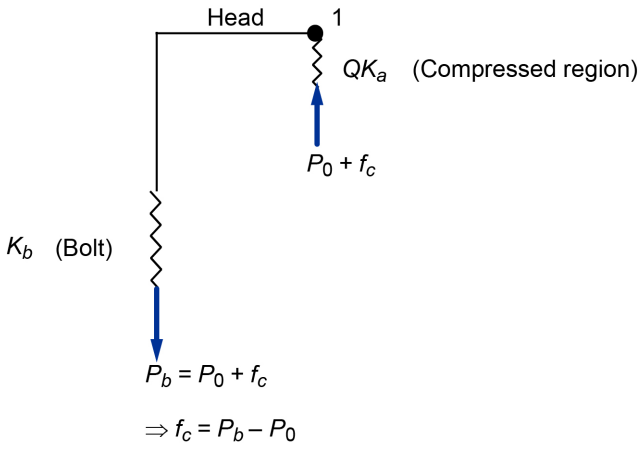

Figure 11.—Free-body diagram of clamping load path in PBJ under tensile load.

The external tensile load being reacted in the clamping load path results in a reaction force f_c in addition to the already existing preload P_0. The reaction force along this load path, $P_b - P_0$, is of constant magnitude, being a compressive force in the compressed region and a tensile force P_b of equal magnitude in the bolt (see Figure 11):

$$P_b = P_0 + f_c \tag{16}$$

Neither P_b or f_c is equivalent to P_{ext}. Rather, P_b is an internal combined force of the preload P_0 and the reaction force f_c in the clamping load path, because of the external tensile load.

The relative displacement after preload of points 2 and 4 of the clamping load path $\delta_{1-2,4-5}$ illustrated in Figure 10 can be written invoking Equation (16) and using Hooke's Law in terms of the force f_c after preload, reacted by the clamping load path, and the clamping load-path stiffness $K_{1-2,4-5}$, as

$$\delta_{1-2,4-5} = \frac{f_c}{K_{1-2,4-5}} = \frac{P_b - P_0}{K_{1-2,4-5}} \tag{17}$$

This displacement is due to mechanical loads only. Note the displacements due to thermal loads will be addressed later.

Since the displacement of the relieving and clamping load paths as given in Equations (15) and (17), respectively, represent the relative displacement of points 2 and 4 after preload, they are equivalent and may be equated and rearranged, giving

$$P_b = P_0 + \frac{K_{1-2,4-5}}{K_{eff}} P_{ext} \tag{18}$$

Substituting Equations (13) and (14) into Equation (18), combining terms, and simplifying results in

$$P_b = P_0 + \frac{QK_aK_b}{RK_a(QK_a + K_b) + QK_aK_b} P_{ext} \tag{19}$$

Factoring out QK_a from the numerator and denominator of Equation (19) and rearranging gives

$$P_b = P_0 + \frac{K_b}{R\left(K_a + \frac{K_b}{Q}\right) + K_b} P_{ext} \tag{20}$$

Substituting Equation (8) into Equation (20) gives

$$P_b = P_0 + \frac{K_b}{R\left[K_a + \left(1 - \frac{1}{R}\right)K_b\right] + K_b} P_{ext} \tag{21}$$

Upon simplifying Equation (21),

$$P_b = P_0 + \frac{1}{R}\left(\frac{K_b}{K_a + K_b}\right) P_{ext} \tag{22}$$

Equation (22) is in the familiar form of the traditional bolt tensile load equation (without the thermal load term), expressed as

$$P_b = P_0 + n\phi P_{ext} \tag{23}$$

where n is denoted as the SBLIF because it is expressed exclusively in terms of stiffness,

$$n = \frac{1}{R} \tag{24}$$

and ϕ is the stiffness factor,

$$\phi = \left(\frac{K_b}{K_a + K_b}\right) \tag{25}$$

The SBLIF represented in Equation (24) is expressed in terms of the stiffness coefficient of the relieving load path. It may also be expressed in terms of the compressed region as shown in Section 2.1, “Stiffness-Based Load Introduction Factor (SBLIF).”

Both n and ϕ have been shown to be inherent products of the derivation of the traditional bolt tensile load equation. The stiffness factor is a function of the bolt and clamped-members’ tension load-path stiffnesses. It should be mentioned at this point that it is not necessary to separate out the LIF and the stiffness factor, but it is done here so that the reader can see the derivation of the bolt tensile load equation in its popular form. The bolt tensile load equation will be derived in its fundamental form without these two factors after the complete derivation of the traditional bolt tensile load equation with thermal loading included. It is also worth noting that aside from the assumed location of the loading planes, nothing else has been assumed about the geometry of the compression zone or the clamped-members’ tensile load path in deriving the bolt tensile load equation.

2.1 Stiffness-Based Load Introduction Factor (SBLIF)

As mentioned previously, the LIF represented in Equation (24) is expressed in terms of the stiffness coefficient of the relieving load path. By substituting Equation (7) into Equation (24), the SBLIF may also be expressed in terms of the stiffness coefficient of the compressed region:

$$n = 1 - \frac{1}{Q} \tag{26}$$

To provide continuity with Reference 1, Equation (2) is substituted into Equation (24), and Equation (4) into Equation (26), to obtain the SBLIF in terms of the stiffness coefficients of the relieving load path and compressed regions *A*, *B*, *C*, and *D*, as presented in Reference 1 and shown in Figure 8(a):

$$n = \frac{B + C}{BC} \tag{27}$$

$$n = 1 - \frac{A + D}{AD} \tag{28}$$

The SBLIF can be expressed by either the stiffness coefficients of the relieving load path, Equations (24) and (27), or the stiffness coefficients of the compressed region as shown in Equations (26) and (28). As mentioned previously, there is no advantage in using the four stiffness coefficients *A*, *B*, *C*, and *D*; rather, only the two stiffness coefficients *R* and *Q* are used.

The SBLIF, given in Equation (24) in terms of the stiffness coefficient of the relieving load path *R*, may be modeled analytically using *N* individual stiffness elements. The choice of stiffness element types to use in modeling the relieving load path is left up to the analyst. This section of the report lays out the general concepts. Examples of how to calculate the SBLIF using frustum stiffness elements are shown in Appendix C and Appendix H.

Taking the reciprocal of Equation (11), giving the flexibility of the relieving load path, and representing it in terms of the flexibilities of *N* individual stiffness elements, each of stiffness K_i, gives

$$\frac{1}{K_{2-4}} = \frac{1}{RK_a} = \left(\sum_{i=1}^{N} \frac{1}{K_i} \right)_{relieving} \tag{29}$$

Equation (29) appears to be like Equation (9), but it is not the same. Equation (9) involves *S*, the number of (whole and partial thickness) members constituting the relieving load path, whereas Equation (29) involves *N*, the number of stiffness elements representing *S* number of (whole and partial thickness) members comprising the relieving load path. Although it is possible that *S* could equal *N*, it would not generally be the case (see Appendix C, where $S = 3$ and $N = 4$).

Solving Equation (29) for $1/R$ and substituting into Equation (24), the SBLIF is expressed in terms of the *N* individual stiffness elements, each of stiffness K_i, comprising the relieving load path:

$$n = \frac{1}{R} = K_a \left(\sum_{i=1}^{N} \frac{1}{K_i} \right)_{relieving} \tag{30}$$

In like manner, the SBLIF, as expressed in Equation (26) in terms of the stiffness coefficient *Q*, may be modeled analytically using *M* individual stiffness elements. The flexibility of the compressed region of

Figure 8(c) is obtained by starting with the flexibility of the clamping load path, Equation (12), without the bolt flexibility, giving

$$\frac{1}{K^*_{1-2,4-5}} = \frac{1}{QK_a} \tag{31}$$

where $K^*_{1-2,4-5}$ is the stiffness of the compressed region; the superscript (*) signifies that the bolt flexibility is not included.

Representing the flexibility of the compressed region in terms of the flexibilities of M individual stiffness elements, each of stiffness K_i,

$$\frac{1}{QK_a} = \left(\sum_{i=1}^{M} \frac{1}{K_i} \right)_{compressed} \tag{32}$$

Solving Equation (32) for $1/Q$ and substituting into Equation (26), the SBLIF in terms of the flexibility of the stiffness elements representing the compressed region is

$$n = 1 - \frac{1}{Q} = 1 - K_a \left(\sum_{i=1}^{M} \frac{1}{K_i} \right)_{compressed} \tag{33}$$

Equations (30) and (33) provide a way to calculate the SBLIF in terms of individual stiffness elements that represent the relieved load path and compressed region, respectively.

Having derived the bolt tensile load Equation (23) in its most common form, for mechanical loads only, the bolt tensile load equation will be further developed to include the thermal loading term. The expression for the thermal load is developed in Appendix E and combined with Equation (23) to form the traditional bolt tensile load equation including both mechanical and thermal loads.

2.2 Including Bolt Thermal Load

The thermal load is an internal load resulting from a resistance to unconstrained thermal displacement of a body (Ref. 5, p. 110). For the PBJ, the thermal load is created by a temperature change in conjunction with the differences in thermal expansion rates (coefficients) of the bolt α_b and clamped members α_a. The thermal load serves to restrain the thermal displacement of the bolt and the clamped members so that they are in equilibrium.

The thermal load is derived in Appendix E and is

$$P_{th} = \phi K_a L \Delta T (\alpha_a - \alpha_b) \tag{34}$$

where ΔT is the change in temperature from joint equilibrium at preload, and L is the thickness of the clamped members (each of thickness L_i), which have an effective thermal expansion coefficient of

$$\alpha_a = \frac{\sum_{i}^{m} \alpha_i L_i}{L} \tag{35}$$

Because linear behavior is assumed, linear superposition of forces is permitted, and therefore the complete bolt tensile load equation including mechanical and thermal loads is obtained by linearly combining Equation (23) and the thermal load P_{th}, giving

$$P_b = P_0 + n\phi P_{ext} + P_{th} \tag{36}$$

Substituting Equation (34) into Equation (36),

$$P_b = P_0 + n\phi P_{ext} + \phi K_a L \Delta T (\alpha_a - \alpha_b) \tag{37}$$

and combining terms, gives

$$P_b = P_0 + \phi [n P_{ext} + K_a L \Delta T (\alpha_a - \alpha_b)] \tag{38}$$

where n is the SBLIF given previously in Equation (30) or (33).

3.0 Bolt Rupture Load

The external tension load component at bolt rupture P'_{tu}, may be determined by substituting P'_{tu} for P_{ext}, and the bolt allowable ultimate tensile load $P_{tu-allow}$ for P_b, in the bolt tensile load Equation (36):

$$P_{tu-allow} = P_0 + n\phi P'_{tu} + P_{th} \tag{39}$$

Solving for the bolt rupture load in terms of the SBLIF,

$$P'_{tu} = \frac{P_{tu-allow} - (P_0 + P_{th})}{n\phi} \tag{40}$$

4.0 Separation Load

Under an external tensile load, the relieving load path is susceptible to gapping of its faying surfaces should the tensile load become large enough to eliminate the preload from the relieving load path. In this work, joint gapping is a binary event: either a faying surface is completely gapped, or it is not. In reality, joint gapping is usually not a binary event; rather, it is a gradual progression as external tensile load is increased.

At complete joint separation, the clamped members no longer maintain contact, and therefore, no load can pass across their faying surfaces. Consequently, the clamped members no longer help to reduce the bolt load, and the full external load is experienced by the bolt. In this situation, the external tensile load P_{ext} is equal to the bolt tensile load P_b in the bolt tensile load Equation (36). Designating the external load at the onset of complete joint separation as the separation load P_{sep}, and substituting this for P_{ext} and P_b in the bolt tensile load Equation (36), results in

$$P_{sep} = P_0 + n\phi P_{sep} + P_{th} \tag{41}$$

The separation load P_{sep} in terms of the SBLIF becomes

$$P_{sep} = \frac{P_0 + P_{th}}{1 - n\phi} \tag{42}$$

As long as P_{ext} is less than P_{sep}, the bolt tensile load equations developed in this work remain valid.

5.0 Derivation of Fundamental Bolt Tensile Load Equation

In the previous derivation of the bolt tensile load equation, although it was not necessary to factor out a LIF or stiffness factor, it was done to show how the traditional equation is derived. The downside of that form of the equation is that it creates the possibility that the LIF and stiffness factor will be assumed to be independent of each other, which they are not. Their interdependence is shown next.

Upon substituting Equations (29) and (31) into Equation (5),

$$\frac{1}{K_a} = \frac{1}{K_{2-4}} + \frac{1}{K^*_{1-2,4-5}} = \frac{K^*_{1-2,4-5} + K_{2-4}}{\left(K_{2-4}\right)\left(K^*_{1-2,4-5}\right)} \tag{43}$$

Inverting Equation (43), substituting into Equation (25), combining terms, and refining yields

$$\phi = \frac{K_b\left(K_{2-4} + K^*_{1-2,4-5}\right)}{\left(K_{2-4}\right)\left(K^*_{1-2,4-5}\right) + K_b\left(K_{2-4} + K^*_{1-2,4-5}\right)} \tag{44}$$

Now the SBLIF will be expressed in terms of the stiffness of the relieving and tensile load paths. Solving Equation (11) for R and substituting into Equation (24) gives

$$n = \frac{K_a}{K_{2-4}} \tag{45}$$

Then by substituting the reciprocal of Equation (43) into Equation (45),

$$n = \frac{K^*_{1-2,4-5}}{K_{2-4} + K^*_{1-2,4-5}} \tag{46}$$

Multiplying Equation (44) by Equation (46) the product $n\phi$ becomes

$$n\phi = \left(\frac{K^*_{1-2,4-5}}{K_{2-4} + K^*_{1-2,4-5}}\right)\frac{K_b\left(K_{2-4} + K^*_{1-2,4-5}\right)_a}{\left(K_{2-4}\right)\left(K^*_{1-2,4-5}\right) + K_b\left(K_{2-4} + K^*_{1-2,4-5}\right)} \tag{47}$$

Reducing Equation (47) and rearranging produces

$$n\phi = \frac{K_b}{\left(K_{2-4}\right) + K_b\left(\frac{K_{2-4}}{K^*_{1-2,4-5}} + 1\right)} \tag{48}$$

After substituting the reciprocal of Equation (43) in addition to Equations (44) and (48) into Equation (37) and reducing, the fundamental bolt tensile load equation is obtained without explicit representation of the SBLIF or the stiffness ratio:

$$P_b = P_0 + \frac{K_b P_{ext}}{\left(K_{2-4}\right) + K_b\left(\frac{K_{2-4}}{K^*_{1-2,4-5}} + 1\right)} + \frac{K_b L \Delta T\left(\alpha_a - \alpha_b\right)}{K_b\left(\frac{1}{K_{2-4}} + \frac{1}{K^*_{1-2,4-5}}\right) + 1} \tag{49}$$

It can be seen from Equations (44) and (46) that the stiffness ratio and SBLIF are both functions of the relieving load-path stiffness $K_{2\text{–}4}$ and the compressed region stiffness $K^{*}_{1\text{–}2,4\text{–}5}$, and therefore via Equation (34), that the thermal load is too, as shown in Equation (49). Therefore, n, ϕ, and P_{th} are not independent quantities, and changes to them should be consistent.

The fundamental bolt tensile load equation avoids the distraction of dealing with the LIF and stiffness ratios explicitly. However, the fundamental bolt tensile load equation, as does the traditional bolt tensile load equation, still requires engineering judgment to determine the boundaries of the relieving load path and compressed region, which is equivalent to using engineering judgment in determining the location of the loading planes.

Table I presents the values or expressions for n, $n\phi$, and P_b from Equations (46), (48), and (49) as the stiffness of the compressed region and relieving load path are taken to the limits of 0 and ∞.

Reducing the product $n\,\phi$ reduces the mechanical tensile bolt load, as is commonly known, and can be observed from the traditional bolt tensile load Equation (36). The $n\,\phi$ can be reduced by increasing the stiffness of the relieving load path $K_{2\text{–}4}$, decreasing the stiffness of the compressed region $K^{*}_{1\text{–}2,4\text{–}5}$, or doing both simultaneously, as observed from Equation (48). As an example of the insight into the effects of the load-path stiffnesses on bolt load as provided by the spring stiffness model, consider how these stiffnesses affect the bolt tensile load for the PBJ example in Appendix C. By increasing the stiffness of the relieving load path and decreasing the stiffness of the compressed region, first independently and then concurrently in 10-percent increments, $n\,\phi$, and thus the mechanical bolt tensile load, are reduced, as shown in Figure 12.

It can be seen that simultaneously increasing $K_{2\text{–}4}$ and decreasing $K^{*}_{1\text{–}2,4\text{–}5}$ is the most effective way to decrease $n\phi$. Aside from this, and for changes of less than about 80 percent for the stiffnesses of the relieving load path or compressed region, it is more effective in reducing $n\phi$, and consequently the bolt load, to increase the stiffness of the relieving load path rather than decrease the stiffness of the compressed region. Above about an 80-percent stiffness change for each, the opposite is true for this example.

TABLE I.—LIMITS ON LIF, PRODUCT OF LIF AND JOINT STIFFNESS FACTOR, AND BOLT LOAD AS FUNCTION OF THE LIMITS OF STIFFNESSES OF COMPRESSED REGION AND RELIEVING LOAD PATH

Stiffness limits	n	$n\phi$	P_b
$K^{*}_{1\text{–}2,4\text{–}5} \to \infty$	$\to 1$	$\to \dfrac{K_b}{K_{2-4}+K_b}$	$\to P_0 + \dfrac{K_b P_{ext}}{K_b+K_{2-4}} + \dfrac{K_{2-4}K_b L\,\Delta T\left(\alpha_a-\alpha_b\right)}{K_b+K_{2-4}}$
$K^{*}_{1\text{–}2,4\text{–}5} \to 0$	$\to 0$	$\to 0$	$\to P_0$
$K_{2-4} \to \infty$	$\to 0$	$\to 0$	$\to P_0 + \dfrac{K^{*}_{1\text{–}2,4\text{–}5}K_b L\,\Delta T\left(\alpha_a-\alpha_b\right)}{K_b+K^{*}_{1\text{–}2,4\text{–}5}}$
$K_{2-4} \to 0$	$\to 1$	$\to 1$	$\to P_0 + P_{ext}$

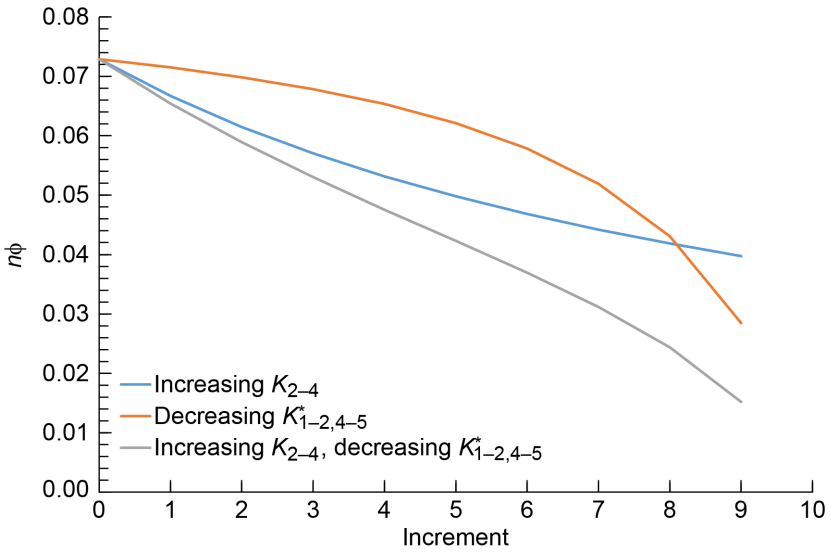

Figure 12.—Change in $n\phi$ for PBJ example in Appendix C from increasing stiffness of relieving load-path K_{2-4}, decreasing stiffness of compressed region $K^{*}_{1-2,4-5}$, and doing both simultaneously. Each increment on the abscissa represents 10-percent increase in K_{2-4} and/or 10-percent decrease in $K^{*}_{1-2,4-5}$.

The fundamental form of the bolt tensile load equation has been derived in terms of three fundamental stiffnesses—those of the relieving load path, the compressed region, and the bolt—without an explicit LIF or stiffness factor. The traditional and fundamental forms of the bolt tensile load equation are equivalent and can be used to approximate the bolt tensile load. If the traditional form of the bolt tensile load equation is used, the analyst will need to explicitly determine the SBLIF using Equation (30) or (33) or the GLIF described next.

6.0 Analytical Approximation of Stiffness-Based Load Introduction Factor

In order to calculate the SBLIF analytically, per Equations (30) and (33), the stiffnesses of the tensile load-path K_a as well as that of either the associated compressed region $K^{*}_{1-2,4-5}$ or the relieving load-path K_{2-4} must be calculated. Because it is a more tractable approach than any other in the analytical realm, K_a is approximated with the stiffness of the compression zone K_c. Likewise, $K^{*}_{1-2,4-5}$ and K_{2-4} are also approximated as stiffnesses of the subregions of the compression zone demarcated by the loading planes. Again, using the stiffness of the compression zone and its subregions in lieu of the corresponding stiffnesses of the tensile load path is acknowledged as an approximation because the clamped-members' compressive and tensile stiffness are not equivalent, as shown by comparing Figure 2(b) and Figure 3.

There have been studies comparing experimental joint compressive stiffness to the compression-zone stiffness predicted by FEA and various other analytical approximations (Ref. 6) as well as comparisons of joint compressive stiffness predicted by FEA and other analytical approaches (Refs. 6 to 8). Compression zones in the shapes of a prolate spheroid, back-to-back frusta, and sleeves have traditionally been used in the approximation of the compressive stiffness of a PBJ. The use of back-to-back frusta with a uniform radial stress distribution has been a popular geometric approximation to the prolate-spheroid compression-zone geometry, provided enough flange acreage exists for the frustra to fully develop. These

studies provide guidance on the half-apex angle to use for the frustra approximation of the compression zone—and thus the compressive stiffness—of the PBJ.

From the works cited in this report, frusta with a half-apex angle from 21.8° to 36°, are advertised to give a reasonably accurate approximation to the experimental joint compressive stiffness. In this report, half-apex angles of 21.8° and 30° will be used as well for coverage between the lowest value of 21.8° and the popular value of 30°. The reader is cautioned that these choices might not yield the most accurate SBLIF for their specific case, and it is up to the analyst to determine the appropriate value.

7.0 Comparison of Geometric and Stiffness-Based Load Introduction Factors

Solving Equation (45) for the flexibility of the relieving load path,

$$\frac{1}{K_{2-4}} = \frac{n}{K_a} \tag{50}$$

which may be expressed in terms of its portion of a tensile load path of arbitrary shape $A(x)$ and arbitrary modulus distribution $E(x)$,

$$\frac{1}{K_{2-4}} = \int_{l_2}^{l_4} \frac{dx}{E(x)A(x)} \tag{51}$$

where x is the through-thickness coordinate of the clamped members, and l_2 and l_4 are the boundaries (loading planes) of the relieving load path as shown in Figure 13.

Similarly, the flexibility of the entire clamped-members' tension load path is

$$\frac{1}{K_a} = \int_0^L \frac{dx}{E(x)A(x)} \tag{52}$$

Equations (51) and (52) follow from Appendix F, Equations (F.1) to (F.6), where the limits of integration have been adjusted appropriately. Substituting Equations (51) and (52) into Equation (50) and rearranging gives a general equation for the SBLIF:

$$\frac{K_a}{K_{2-4}} = \frac{\int_{l_2}^{l_4} \frac{dx}{E(x)A(x)}}{\int_0^L \frac{dx}{E(x)A(x)}} = n \tag{53}$$

The LIF defined in Reference 9 as the ratio of the distance between loading planes to the total thickness of the clamped members is denoted herein as the geometric load introduction factor (GLIF) n_G, because it is defined solely on geometric considerations: the ratio of two lengths. The distance between loading planes is equal to the thickness of the relieving load path. Referring to Figure 13, the GLIF is expressed as

$$n_G = \frac{l_4 - l_2}{L} \tag{54}$$

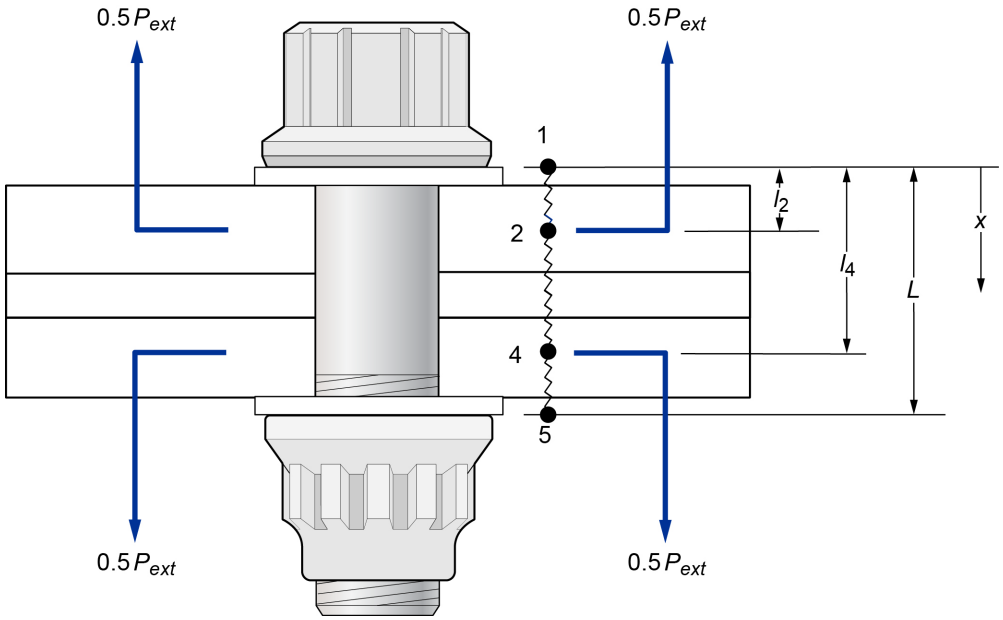

Figure 13.—Loading planes located at points 2 and 4. Points 1, 2, 4, and 5 correspond to those of Figure 8.

Equating Equations (53) and (54) provides the relationship between the SBLIF and the GLIF:

$$\frac{\int_{l_2}^{l_4} \frac{dx}{E(x)A(x)}}{\int_0^L \frac{dx}{E(x)A(x)}} \overset{\text{set}}{=} \frac{l_4 - l_2}{L} \tag{55}$$

Using the identity

$$\int_a^b dx = b - a \tag{56}$$

it can be observed that the only means by which Equation (55) can be satisfied is that $E(x)$ and $A(x)$ are constants or that they vary with x such that their product is a constant for all x within the limits of integration; that is,

$$\left.\begin{matrix} E(x), A(x) \\ E(x)A(x) \end{matrix}\right\} = \text{constant} \quad a \le x \le b \tag{57}$$

This second scenario, although possible, is unlikely in practice.

Therefore, for all practical situations, the GLIF is based on the assumption that the clamped-members' tension load path corresponds to a cross section shape of constant area and uniform modulus of elasticity. This conclusion is also mentioned in Reference 10. In practice, this would be a sleeve-type geometry consisting of a uniform material. The GLIF is inconsistent with clamped-members' tension load paths that are of a nonuniform geometry and/or consisting of materials with different modulus of elasticity. It should be noted that both the SBLIF and the GLIF depend upon an idealized location of the loading planes, and in both cases, this is usually based on engineering judgment.

7.1 Relative Position of Relieving Load Path

The GLIF based on the thickness ratio of the relieving load path and clamped-member thicknesses, does not in general account for the position of the relieving load path within the clamped members. This is apparent from Equation (54) and demonstrated for the two PBJs shown in Figure 14 using a back-to-back frusta approximation of the compression-zone K_c and for two PBJs shown in Figure 15 using a sleeve approximation for K_c. In each of Figure 14 and Figure 15, for case (a) the relieving load path is centered within the clamped members, and in case (b) it is offset closer to the bolt head. In both cases the GLIF is the same, $n_G = 0.4699$. However, the stiffnesses of the relieving load path and compressed regions, being different for the two PBJs shown in Figure 14 and Figure 15, result in different SBLIFs as indicated.

For the PBJ of Figure 14, K_c was modeled as back-to-back frusta with half-apex angle $\theta = 30°$, through-hole diameter of 0.25 in., and bolt head and nut contact surface diameter of 0.375 in. $K_{2\text{–}4}$ and $K^*_{1\text{–}2,4\text{–}5}$ were modeled using six stiffness elements, with the flexibility of each being given by Equation (F.25) and repeated in Figure 14 for convenience.

For the PBJ of Figure 15, K_c was modeled as the stiffness of a sleeve (Ref. 11).

The SBLIF is shown to account for the relative location of the relieving load path within the clamped members, whereas the GLIF does not. From Figure 14, the SBLIFs are 0.231 and 0.186 for cases (a) and (b), respectively, much lower than the GLIF of 0.4699. The GLIF based on the thickness of the relieving load path $l_{2\text{–}4} = 0.5$ in. and that of the clamped members $L = 1.064$ in. gives $n_G = 0.4699$ for both cases (a) and (b), demonstrating its invariance with respect to the relative positions of relieving and compressed regions within the clamped members.

From Figure 15, the SBLIFs are 0.4841 and 0.3426 for cases (a) and (b), respectively, the former being slightly larger and the latter being less than the GLIF of 0.4699. The GLIF based on thickness of relieving load path $l_{2\text{–}4} = 0.5$ in. and that of the clamped member's $L = 1.064$ in., gives $n_G = 0.4699$ for both cases (a) and (b), demonstrating its invariance with respect to relative positions of relieving and compressed regions within the clamped members. It should be noted that the sleeve representation of K_c for the PBJ of Figure 15 would have produced a SBLIF equivalent to that of the GLIF, had the modulus of elasticity of all the clamped members been the same. For this study it can be concluded that the use of the GLIF is more conservative for bolt mechanical load when compared with a SBLIF based on back-to-back frustra, whereas a conclusion on GLIF conservativism cannot be reported from this limited study when compared with a SBLIF based on a sleeve-compression-stiffness profile.

7.2 Clearance Hole and Clamped-Member Thickness

The data in Figure 16 illustrate the difference in magnitude between the GLIF and SBLIF for a PBJ with two flanges of equal thickness without washers. The SBLIF for the PBJ shown there was calculated using a $\theta = 30°$ back-to-back frusta approximation of K_c, for six through-hole diameters ranging from 0.19 in., up to 0.75 in., for each of combined clamped-member thicknesses ranging from 0.25 to 2.0 in. This was done for three different loading-plane locations, each symmetric about the flange-to-flange faying surface. The selection of these loading-plane locations resulted in GLIFs of 0.25, 0.50, and 0.75. For this joint configuration the SBLIF does not change if the modulus of elasticity for each clamped member, E_1 and E_2, are different.

Since the GLIF is equivalent to the SBLIF for a cylindrical compression zone for this particular joint, Figure 16 can also be interpreted as illustrating the difference in the SBLIF when modeling the compression zone as a cylinder as opposed to back-to-back frusta.

Stiffness element, i	Modulus of elasticity, E_i, psi	Case (a) Minor diameter, D_i, in.	Case (a) Thickness, t_i, in.	Case (a) Flexibility,[a] $1/K_i$, in./lb	Case (b) Minor diameter, D_i, in.	Case (b) Thickness, t_i, in.	Case (b) Flexibility,[a] $1/K_i$, in./lb
1	2.90×10^{7}	0.375000	0.032	1.53260×10^{-8}	0.375000	0.032	1.53260×10^{-8}
2	2.90×10^{7}	0.411950	0.25	5.02977×10^{-8}	0.411950	0.1	2.87036×10^{-8}
3	2.90×10^{7}	0.700626	0.25	1.74817×10^{-8}	0.527420	0.4	3.90759×10^{-8}
6	2.90×10^{7}	0.375000	0.032	1.53260×10^{-8}	0.375000	0.032	1.53260×10^{-8}
5	1.00×10^{7}	0.411950	0.25	1.45863×10^{-7}	0.411950	0.4	1.80677×10^{-7}
4	1.00×10^{7}	0.700626	0.25	5.06971×10^{-8}	0.873831	0.1	1.58830×10^{-8}
		$1/K_{2-4} = 1/K_3 + 1/K_4 = 6.81788\times10^{-8}$ in./lb $K_{2-4} = 1.46673\times10^{7}$ lb/in. $1/K^*_{1-2,4-5} = 1/K_1 + 1/K_2 + 1/K_5 + 1/K_6 = 2.26813\times10^{-7}$ in./lb $K^*_{1-2,4-5} = 4.40892\times10^{6}$ lb/in. $n = K^*_{1-2,4-5}/(K_{2-4} + K^*_{1-2,4-5}) = 0.231$			$1/K_{2-4} = 1/K_3 + 1/K_4 = 5.49589\times10^{-8}$ in./lb $K_{2-4} = 1.81954\times10^{7}$ lb/in. $1/K^*_{1-2,4-5} = 1/K_1 + 1/K_2 + 1/K_5 + 1/K_6 = 2.40033\times10^{-7}$ in./lb $K^*_{1-2,4-5} = 4.16610\times10^{6}$ lb/in. $n = K^*_{1-2,4-5}/(K_{2-4} + K^*_{1-2,4-5}) = 0.186$		

[a]Determined from Equation (F.25),

$$\frac{1}{K_i} = \frac{1}{\pi E_i D_t \tan(\theta)} \ln\left[\frac{\left(t_i \tan(\theta) + \frac{D_i - D_t}{2}\right)\left(\frac{D_i + D_t}{2}\right)}{\left(t_i \tan(\theta) + \frac{D_i + D_t}{2}\right)\left(\frac{D_i - D_t}{2}\right)}\right]$$

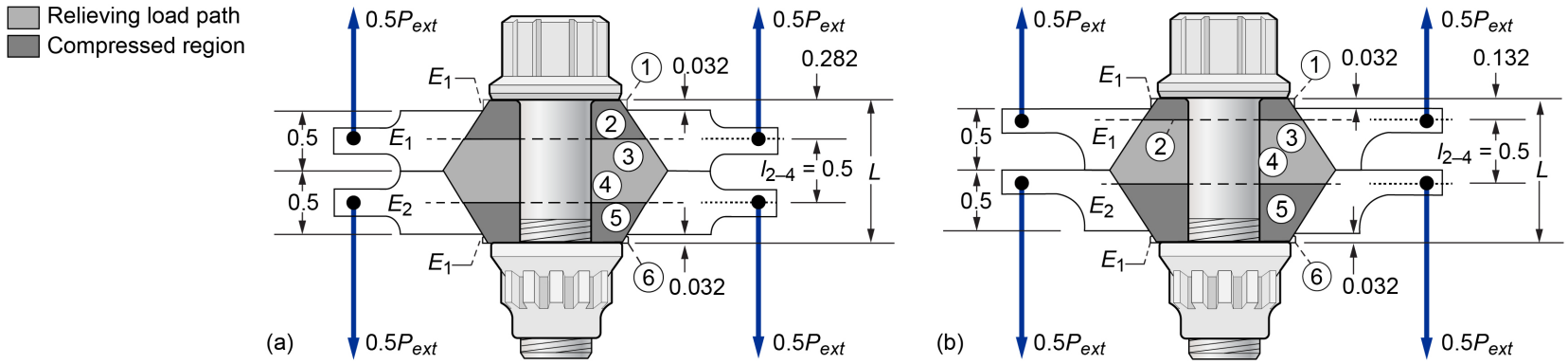

Figure 14.—Comparison of SBLIF and GLIF for PBJ, using back-to-back frusta compression zone with 30° half-apex angle, θ. Through-hole diameter is 0.25 in., bolt head and nut contact area diameter is 0.375 in., $E_1 = 29\times10^6$ psi, and $E_2 = 10\times10^6$ psi. (a) Relieving load path is centered within clamped members. (b) Relieving load path is offset closer to bolt head.

Stiffness element, i	Modulus of elasticity, E_i, psi	Case (a) Thickness, t_i, in.	Case (a) Flexibility,[a] $1/K_i$, in./lb	Case (b) Thickness, t_i, in.	Case (b) Flexibility $1/K_i$, in./lb
1	2.90×10^{7}	0.032	8.30126×10^{-9}	0.032	8.30126×10^{-9}
2	2.90×10^{7}	0.25	6.48536×10^{-8}	0.1	2.59414×10^{-8}
3	2.90×10^{7}	0.25	6.48536×10^{-8}	0.4	1.03766×10^{-7}
6	2.90×10^{7}	0.032	8.30126×10^{-9}	0.032	8.30126×10^{-9}
5	1.00×10^{7}	0.25	1.88075×10^{-7}	0.4	3.00921×10^{-7}
4	1.00×10^{7}	0.25	1.88075×10^{-7}	0.1	7.52301×10^{-8}
		$1/K_{2-4} = 1/K_3 + 1/K_4 = 2.52929\times10^{-7}$ in./lb $K_{2-4} = 3.95368\times10^{6}$ lb/in. $1/K^*_{1-2,4-5} = 1/K_1 + 1/K_2 + 1/K_5 + 1/K_6 = 2.69531\times10^{-7}$ in./lb $K^*_{1-2,4-5} = 3.71014\times10^{6}$ lb/in. $n = K^*_{1-2,4-5}/(K_{2-4} + K^*_{1-2,4-5}) = 0.4841$		$1/K_{2-4} = 1/K_3 + 1/K_4 = 1.78996\times10^{-7}$ in./lb $K_{2-4} = 5.58672\times10^{6}$ lb/in. $1/K^*_{1-2,4-5} = 1/K_1 + 1/K_2 + 1/K_5 + 1/K_6 = 3.43464\times10^{-7}$ in./lb $K^*_{1-2,4-5} = 2.91151\times10^{6}$ lb/in. $n = K^*_{1-2,4-5}/(K_{2-4} + K^*_{1-2,4-5}) = 0.3426$	

[a]Determined with equation from Ref. 11,

$$\frac{1}{K_i} = \frac{4t_i}{\pi E_i\left[\left(D_H + 0.1l_j\right)^2 - D_h^2\right]}$$

D_H = diameter of bolt head = 0.375 in., D_h = diameter of clearance hole = 0.25 in., and $l_j = L$ = thickness of clamped members = 1.064 in.

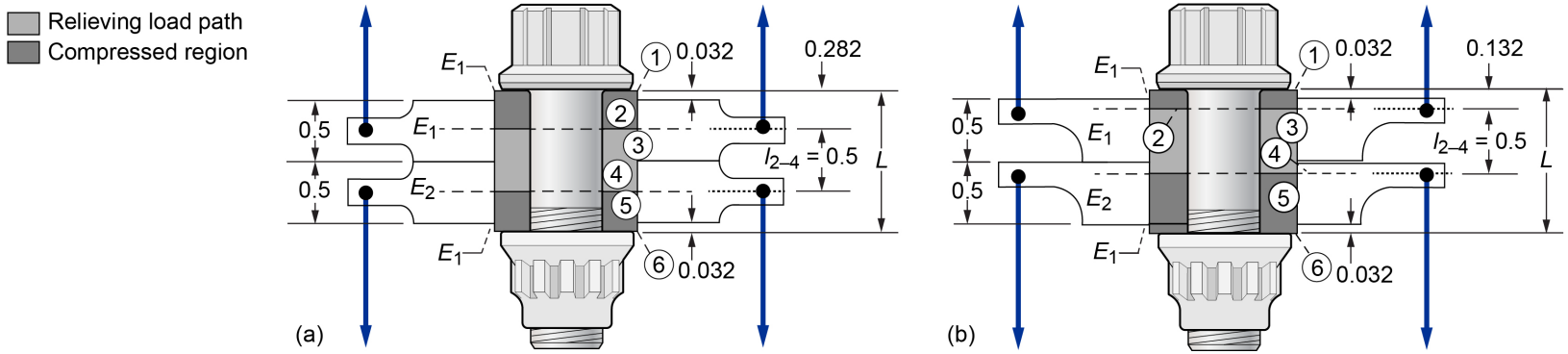

Figure 15.—Comparison of GLIF and SBLIF for PBJ, using cylindrical compression zone. Through-hole diameter is 0.25 in., bolt head and nut contact area diameter is 0.375 in., and moduli $E_1 = 29\times10^6$ psi, and $E_2 = 10\times10^6$ psi. (a) Relieving load path is centered within clamped members. (b) Relieving load path is offset closer to bolt head.

$n_G = l_{2–4}/L = 0.25$					
Bolt through-hole diameter, in.	L, in.				
	0.25	0.50	0.75	1.00	2.00
0.190	0.157	0.118	0.096	0.081	0.050
0.250	0.171	0.134	0.111	0.095	0.061
0.375	0.190	0.156	0.134	0.118	0.080
0.500	0.201	0.171	0.150	0.134	0.095
0.625	0.209	0.182	0.162	0.146	0.108
0.750	0.215	0.190	0.171	0.156	0.118

$n_G = l_{2–4}/L = 0.5$					
Bolt through-hole diameter, in.	L, in.				
	0.25	0.50	0.75	1.00	2.00
0.190	0.357	0.285	0.239	0.207	0.136
0.250	0.381	0.315	0.270	0.238	0.162
0.375	0.412	0.356	0.315	0.283	0.205
0.500	0.430	0.381	0.344	0.315	0.238
0.625	0.442	0.399	0.365	0.338	0.263
0.750	0.450	0.412	0.381	0.356	0.283

$n_G = l_{2–4}/L = 0.75$					
Bolt through-hole diameter, in.	L, in.				
	0.25	0.50	0.75	1.00	2.00
0.190	0.622	0.540	0.480	0.433	0.315
0.250	0.647	0.576	0.521	0.478	0.361
0.375	0.677	0.621	0.576	0.538	0.431
0.500	0.693	0.647	0.609	0.576	0.478
0.625	0.703	0.665	0.631	0.602	0.512
0.750	0.710	0.677	0.647	0.621	0.538

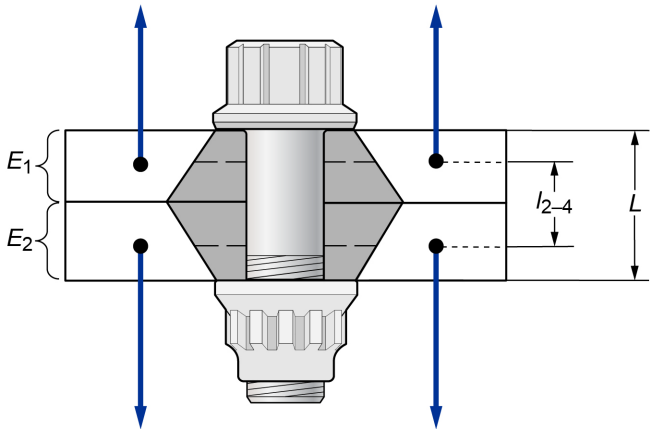

Figure 16.—Comparison of SBLIF and GLIF for PBJ with two flanges of equal thickness. Minor diameter of compression zone under bolt head and nut is assumed to be 1.5× bolt diameter.

For the cases evaluated in Figure 16, the GLIF is greater than the SBLIF, $n_G > n$, which means that opportunities may exist to use smaller diameter and/or lower strength bolts to save weight and possibly cost, if the SBLIF is used instead of the GLIF, or equivalently, the alternative form of the bolt tensile load (Equation (49)) is used to determine bolt load.

Detailed calculations of the SBLIF and GLIF for a PBJ with a countersunk fastener is presented in Appendix C. The SBLIF results in about a 39 percent lower external bolt tensile load than would be calculated using the GLIF.

7.3 Comparison With Finite Element Analysis

In Reference 2, section A.5, a hypothetical pure tension joint, as shown in Figure 17, was conceived and analyzed using FEA (see Appendix G for details not shown in Ref. 2) to determine an upper-bound estimate of the amount of external tensile load reacted by a fastener. This PBJ in pure tension joins two identical fittings separated by a sleeve. A secant-line load-deflection curve beginning from initial preload up to total joint separation has an average slope $(n\phi)_{FEA}$ of 0.25, meaning that on the average, 25 percent of the tension load is being reacted by the bolt. A comparison of the GLIF and SBLIF with that predicted by FEA is presented in Appendix H and shown in Table H.1, which is presented here for convenience.

FEA of a PBJ can yield the product $(n\phi)_{FEA}$, but not the finite-element-based LIF, n_{FEA}, directly. To determine n_{FEA}, the product $(n\phi)_{FEA}$ must be divided by the stiffness ratio ϕ. Since ϕ based on FEA was not a goal of the aforementioned analysis, it was determined analytically herein. Because ϕ is a function of the bolt and clamped-member stiffness, and since the latter is approximated as that of the compression zone using the stiffness of a cylinder and frustra, the stiffness ratio is a function of θ, the frustra half-apex angle, chosen using engineering judgment. This results in n_{FEA} being a function of θ. This is the reason that n_{FEA} has different values in Appendix H, Table H.1, where the half-apex angles $\theta = 30°$ and 21.8° were used, respectively, to attempt to bracket the comparison. In reality, n_{FEA} should be based on the stiffness characteristics of the joint, as determined solely by FEA.

TABLE H.1.—COMPARISON OF FINITE ELEMENT, GEOMETRIC, AND STIFFNESS-BASED LIF FOR PURE TENSION JOINT OF APPENDIX G WITH DIFFERENT HALF-APEX ANGLES[a]
[$n\phi = 0.25$.]

(a) $\theta = 30°$

LIF	Without bolt head and nut flexibility $\phi_c(\theta) = 0.325$	With bolt head and nut flexibility $\phi_c(\theta) = 0.309$
$n_{FEA}(\theta)$	0.77	0.81
n_G	0.9 (17%)	0.9 (11%)
$n(\theta)$	0.71 (–8%)	0.71 (–12%)

(b) $\theta = 21.8$

LIF	Without bolt head and nut flexibility $\phi_c(\theta) = 0.351$	With bolt head and nut flexibility $\phi_c(\theta) = 0.334$
$n_{FEA}(\theta)$	0.71	0.75
n_G	0.9 (27%)	0.9 (20%)
$n(\theta)$	0.71 (0 %)	0.71 (–5%)

[a]Percent difference (rounded) between the predicted and FEA LIF (Appendix G) is shown in parentheses.

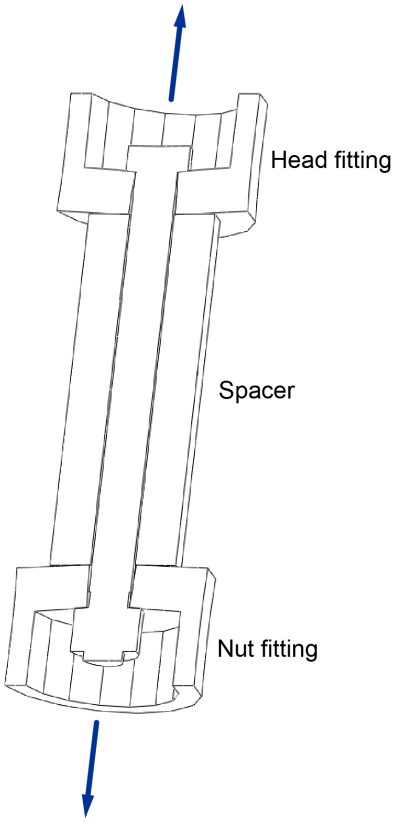

Figure 17.—Pure tension joint.

In like manner, the approximation of the bolt stiffness affects the calculation of ϕ, and hence n_{FEA}. To also bracket the effects due to bolt stiffness approximation, the bolt stiffness was determined assuming both a rigid and flexible bolt head and nut (Ref. 10).

As noted above, n_{FEA} is based on a combination of FEA and analytical approximations, whereas the GLIF and SBLIF are strictly analytical. A few observations can be made from Table H.1 for this pure tension joint example, where all comparisons are made against n_{FEA}.

- The GLIF is larger than n_{FEA} and the SBLIF.
- The SBLIF ranges from exact to 12 percent unconservative when compared with n_{FEA} for the two half-apex angles assumed, and with the inclusion or exclusion of bolt head and nut flexibilities in the determination of ϕ, and thus n_{FEA}. This emphasizes that the accuracy of the SBLIF is dependent upon the accuracy of the PBJ load-path approximations and can offer excellent results but not conservatism.

As can be seen from Table H.1(a) and noted in Appendix H, the SBLIF results in about a 21 percent lower external bolt tensile load than would be calculated using the GLIF.

7.4 Relative Conservatism Between SBLIF and GLIF

Having compared the GLIF n_G and SBLIF n for various specific examples, it seemed useful to consider a mathematical relationship between them. Setting n in the form of Equation (45) equal to n_G results in an equation for n_G in terms of the stiffnesses of the clamped-member tensile load path K_a and the relieving load path $K_{2\text{–}4}$:

$$\frac{K_a}{K_{2-4}} \overset{\text{set}}{=} n_G \tag{58}$$

Alternatively, setting n in the form of Equation (46) equal to n_G results in an equation for n_G in terms of the stiffnesses of the compressed region $K^*_{1-2,4-5}$ and relieving load-path $K_{2\text{–}4}$:

$$\frac{K^*_{1-2,4-5}}{K_{2-4} + K^*_{1-2,4-5}} \overset{\text{set}}{=} n_G \tag{59}$$

By manipulating Equation (59) the ratio on the left-hand side can be simplified to be more informative:

$$\frac{K^*_{1-2,4-5}}{K_{2-4}} \overset{\text{set}}{=} \left(\frac{n_G}{1 - n_G} \right) \tag{60}$$

Equations (58) and (60) are plotted in Figure 18(a) and (b), respectively, for $0.01 \le n_G \le 0.99$. Points on the curves indicate where the GLIF and SBLIF are equal. Because the GLIF is larger than the SBLIF to the left of the curves, the GLIF produces higher bolt and joint separation loads compared with those predicted using the SBLIF. To the right of the curves, the opposite is true.

For example, consider a GLIF of 0.5. Inserting $n_G = 0.5$ into Equation (58) or (60) indicates that the ratio of stiffnesses (SBLIF) on the left-hand side of Equations (58) and (60) must equal 0.5 and 1, respectively, for the SBLIF and GLIF to be equal. From Equation (58), if the relieving load-path stiffness $K_{2\text{–}4}$ is more than twice that of the tensile load-path stiffness K_a, the ratio of stiffnesses—and consequently the SBLIF—will be less than the GLIF of 0.5. Likewise from Equation (60), if $K_{2\text{–}4}$ is larger than the compressed load-path stiffness $K^*_{1-2,4-5}$, the ratio of stiffnesses—and consequently the SBLIF—will be less than the GLIF of 0.5. In both cases, the GLIF of 0.5 would be more conservative than the SBLIF with respect to bolt rupture. At the same time, the GLIF would be less conservative than the SBLIF with respect to joint separation, predicting a higher separation load.

Equations (58) and (60) and their graphs shown in Figure 18 apply to all PBJs (with two loading planes) since there were no restrictions placed on the shape of the clamped-member's tension load path, or its modulus of elasticity distribution.

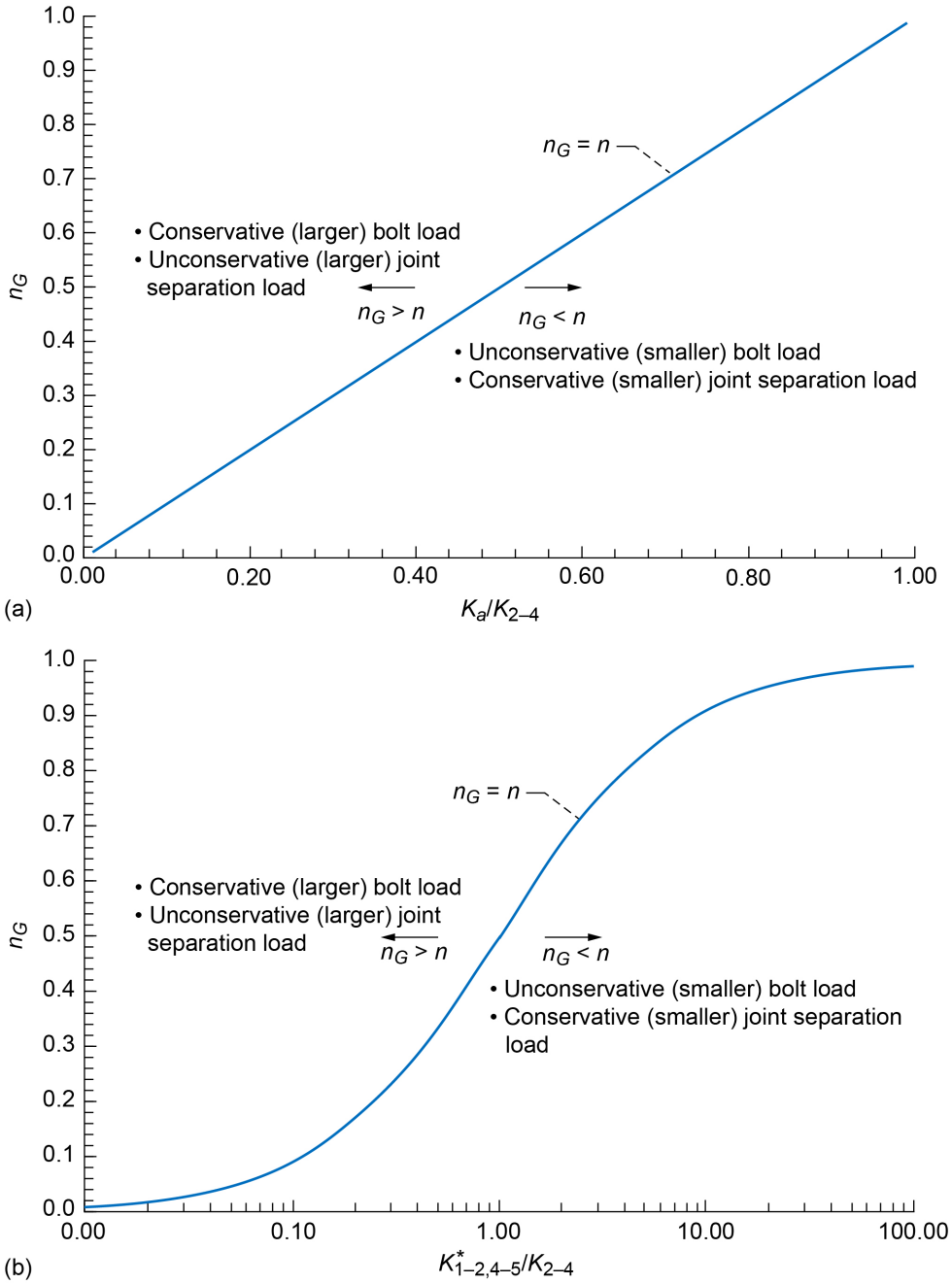

Figure 18.—Comparison of GLIF and SBLIF for PBJs. (a) In terms of stiffnesses of clamped-member tensile load path and relieving load path. (b) In terms of stiffnesses of compressed region and relieving load path.

7.5 Comparison With Experiment

Boenick (Ref. 3) used a clever experimental setup to investigate the loads reacted by a fastener of 7.8 mm diameter that clamped two cylindrical flange members of 39 mm thickness, each having external threads. The fastener longitudinal axis was collinear with the flange members' axes. The concentric external load was applied to the cylindrical flange members at certain distances above their faying surface by a sleeve that had an internal thread engagement length of 6 mm at the sleeve opening, engaging the external thread of the cylindrical flanges (see Figure 19). The sleeves were connected to a tensile testing machine for load application. Four cylindrical flange members with diameters of 80, 60, 40, and 20 mm were investigated. The fastener through-hole diameter was 10 mm. The fastener had a boss of 10 mm diameter coincident with the faying surface of the flanges to keep them concentric. The fastener tensile stiffness was measured to be 11.82 kp/μm (115.9 N/μm). The compressive stiffness (compression zone stiffness) of the cylindrical flanges were measured and presented graphically in Figure 40 of Reference 3 and were digitized using the software of Reference 12 to be 117 kp/μm (1,147 N/μm) for the 80-mm-diameter flanges, 121 kp/μm (1,187 N/μm) for the 60-mm-diameter flanges, 111 kp/μm (1,089 N/μm) for the 40-mm-diameter flanges, and 47 kp/μm (461 N/μm) for the 20-mm-diameter flanges. It should be noted that kp is the kilopond (see Ref. 13), which is equal to 9.80665 N.

Concentric external tensile loads were applied to the preloaded cylindrical flanges at discrete locations from their faying surface. Four preload levels of 30, 50, 70, and 90 percent of bolt yield were employed as well. Fastener loads above preload were recorded as a function of externally applied tension load.

In Figure 53 of Reference 3, for each of the four different flange diameters, Boenick plotted the ratio of (bolt load above preload)/(applied tensile load) on the ordinate, which is equivalent to the product $n\phi$, versus the ratio of (distance between load application points)/(clamped-member thickness) on the abscissa, which is equivalent to the GLIF. Figure 53 was digitized using the software of Reference 12. By dividing the ordinate by the stiffness factor ϕ_c obtained from the previously mentioned measured bolt and joint compression zone stiffnesses,[3] the experimental LIFs n_{exp} were obtained,

$$n_{exp} = \frac{n\phi}{\phi_c} > n \tag{61}$$

as shown in Figure 20, providing a comparison to the GLIF and the SBLIF. If ϕ_c in Equation (61) were equal to ϕ, then it would be that $n_{exp} = n$. However, since $\phi_c < \phi$ (as shown in Appendix B), $n_{exp} > n$, and therefore, the n_{exp} form an upper bound.

Again, ϕ_c is based on the experimental compressive stiffness of the preloaded cylindrical flanges K_c and not their stiffness under tensile load K_a. Using K_c in lieu of K_a is not physically correct but is acknowledged as an approximation (see Appendix B).

[3]Example calculation of joint stiffness for 80-mm flanges (stiffness values are in kp/μm):

$$\phi_c = \frac{K_b}{K_b + K_c} = \frac{11.82\,(\text{kp/μm})}{11.82\,(\text{kp/μm}) + 117\,(\text{kp/μm})} = 0.0918$$

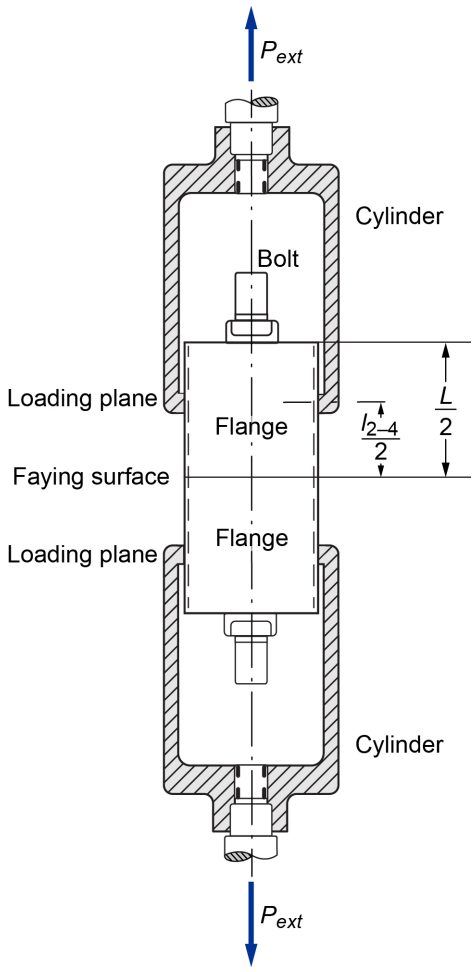

Figure 19.—Experimental setup of Reference 3 used to investigate effects of varying locations of load introduction on bolt load.

The GLIF ends up being represented as a 45° line on the plots because the calculated GLIFs represented on the ordinate are the same as the nondimensional load input locations plotted on the abscissa. The SBLIFs were calculated using a combination of frustra and cylindrical stiffnesses with frusta half-apex angles of 30°. The calculation of the SBLIFs for the comparison are presented in Appendix I.

It can be seen from Figure 20 that the GLIF is larger than the experimental LIF for nearly all locations of the loading planes and preload levels for flange diameters of 80, 60, and 40 mm. For these cases, the SBLIF more accurately predicts the experimental LIF than the GLIF, but the SBLIF can be unconservative. Both the GLIF and SBLIF track the experimental LIF well across the loading-plane spectra for the flanges of a 20-mm diameter, as shown in part (d) of Figure 20. In this case, the relatively close approximation of the GLIF to the experimental LIF is to be expected, since the 20-mm-diameter flanges limit the flange stiffness to that of a sleeve, which is the implicit assumption behind the GLIF as indicated in Equation (57) and the text immediately following it.

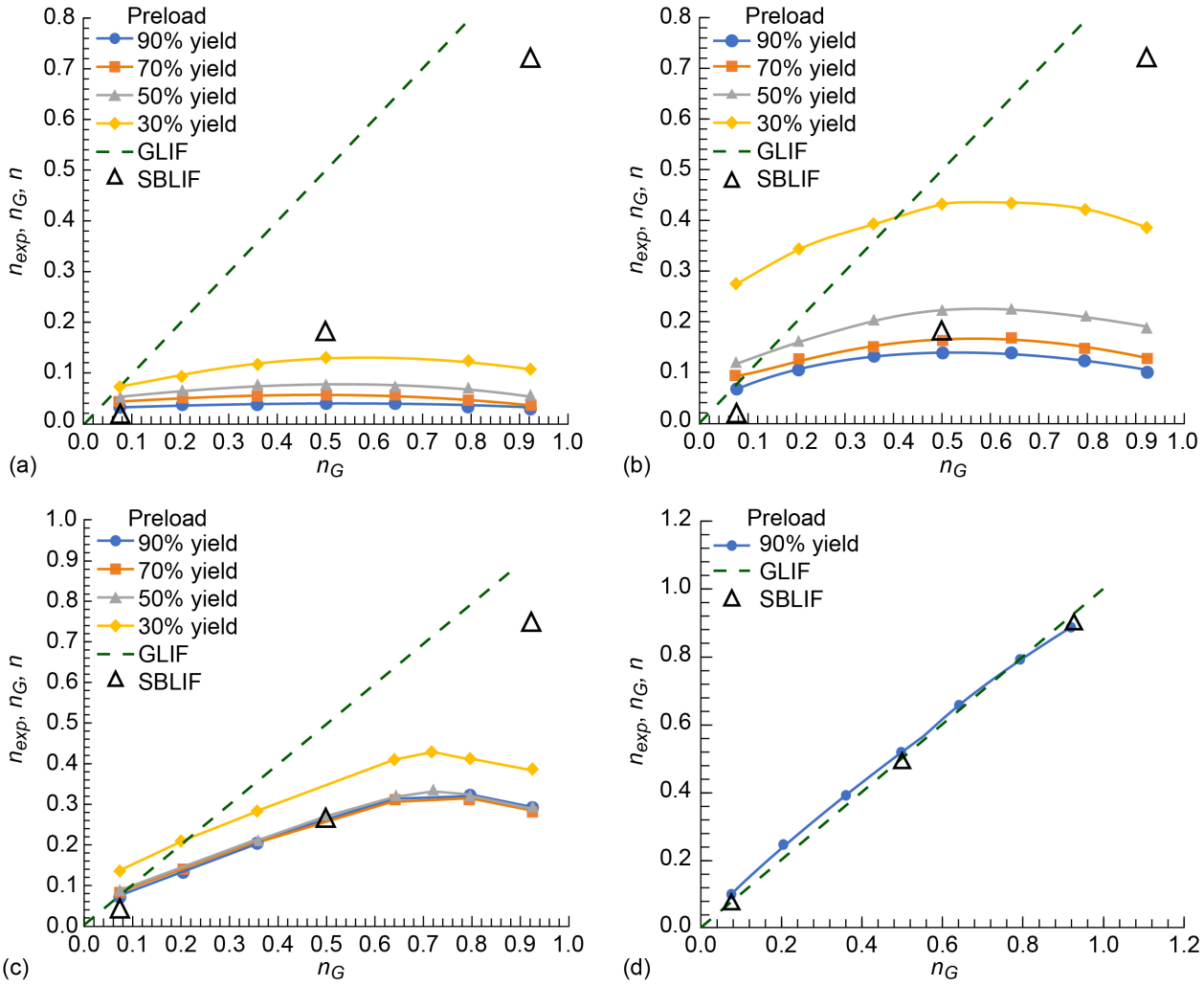

Figure 20.—Comparison of GLIF and SBLIF with PBJ experiment for flanges with different diameters. Assumed $K_c = K_a$. (a) 80 mm. (b) 60 mm. (c) 40 mm. (d) 20 mm.

8.0 Effect of SBLIF on Graphical Aids

The SBLIF permeates nearly all aspects of PBJ analyses including the graphical aids sometime used by analysts, such as the joint diagram shown in Figure 21 and the various $n\phi$ diagrams as shown in Figure 22 to Figure 25. The following sections will discuss the role of the LIF in each:

8.1 Joint Diagram

Quite often in the open literature, a bolted-joint diagram is used to explain the effects of the LIF on the bolted joint. The joint diagram is a plot of the load-deflection trajectories associated with the various load paths within the PBJ and is developed in Appendix J.

Consider the joint diagram of Figure 21. Shown are the load-deflection trajectories for the bolt, preload, clamping, and relieving load paths. The load-deflection trajectories of the bolt and the preload load path are invariant with respect to the SBLIF because it only comes into play after preload.

During the preload phase, the load-deflection trajectories of the bolt and preload load paths converge at the preload level $P_0 + P_{th}$.

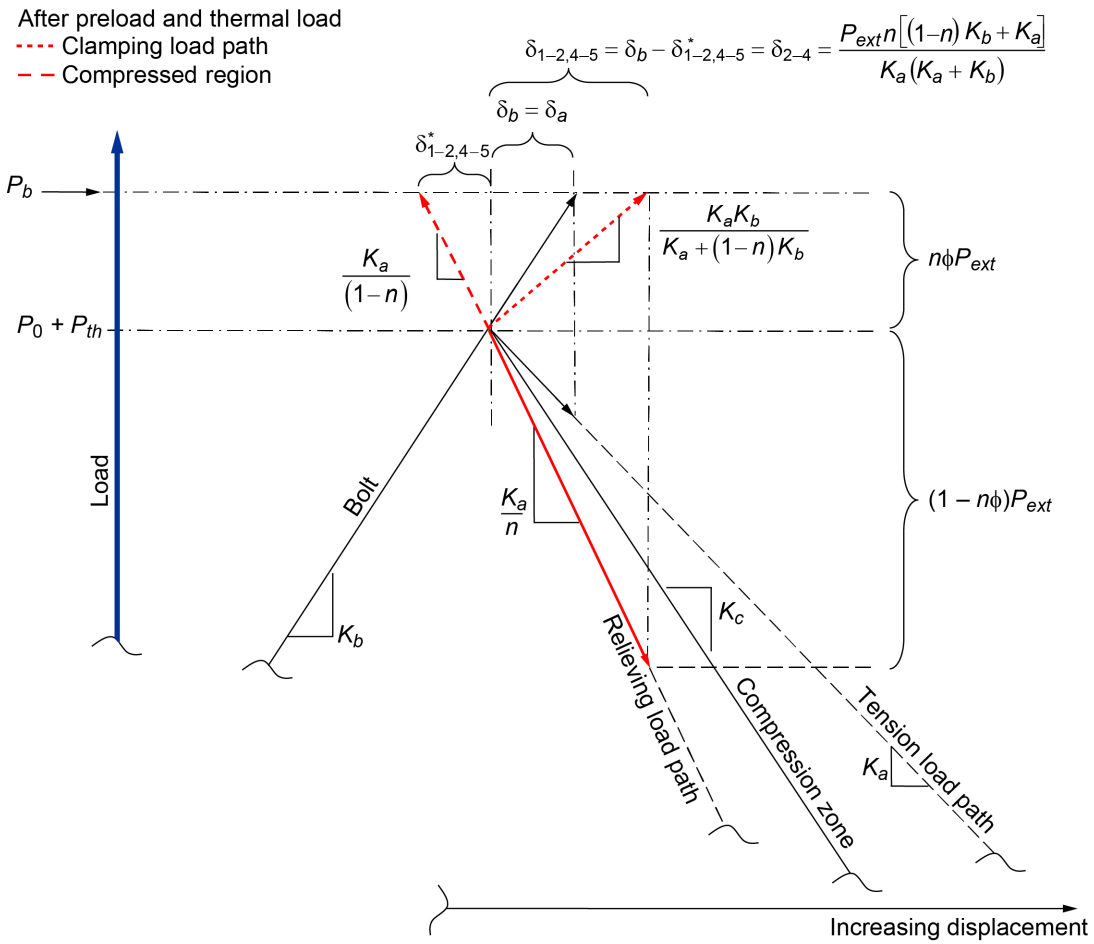

Figure 21.—PBJ joint diagram, including relationship between load paths and SBLIF, where δ_a is contraction or expansion of clamped member and δ_b is displacement of bolt.

The clamping and relieving load paths are explicitly active during joint tensile loading after the preload phase, and thus their load-deflection trajectories are shown to originate from the point of preload and thermal load $P_0 + P_{th}$. The slopes of the clamping and relieving load-path trajectories vary with the magnitude of the SBLIF. As the external load is increased, the clamping load increases along its load-deflection trajectory. At the same time, the relieving load continues to decrease along its trajectory towards the point of zero load. At the point the relieving load-path trajectory reaches zero load, the faying surfaces of the relieving load path have gapped.

As can be seen from Figure 21, when the SBLIF equals 1, the clamping load path is the same as the bolt load-deflection trajectory, and the relieving load path is the same as the tensile load-deflection trajectory of the joint.

The amount of external load being reacted by the clamping load path (and thus the bolt), which is $n\phi P_{ext}$, and the relieving load path, which is $(1 - n\phi)P_{ext}$, are the vertical distances from the end of their current trajectories to the point of preload plus thermal load $P_0 + P_{th}$ as shown in Figure 21. Their sum equals the external load P_{ext}, and when this external load equals the bolt load P_b, complete separation of the relieving load-path faying surfaces (joint separation) has occurred. Prior to joint separation, the displacement of the clamping and relieving load-path trajectories, $\delta_{1-2,4-5}$ and δ_{2-4}, respectively, are equal as shown in Figure 21.

8.2 $n\phi$ Diagram

The bolt tensile load Equation (36) is of the form of an equation for a line; it is slightly rearranged and repeated here for convenience:

$$P_b = (P_0 + P_{th}) + n\phi P_{ext} \tag{62}$$

where the ordinate intercept is the sum of the preload and thermal load, and the slope is the product of the SBLIF and the stiffness factor $n\phi$. The bolt tension load P_b may be plotted on the ordinate, and the external tension load P_{ext}, plotted on the abscissa. Changes in the slope $n\phi$ of the bolt tensile load equation because of changes in PBJ stiffness can be observed as well as the resulting intercept of the bolt-load trajectory with the separation curve and allowable ultimate bolt load, indicating whether the bolt ruptures prior to or after joint separation, which is explained next. Generic idealized examples of these plots are shown in Figure 22 to Figure 25. Figure 22 represents the case where the PBJ has separated before the bolt ruptures. This is indicated by the intersection of the bolt-load trajectory and the separation line occurring below the ultimate allowable bolt load.

The bolt-load trajectory starts with a preload and thermal load. As the external tension load is increased, the bolt-load trajectory is traversed until it reaches the separation line of slope equal to 1. At this point, the external tension load is solely reacted by the bolt, because the faying surfaces of the relieving load path have separated, no longer helping to reduce the bolt load. As the external tension load is increased further, the bolt-load trajectory proceeds up the separation curve until the ultimate allowable bolt load is reached, indicating bolt failure. The preload does not contribute at the time or point of bolt failure because it was previously lost from joint separation. It is implicitly assumed that in addition to the bolt, no other joint members have failed prior to reaching bolt ultimate allowable load.

Figure 23 shows the case where under maximum preload the bolt fails before the PBJ separates. This is illustrated by the bolt-load trajectory intercepting the ultimate allowable bolt load prior to the separation curve. Here, the preload does contribute at the time or point of bolt failure.

The most accurate way to determine the bolt load, aside from testing, is by the use of FEA. FEA is especially useful for incorporating linear or nonlinear geometric effects such as gapping and prying action in addition to linear or nonlinear material properties. Even though FEA permits the analyst to directly determine the stress state of the bolt and all joint members, it can give rise to debate about localized high stresses caused by finite element modeling artifacts. To avoid this, it can be more straight forward to extract the product $n\phi$ from the FEA to determine the bolt tensile load using Equation (36) and subsequently calculate the bolt margins of safety.

Although it is beyond the scope of this report to provide detailed FEA modeling guidance (model fidelity, mesh density, choice of elements, boundary conditions, and material properties), the FEA methodology to determine $n\phi$ consists of the following general steps:

1. Explicitly model the clamped members, bolt(s), nut(s), and washer(s) to the appropriate level of detail.
2. Use the appropriate linear or nonlinear material properties.
3. Apply a preload to the bolt(s). To obtain preload, contact between the members must be incorporated as appropriate.
4. For the current preload, apply a range of external loads to the joint.
5. Plot the tensile load reacted by the bolt(s) versus the tension component of the external load(s) as shown in Figure 24. The tensile load reacted by the bolts is the total bolt load minus the preload.
6. Calculate $n\phi$ for each bolt (i.e., the slope(s) of the curve(s) in step 5), and plot it versus the tension component of external load as shown in Figure 25.
7. Go to step 3 and repeat for another preload level until the range of preloads are adequately covered.

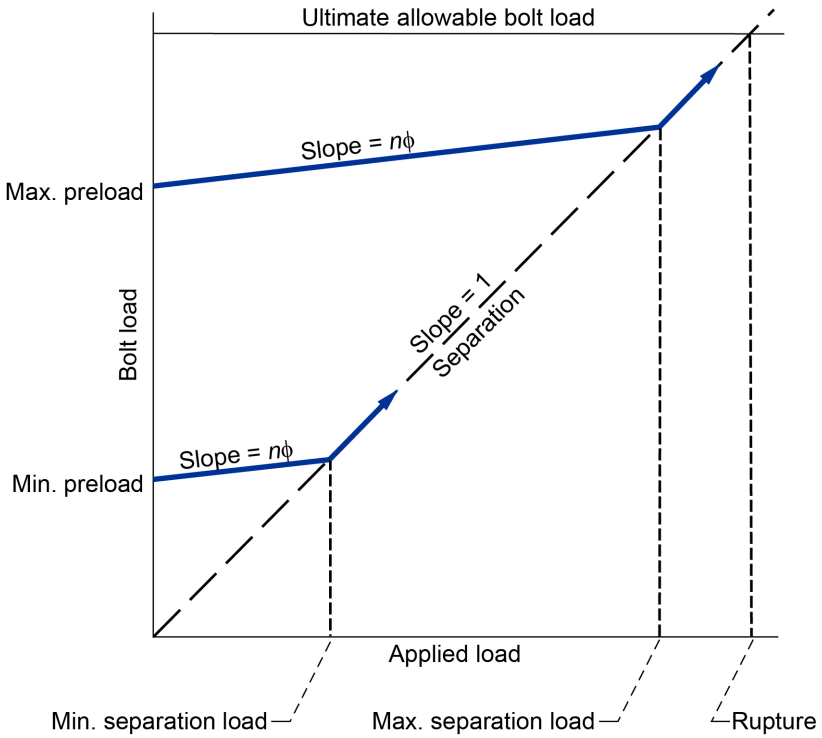

Figure 22.—Bolt tension load versus applied tension load for PBJ when separation occurs before rupture (linear theory).

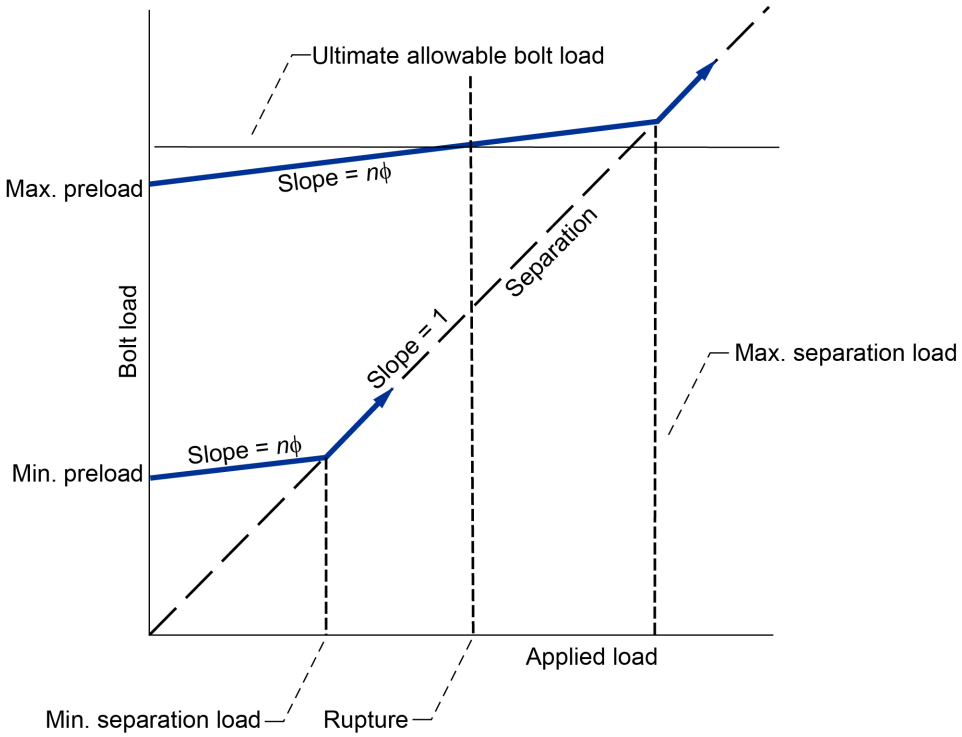

Figure 23.—Bolt tension load versus applied tension load for PBJ when bolt ruptures before joint separation under maximum preload (linear theory).

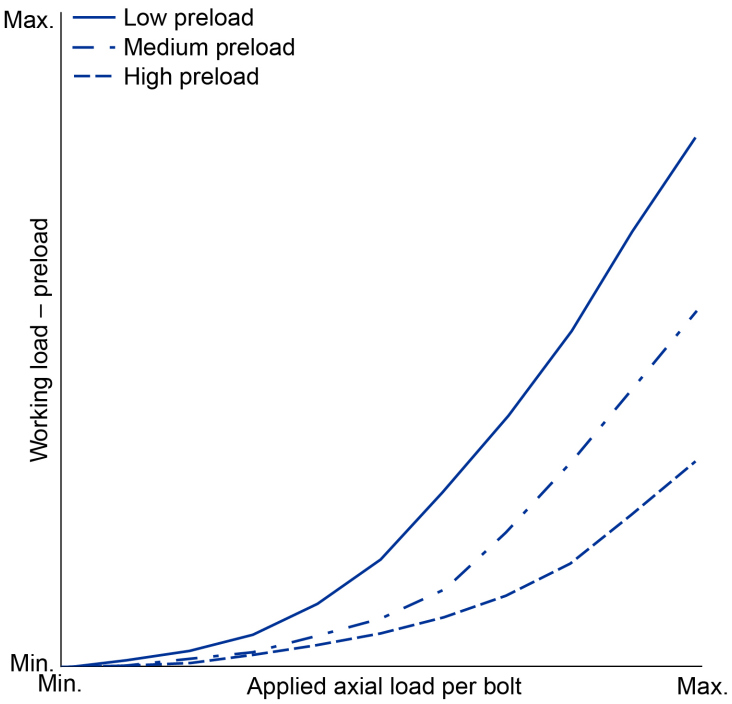

Figure 24.—Bolt tension load above preload versus applied tension load for PBJ, obtained from FEA. Based on analysis performed by Gary Drlik (HX5).

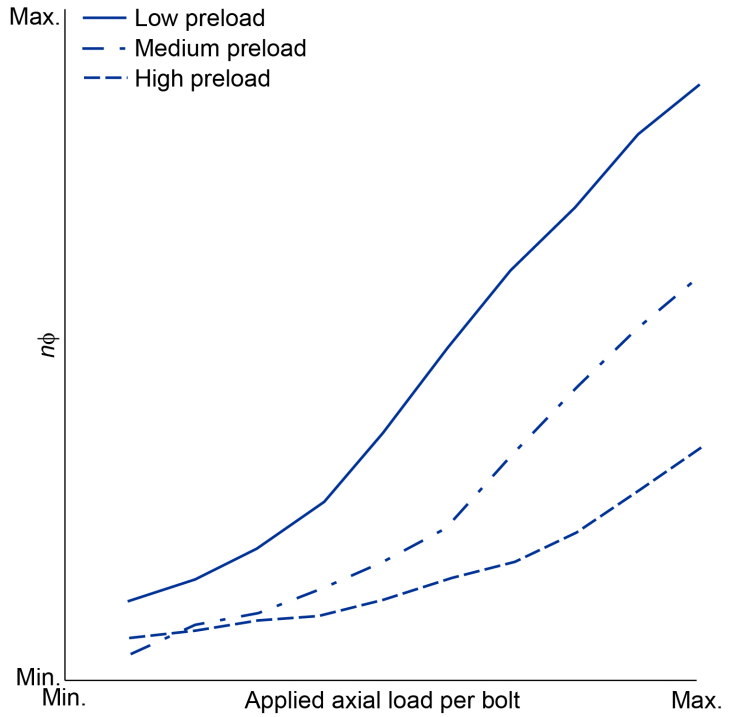

Figure 25.—$n\phi$ versus applied tension load for PBJ, obtained as slope of curves in Figure 24. Based on analysis performed by Gary Drlik (HX5).

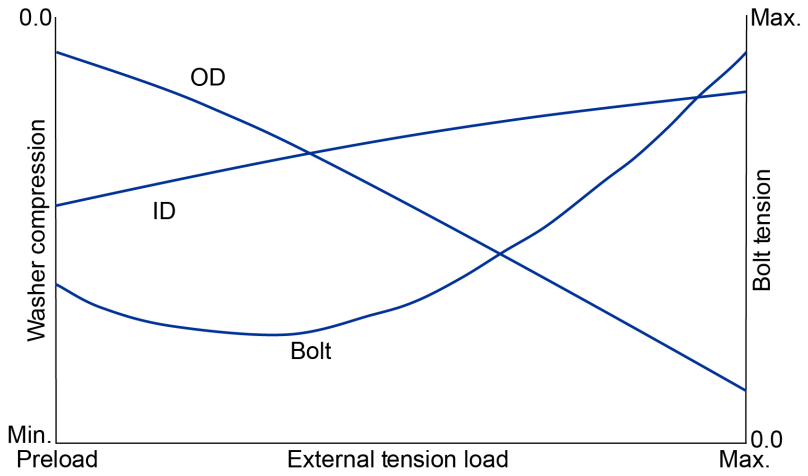

Figure 26.—Initial unloading of bolt preload observed computationally in some cases, due to geometric effects. Courtesy James Smith (Ref. 14).

In some situations, the FEA results for PBJs have indicated an initial reduction in the bolt preload upon the initiation of the external tensile load. As the external tension load component is further increased, this initial unloading is reversed, and the bolt experiences increased tension loading. This would be observed by an initial negative slope and dip in the bolt-load trajectory. One scenario causing this initial decrease in preload was explained by James Smith (Ref. 14) as follows: Initially, when the PBJ is solely under preload, there is higher compression on the inside diameter (ID) of the washer than on the outside diameter (OD), due to the flexibility of the bolt head. As the PBJ is loaded above preload in tension, the prying action puts more load on the OD of the washer, relieving its ID. By extracting the bolt tensile and washer compressive forces, it can be observed from Figure 26 that the compressive-force trajectory of the washer ID crosses over the compressive-force trajectory of the OD at the inflection point in the bolt-tensile-load trajectory. This inflection point of the bolt-tensile-load trajectory signifies the beginning of the bolt tensile load after preload.

9.0 Conclusions

The load introduction mechanism within a preloaded bolted joint (PBJ) consists of the load paths by which an external load enters and travels through its members. It was previously shown that this load introduction mechanism is naturally accounted for in the derivation of the bolt tensile load equation, and may be represented as an inherent factor, denoted as the stiffness-based load introduction factor (SBLIF).

The spring stiffness model and consequently the SBLIF provide unique insights into the behavior of a PBJ. Expanding upon previous work, it was shown that the SBLIF, joint stiffness factor, and the thermal load are all functions of the stiffness of the clamped-member tension load path, or alternatively, the stiffnesses of the relieving load path and clamped region within a PBJ. Therefore, the SBLIF, stiffness factor, and thermal load should not be treated as independent variables.

Mathematical expressions for the SBLIF in terms of the stiffness of the clamped-member tension load path, relieving load path, and compressed region of a PBJ allow for a varying stiffness distribution through the clamped-member thickness. As such, the SBLIF is better suited to represent the load introduction mechanism as opposed to the traditional geometric load introduction factor (GLIF), which is a simple thickness ratio, theoretically restricted to constant-stiffness distributions through the thickness of the clamped members. The GLIF is further limited because it does not account for the relative position of

the relieving load path within the PBJ, whereas the SBLIF is not likewise restricted. Mathematical relationships between the SBLIF and the GLIF were developed.

Comparisons between the SBLIF, GLIF, LIF from experiment, and LIF from finite element analysis (FEA) were presented. With the LIF results from experiment and FEA as a benchmark, the SBLIF determined by traditional load-path stiffness approximations was shown to be capable of greater accuracy than the GLIF. The accuracy of the SBLIF is only limited by the degree to which the load-path stiffnesses can be approximated. The GLIF generally attributes more of the externally applied tensile load to the bolt than does the SBLIF, potentially resulting in heavier and/or more costly bolted joints. Depending upon the stiffness approximations used, the SBLIF could underpredict the mechanical tensile load and thus be unconservative. To mitigate this possibility, an average or some combination of the SBLIF and GLIF values may be considered as the LIF.

Step-by-step examples demonstrating the calculation of the SBLIF using traditional stiffness approximations were presented. To provide a clearer understanding of the relationship between the SBLIF and joint diagrams, the load-displacement relationships of the load paths in a PBJ, were developed. Formulas for the key coordinates of the joint diagram in terms of the SBLIF, with or without a thermal load, were provided and are useful for programming.

The compression zone stiffness (i.e., the stiffness of the preload load path) has historically been used in lieu of the clamped-member's tensile load-path stiffness to determine bolt tensile load. This historically inconsistent practice is likely due to the tractability of calculating the compression zone stiffness as opposed to the clamped-members' tensile load-path stiffness. It has been shown that this practice amplifies the bolt thermal load: a positive thermal load will become more positive, and a negative thermal load will become more negative. An inequality has been provided to evaluate the effect of this practice on the predicted bolt load.

The following additional specific conclusions of this work have been determined:

1. The bolt mechanical tensile load can be reduced by increasing the stiffness of the relieving load path $K_{2–4}$, decreasing the stiffness of the compressed region $K^{*}_{1–2,4–5}$, or doing both simultaneously.
2. Reducing $K^{*}_{1–2,4–5}$ will decrease both the bolt mechanical and thermal loads, reducing the bolt load towards the preload level.
3. Reducing $K_{2–4}$ will increase the bolt mechanical tensile load and decrease the bolt thermal load, driving the bolt load towards the sum of the preload and external load.

Appendix A.—Nomenclature

A.1 Symbols

A	cross-sectional area (Appendix F)
A, B, C, D	stiffness coefficients, multipliers of K_a
D_h	bolt head diameter (Figure C.1)
D_i	minor diameter of frustra stiffness element i (Figure C.3)
D_L	diameter of lower end of compression zone (Figure D.1)
D_{max}	maximum diameter of compression zone (Figure D.1)
D_t	clearance hole diameter (Figure C.1, Figure C.3, and Figure F.3)
D_U	diameter of upper end of compression zone (Figure D.1)
E	modulus of elasticity
e	displacement
F_c	force in clamping load path including preload and thermal load
F_r	force in relieving load path including preload and thermal load
F_{ty}	tensile yield stress
f_c	force in clamping load path excluding preload and thermal load
i	summation index; index of clamped member, stiffness element, area, or modulus of elasticity
$K_{1–2,4–5}$	stiffness of clamping load path counterclockwise from points 2 to 4 (i.e., 2–1–5–4) in Figure 9
$K^*_{1–2,4–5}$	stiffness of compressed region
$K_{2–4}$	stiffness of relieving load path
K_a	stiffness of clamped members (including washer(s)) under external load; stiffness of clamped-members' tension load path
K_b	stiffness of bolt
K_c	stiffness of compression zone; usually used as an approximation to K_a
K_{eff}	combined stiffness of clamping and relieving load paths reacting to external tensile loading, $= K_{2–4} + K_{1–2,4–5}$
$K_{flanges}$	stiffness of load path along flanges or structure of bolted joint
K_i	stiffness of an individual clamped member or stiffness element. Index i runs from 1 to m for clamped members comprising the compression zone, 1 to M for stiffness elements comprising the compressed region, 1 to S for members comprising the relieving load path, and 1 to N for stiffness elements comprising the relieving load path.
L	thickness of clamped members (Figure 14)
L_b	effective length of bolt; length used to determine stiffness of bolt (Figure E.2)
L_c	thickness of compression zone (Figure C.2)
L_h	countersunk bolt-head depth (Figure C.1)
L_i	thickness of an individual clamped member, where index i runs from 1 to m
L_{th}	unconstrained thermal displacement of clamped members
l_2	beginning coordinate of relieving load path (Figure 13)

$l_{2–4}$	thickness of relieving load path (Figure 14)
l_4	ending coordinate of the relieving load path (Figure 13)
M	maximum number of stiffness elements comprising the compressed region
m	maximum number of clamped members
N	maximum number of stiffness elements comprising the relieving load path
n	stiffness-based load introduction factor, SBLIF
n_{exp}	LIF determined indirectly from experiment
n_{FEA}	LIF determined indirectly from finite element analysis (Appendix H)
n_G	geometric load introduction factor, GLIF
P	load applied in x-direction
P_0	bolt preload
P_b	bolt tensile load
P_{ext}	external tensile load applied to PBJ
P_{sep}	external load at onset of complete joint separation
P_{th}	tensile load in bolt caused by a thermal load
$P_{tu–allow}$	allowable ultimate tensile load of bolt
P'_{tu}	external tensile load causing bolt rupture
Q	stiffness coefficient of compressed region, multiplier of K_a
R	stiffness coefficient of relieving load path, multiplier of K_a
Δr	difference in radius between ends of frustrum element (Figure C.3 and Figure F.3)
r_{in}	frustrum inner radius. (Figure F.3)
r_o	frustrum outer radius (Figure F.3)
S	number of members of whole and partial thickness, constituting the relieving load path
ΔT	change in temperature
t_i	thickness of stiffness element i (Figure C.3 and Figure F.3)
X_d	location of maximum diameter along bolt axis (Figure D.1)
x	coordinate along or parallel to bolt axis
α_a	effective thermal expansion coefficient of clamped members
α_b	thermal expansion coefficient of bolt
α_i	thermal expansion coefficient of individual clamped member, where index i runs from 1 to m (Figure E.1)
δ	displacement
δ_a	displacement of compression zone (Figure 21)
δ_b	displacement of bolt (Figure 21)
δ_{b_0}	displacement of bolt at preload
δ_{c_0}	displacement of compression zone at preload
$\delta_{b_{th}}$	displacement of bolt shank due to thermal load

δL_{th}	total displacement of clamped members due to temperature change
$\delta_{1-2,4-5}$	displacement of the clamping load path; see Figure 21 and Section A.3, “Definitions”
δ_{2-4}	displacement of relieving load path; see Figure 21 and Section A.3, “Definitions”
$\delta^{*}_{1-2,4-5}$	displacement of compressed region; see Figure 21 and Section A.3, “Definitions”
λ	arbitrary constant (Eq. (B.8))
ϕ	stiffness factor
ϕ_c	stiffness factor based on compression zone stiffness, K_c
σ_{ax}	axial stress
σ_{vm}	von Mises stress
θ	half-apex angle of frustum (Figure C.3)

A.2 Acronyms

FEA	finite element analysis
GLIF	geometric load introduction factor
ID	inside diameter
LIF	load introduction factor
OD	outside diameter
PBJ	preloaded bolted joint
SBLIF	stiffness-based load introduction factor

A.3 Definitions

bolt tension load path	One of two load paths through a PBJ reacting preload only. Load path consisting solely of the bolt. Depicted in terms of bolted-joint members in Figure 6 and in terms of spring stiffnesses in Figure 7.
clamping load path	One of two load paths reacting the (post-preload) external tension loads applied to a PBJ. Load path consisting of the bolt and compressed region. Depicted in terms of bolted-joint members in Figure 5 and in terms of spring stiffnesses in Figure 9 and Figure 10.
clamped member	Any component clamped between the bolt and an internally threaded component (nut, insert, or threaded member itself). Depending on the context, a clamped member of whole or partial thickness may be implied.
clamped-member tension load path	Load path through the clamped members created by the external tension load applied to the PBJ.
compressed region	Members, of whole or partial thickness, of the clamping load path, excluding the bolt, that are compressed in reaction to an external tensile load; see Figure 5

compression zone	One of two load paths reacting the preload applied to a PBJ: the load path comprising the compression zone. Consists of members clamped between the bolt head and the internally threaded component, possibly including a portion of the internally threaded component. Depicted in terms of bolted-joint members in Figure 6 and in terms of spring stiffnesses in Figure 7. Geometric envelope of the compression load path during the preload phase as shown in Figure 6.
faying surface	Contacting surfaces at the interface between members and components.
Hooke's Law	States that stress σ is proportional to strain ε; that is, $\sigma = E\varepsilon$, where E is the modulus of elasticity. In terms of dimensions, this is expressed as $\left(\frac{\text{lb}}{\text{in}^2}\right)=\left(\frac{\text{lb}}{\text{in}^2}\right)\left(\frac{\text{in.}}{\text{in.}}\right)$. Through dimensional analysis, multiplying both sides by the units of area in^2, Hooke's Law is transformed dimensionally into $\text{lb}=\left(\frac{\text{lb}}{\text{in.}}\right)\text{in.}$, which means that force F, is proportional to displacement δ and is written as $F = k\delta$, where k is a spring constant. This latter form of Hooke's Law is used in the current work.
internally threaded component	Component with internal threads such as a nut, insert, or clamped member; the internal threads engaging the external threads of the bolt.
joint	Assembled combination of a fastener, an internally threaded component (such as a nut, insert, or threaded member), and the region of all members clamped between them.
load path	Continuous path through the joint members beginning and ending where the external tension load enters and exits the joint, respectively. This path consists of the joint members that exhibit primary displacements in response to the external tension load.
loading planes	Discrete planes located where the external loads are idealized (by engineering judgment) to enter the clamped members; assumed to be perpendicular to the bolt shank.
member	Any component of a PBJ: the bolt, an internally threaded component (such as a nut, insert, or threaded member itself), and any member clamped between them. Depending upon the context, a member of whole or partial thickness may be implied.
region	Member or group of members, of whole and partial thickness, whose boundaries do not coincide with the boundaries of a load path.
relieving load path	One of two load paths reacting the (post-preload) external tension loads applied to a PBJ. The load path consists of members of whole or partial thickness located between the loading planes, which increase in thickness in reaction to an external

	tension load applied to the PBJ. This is depicted in terms of bolted-joint members in Figure 5 and in terms of spring stiffnesses in Figure 9 and Figure 10.
stiffness element	Element used to represent the stiffness of a whole or portion of a member.

Appendix B.—Using K_c in Place of K_a

The compression zone stiffness (i.e., the stiffness of the preload load-path) K_c of the preloaded bolted joint (PBJ) has historically been used in lieu of the clamped-member's tensile load-path stiffness K_a to determine bolt tensile load. This historically inconsistent practice is likely due to the tractability of calculating the compression zone stiffness as opposed to the clamped-members' tensile load-path stiffness. It has been shown that this practice amplifies the bolt thermal load: a positive thermal load will become more positive, and a negative thermal load will become more negative. An equality is presented that must be satisfied in order for the use of K_c to be conservative.

It is documented through finite element analysis (Refs. 4 and 11) that the load path in the PBJ solely under preload is confined to a volume between the bolt head and the internal threaded component (nut, insert, or internal threaded flange) known as the compression zone. The stiffness of this compression zone is denoted as K_c.

When external tensile loads are applied to the PBJ, the load is applied at some distance from this compression zone, and so the load path now consists of the compression zone in addition to some length of flange or structure between the compression zone and applied tensile load. Let the stiffness of this additional load path along the flanges or structure be denoted as $K_{flanges}$. The stiffnesses K_c and $K_{flanges}$ act in series to produce the tensile load-path stiffness of the clamped members and is denoted as K_a. This is expressed mathematically as follows:

$$\frac{1}{K_a} = \frac{1}{K_c} + \frac{1}{K_{flanges}} = \frac{K_{flanges} + K_c}{(K_c)(K_{flanges})} \tag{B.1}$$

Solving for K_c,

$$K_c = K_a\left(1 + \frac{K_c}{K_{flanges}}\right) \tag{B.2}$$

which shows that $K_c > K_a$ and consequently that for the stiffness factors, $\phi_c < \phi$ as shown:

$$\phi_c = \frac{K_b}{K_b + K_c} < \frac{K_b}{K_b + K_a} = \phi \tag{B.3}$$

Now consider the bolt tensile load Equation (37),

$$P_b = P_0 + n\phi P_{ext} + \phi K_a L\Delta T(\alpha_a - \alpha_b) \tag{37}$$

where P_b = bolt tensile load
P_0 = bolt preload
n = stiffness-based load introduction factor, SBLIF, based on load path tensile stiffnesses
ϕ = stiffness factor based on clamped-member tensile load-path stiffness K_a
P_{ext} = external load applied to PBJ
ϕ_c = stiffness factor based on compression zone stiffness K_c
K_a = clamped-member stiffness of tensile load path
K_c = stiffness of compression zone
L = thickness of clamped members

ΔT = change in temperature from time of joint preload equilibrium
α_a = effective thermal expansion coefficient of clamped members
α_b = thermal expansion coefficient of bolt

Writing Equation (37) in consistent terms, using K_a for the tensile stiffness under a tensile load,

$$P_b = P_0 + \frac{K_a}{(K_{2-4})_a}\left(\frac{K_b}{K_b + K_a}\right)P_{ext} + \left(\frac{K_b}{K_b + K_a}\right)K_a L_b \Delta T(\alpha_a - \alpha_b) \tag{B.4}$$

where K_b is the stiffness of the bolt, $(K_{2-4})_a$ is the stiffness of the relieving load path under the tensile load, and Equations (25) and (45) have been employed.

To investigate the result of using K_c instead of K_a to determine the bolt loading, we substitute K_c for K_a and for consistency substitute $(K_{2-4})_c$ for $(K_{2-4})_a$ in Equation (B.4), where $(K_{2-4})_c$ is the relieving load-path stiffness of the compression zone. This results in

$$P_b = P_0 + \frac{K_c}{(K_{2-4})_c}\left(\frac{K_b}{K_b + K_c}\right)P_{ext} + \left(\frac{K_b}{K_b + K_c}\right)K_c L_b \Delta T(\alpha_a - \alpha_b) \tag{B.5}$$

One way for the mechanical bolt load as determined from Equation (B.5) to be more conservative than that determined from Equation (B.4) is if

$$\frac{K_c}{(K_{2-4})_c}\left(\frac{K_b}{K_b + K_c}\right) > \frac{K_a}{(K_{2-4})_a}\left(\frac{K_b}{K_b + K_a}\right) \tag{B.6}$$

Conservatism, or lack thereof, may be evaluated from Equation (B.6).

One way for the thermal bolt load determined from Equation (B.5) to be amplified above that determined from Equation (B.4) is if

$$K_c\left(\frac{K_b}{K_b + K_c}\right) > K_a\left(\frac{K_b}{K_b + K_a}\right) \tag{B.7}$$

Writing K_c in terms of K_a,

$$K_c = \lambda K_a \tag{B.8}$$

where λ is an arbitrary constant. Substituting Equation (B.8) into Equation (B.7) gives

$$\lambda K_a\left(\frac{K_b}{K_b + \lambda K_a}\right) > K_a\left(\frac{K_b}{K_b + K_a}\right) \tag{B.9}$$

and then reducing yields

$$\frac{\lambda}{K_b + \lambda K_a} > \frac{1}{K_b + K_a} \tag{B.10}$$

Upon solving Equation (B.10) for λ,

$$\lambda > 1 \tag{B.11}$$

Therefore, λ must be greater than 1 for Equation (B.7) to be true, but this means from Equation (B.8) that K_c must be greater than K_a for Equation (B.7) to be true, which in this case means that the magnitude of the bolt thermal load predicted by Equation (B.5) is greater than that predicted by Equation (B.4). Therefore, the use of the compression zone stiffness will result in an amplified thermal load: a positive thermal load will become more positive, and a negative thermal load will become more negative.

Appendix C.—Calculating Stiffness-Based and Geometric Load Introduction Factors

This appendix provides an example of how to calculate the stiffness-based and geometric load introduction factors for a preloaded bolted joint (PBJ) consisting of a through-bolted countersunk fastener clamping three flanges. The joint reacts a tension load originating in the upper and lower flanges.

C.1 Stiffness-Based LIF

The stiffness of the clamped-member tension load-path K_a of Figure C.1 will be approximated as the stiffness of the compression-zone K_c using frusta. This compression zone, as shown in Figure C.2, consists of individual frustum elements (shown in Figure C.3) arranged in series. The geometry of each individual frustum element corresponds to an assumed half-apex angle and results from the pertinent PBJ features shown in Figure C.1.

The stiffness of a single frustum element K_i as shown in Figure C.3 is derived in Appendix F and is presented here for convenience:

$$K_i = \frac{\pi E_i D_t \tan(\theta)}{\ln\left\{\frac{[2t_i \tan(\theta) + D_i - D_t](D_i + D_t)}{[2t_i \tan(\theta) + D_i + D_t](D_i - D_t)}\right\}} \tag{F.27}$$

where E_i is the modulus of elasticity of the frustum element i, D_i is the minor diameter corresponding to the smaller end of frustum element i, D_t is the through-hole diameter, t_i is the frustum thickness, and θ is the frustum half-apex angle.

For this particular joint configuration, the individual frustum elements are arranged as shown in Figure C.2. Note that the back-to-back frusta are not symmetric about a midplane perpendicular to the bolt axis because the bolt head and nut diameters are different.

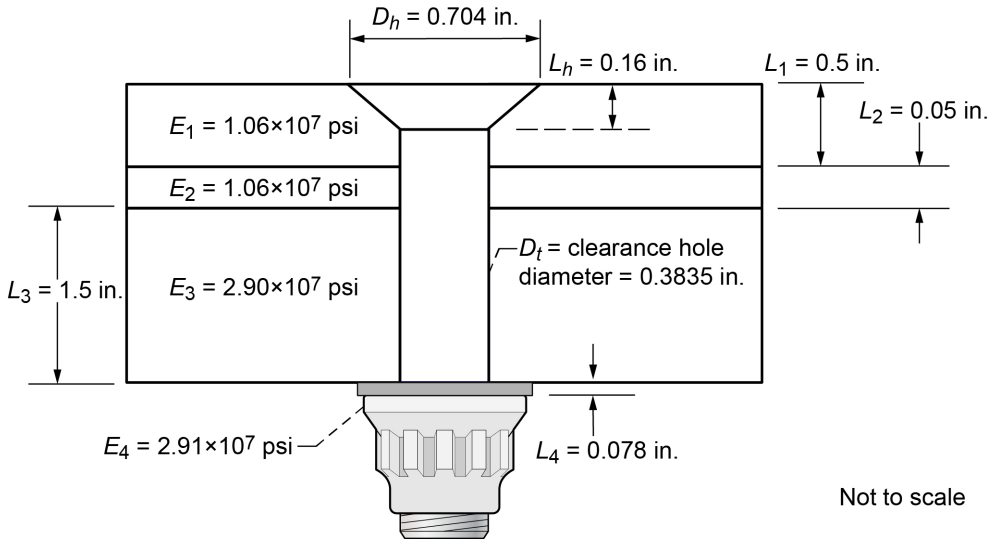

Figure C.1.—PBJ detail.

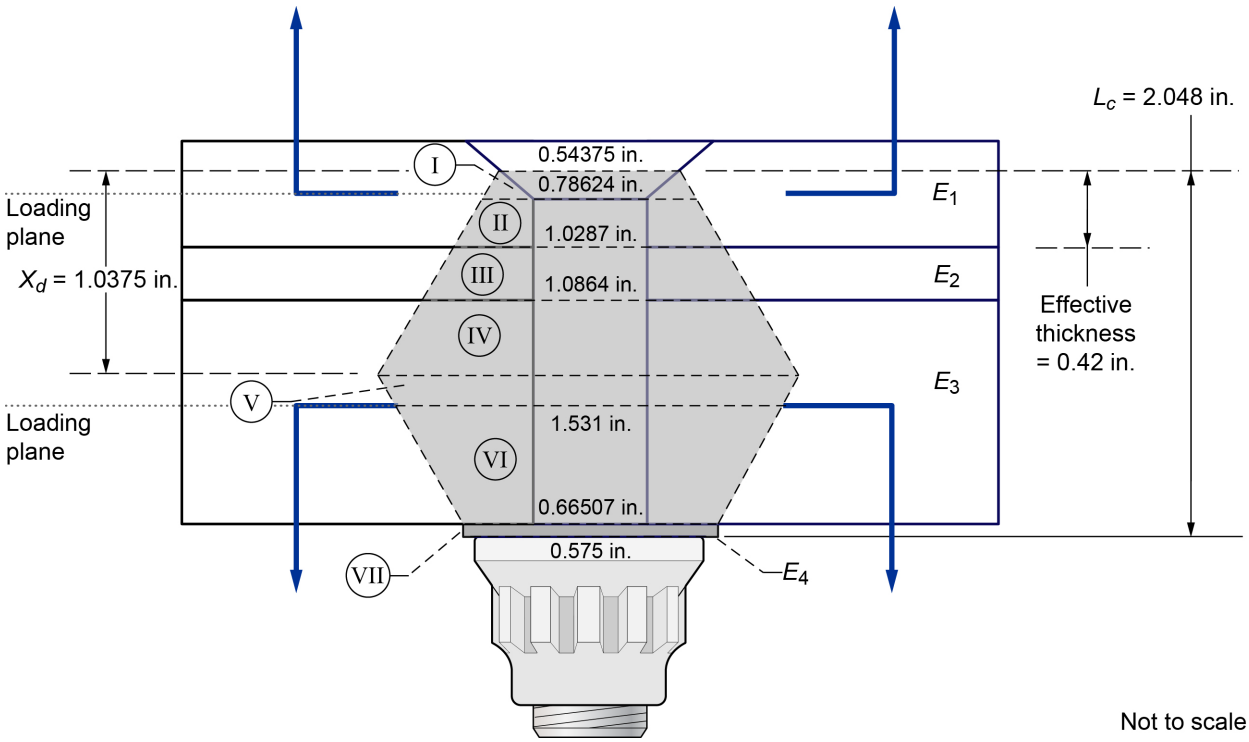

Figure C.2.—PBJ frustum stiffness elements I to VII arranged in series to form compression zone of thickness L_c with maximum diameter located at X_d.

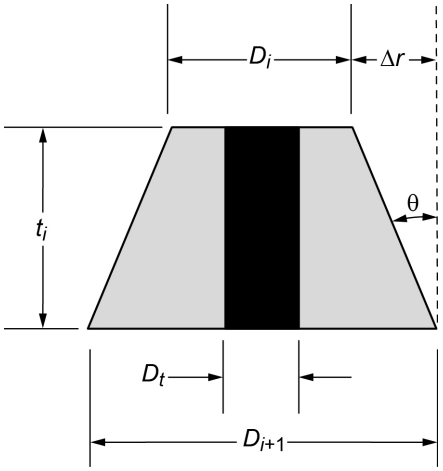

Figure C.3.—Dimensions of PBJ frustum element *i*.

It can be observed from the single frustum element shown in Figure C.3 that

$$\Delta r = t_i \tan(\theta) \tag{C.1}$$

Using Equation (C.1) it can also be observed from Figure C.3 that

$$D_{i+1} = D_i + 2\Delta r = D_i + 2t_i \tan(\theta) \tag{C.2}$$

which will be useful in the calculations that follow.

The stiffness of elements I through VII (Figure C.2) are calculated below using the geometry of Figure C.1 and the compression-zone half-apex angle θ = 30°.

C.1.1 Stiffness Element I

It is assumed based on engineering judgment that D_1 is the average of the fastener-head diameter and the through-hole diameter, and is calculated as

$$D_1 = \frac{(D_h + D_t)}{2} = \frac{(0.704 + 0.3835)}{2} = 0.54375 \text{ in.} \tag{C.3}$$

The location of the average diameter D_1 is located at half the flange countersink depth, which is assumed to be the same as L_h.

The effective thickness of the clamped member 1 (see Figure C.2) extends from the location of this average diameter to the bottom of the clamped member 1. The thickness of stiffness element I extends from the location of this average diameter to the top loading plane, which is assumed located at midplane of the effective thickness of clamped member 1. This is expressed mathematically as

$$t_I = \frac{\left(L_1 - \frac{l_h}{2}\right)}{2} = \frac{\left(0.5 - \frac{0.16}{2}\right)}{2} = 0.21 \text{ in.} \tag{C.4}$$

Using Equation (F.27), the stiffness of element I is

$$K_I = \frac{\pi(1.06\times10^7)(0.3835)\tan(30)}{\ln\left[\frac{(2(0.21)\tan(30)+0.54375-0.3835)(0.54375+0.3835)}{(2(0.21)\tan(30)+0.54375+0.3835)(0.54375-0.3835)}\right]} \tag{C.5}$$

$$= 10,697,723.5641 \text{ lb/in.}$$

C.1.2 Stiffness Element II

The thickness of stiffness element II is the distance from the top loading plane to the bottom of clamped member 1. This is equivalent to the thickness of stiffness element I, since the loading plane divides the effective thickness of the clamped member 1 equally.

$$t_{II} = t_I = 0.21 \text{ in.} \tag{C.6}$$

Using Equation (C.2) the minor diameter of element II is

$$D_{II} = D_I + 2(t_I)\tan(30) = 0.54375 + 2(0.21)\tan(30) = 0.78624 \text{ in.} \tag{C.7}$$

and using Equation (F.27) the stiffness is

$$K_{II} = \frac{\pi(1.06\times10^7)(0.3835)\tan(30)}{\ln\left\{\frac{[2(0.21)\tan(30)+0.78624-0.3835](0.78624+0.3835)}{[2(0.21)\tan(30)+0.78624+0.3835](0.78624-0.3835)}\right\}} \tag{C.8}$$

$$= 26,060,911.7106 \text{ lb/in.}$$

C.1.3 Stiffness Element III

The thickness of stiffness element III is equivalent to the thickness of the second flange:

$$t_{\mathrm{III}} = 0.050 \text{ in.} \tag{C.9}$$

It should be mentioned that stiffness elements II and III could have alternatively been treated as one stiffness element since the modulus of elasticity is the same for both.

Using Equation (C.2) the minor diameter of stiffness element III is

$$D_{\mathrm{III}} = D_{\mathrm{II}} + 2(t_{\mathrm{II}})\tan(30) = 0.78624 + 2(0.21)\tan(30) = 1.0287 \text{ in.} \tag{C.10}$$

and using Equation (F.27) the stiffness is

$$\begin{aligned} K_{\mathrm{III}} &= \frac{\pi(1.06\times10^{7})(0.3835)\tan(30)}{\ln\left[\dfrac{(2(0.05)\tan(30)+1.0287-0.3835)(1.0287+0.3835)}{(2(0.05)\tan(30)+1.0287+0.3835)(1.0287-0.3835)}\right]} \\ &= 161{,}571{,}728.376 \text{ lb/in.} \end{aligned} \tag{C.11}$$

C.1.4 Stiffness Element IV

The thickness of stiffness element IV will be determined by either the maximum compression-zone diameter or the bottom loading plane, whichever is nearer the bottom of stiffness element III (top of stiffness element IV).

Equation (D.6) will be used to determine the location of the maximum diameter of the compression zone. To use Equation (D.6), the thickness of the compression zone and the diameters of both ends first need to be determined. Referring to Figure C.1, the thickness of the compression zone is

$$L_c = L_1 - \frac{l_h}{2} + L_2 + L_3 + L_4 = 0.5 - \frac{0.16}{2} + 0.05 + 1.5 + 0.078 = 2.048 \text{ in.} \tag{C.12}$$

The diameter of the lower end of the compression zone is equal to the diameter of the nut, which is given as

$$D_{\mathrm{VII}} = 0.575 \text{ in.} \tag{C.13}$$

and the diameter of the top end of the compression-zone D_1 was already determined for stiffness element I to be 0.54375 in. The location of the maximum compression-zone diameter with respect to the top of the compression zone is obtained using Equation (D.6) from Appendix D and is

$$X_d = \frac{L_c}{2} + \frac{(D_{\mathrm{VII}} - D_1)}{4\tan(\theta)} = \frac{2.048}{2} + \frac{(0.575 - 0.54375)}{4\tan(30)} = 1.0375 \text{ in.} \tag{C.14}$$

The location of the bottom loading plane at the midplane of clamped member 3 is determined as follows:

$$L_1 - \frac{l_h}{2} + L_2 + \frac{L_3}{2} = 0.5 - \frac{0.16}{2} + 0.05 + \frac{1.5}{2} = 1.22 \text{ in.} \tag{C.15}$$

Since the maximum compression-zone diameter is nearer the top of stiffness element IV than is the lower loading plane, the location of the maximum diameter of the compression zone is used as the bottom of stiffness element IV. Therefore, the thickness of stiffness element IV is

$$t_{\mathrm{IV}} = X_d - t_{\mathrm{I}} - t_{\mathrm{II}} - t_{\mathrm{III}} = 1.0375 - 0.21 - 0.21 - 0.05 = 0.5675 \text{ in.} \tag{C.16}$$

Using Equation (C.2) the associated minor diameter is

$$D_{\mathrm{IV}} = D_{\mathrm{III}} + 2(t_{\mathrm{III}})\tan(30) = 1.0287 + 2(0.05)\tan(30) = 1.0864 \text{ in.} \tag{C.17}$$

and using Equation (F.27) the stiffness is

$$\begin{aligned} K_{\mathrm{IV}} &= \frac{\pi\left(2.9\times10^{7}\right)(0.3835)\tan(30)}{\ln\left\{\dfrac{[2(0.5675)\tan(30)+1.0864-0.3835](1.0864+0.3835)}{[2(0.5675)\tan(30)+1.0864+0.3835](1.0864-0.3835)}\right\}} \\ &= 69,552,630.2608 \text{ lb/in.} \end{aligned} \tag{C.18}$$

Equation (F.27) provides the stiffness of a frustum element in terms of the minor diameter of the frustum. Because of this, it is more convenient to calculate the stiffness of element VII next, followed by elements VI and V.

C.1.5 Stiffness Element VII

The minor diameter of this stiffness element is equal to the nut diameter, which was given previously and is

$$D_{\mathrm{VII}} = 0.575 \text{ in.} \tag{C.19}$$

The thickness of this stiffness element is equal to the thickness of the washer and is

$$t_{\mathrm{VII}} = 0.078 \text{ in.} \tag{C.20}$$

and using Equation (F.27) the stiffness is

$$\begin{aligned} K_{\mathrm{VIII}} &= \frac{\pi\left(2.91\times10^{7}\right)(0.3835)\tan(30)}{\ln\left\{\dfrac{[2(0.078)\tan(30)+0.575-0.3835](0.575+0.3835)}{[2(0.078)\tan(30)+0.575+0.3835](0.575-0.3835)}\right\}} \\ &= 68,460,194.9079 \text{ lb/in.} \end{aligned} \tag{C.21}$$

C.1.6 Stiffness Element VI

Starting with Equation (C.2), a rearrangement of its indices to accommodate the current situation of working from stiffness element VI backwards at this point becomes

$$D_{\mathrm{VI}} = D_{\mathrm{VII}} + 2(t_{\mathrm{VI}})\tan(30) = 0.575 + 2(0.078)\tan(30) = 0.66507 \text{ in.} \tag{C.22}$$

Stiffness element VI extends from the lower loading plane to the washer, and therefore its thickness is equal to half of the thickness of clamped member 3 and is

$$t_{\mathrm{VI}} = \frac{L_3}{2} = \frac{1.5}{2} = 0.75 \text{ in.} \tag{C.23}$$

and using Equation (F.27) the stiffness is,

$$\begin{aligned} K_{\mathrm{VI}} &= \frac{\pi\left(2.9\times10^{7}\right)(0.3835)\tan(30)}{\ln\left\{\dfrac{[2(0.75)\tan(30)+0.66507-0.3835](0.66507+0.3835)}{[2(0.75)\tan(30)+0.66507+0.3835](0.66507-0.3835)}\right\}} \\ &= 25{,}122{,}134.4416 \text{ lb/in.} \end{aligned} \tag{C.24}$$

C.1.7 Stiffness Element V

Stiffness element V extends from the location of the maximum diameter of the compression zone to the lower loading plane, and this thickness may be calculated as follows:

$$t_{\mathrm{V}} = L_3 - t_{\mathrm{IV}} - t_{\mathrm{VI}} = 1.5 - 0.5675 - 0.75 = 0.1825 \text{ in.} \tag{C.25}$$

Using Equation (C.2) with a rearrangement of its indices to accommodate the current situation of working from stiffness element VI backwards at this point, gives

$$D_{\mathrm{V}} = D_{\mathrm{VI}} + 2(t_{\mathrm{VI}})\tan(30) = 0.66507 + 2(0.75)\tan(30) = 1.5311 \text{ in.} \tag{C.26}$$

and using Equation (F.27) the stiffness is,

$$\begin{aligned} K_{\mathrm{V}} &= \frac{\pi\left(2.9\times10^{7}\right)(0.3835)\tan(30)}{\ln\left\{\dfrac{[2(0.1825)\tan(30)+1.5311-0.3835](1.5311+0.3835)}{[2(0.1825)\tan(30)+1.5311+0.3835](1.5311-0.3835)}\right\}} \\ &= 314{,}376{,}726.529 \text{ lb/in.} \end{aligned} \tag{C.27}$$

C.1.8 Compression-Zone Flexibility

The compression-zone flexibility is the sum of the flexibilities of all seven of the stiffness elements comprising it, and is

$$\frac{1}{K_c} = \sum_{i=\mathrm{I}}^{\mathrm{VII}} \frac{1}{K_i} = 2.1001\times10^{-7} \text{ in./lb} \tag{C.28}$$

C.1.9 Compression-Zone Stiffness

The stiffness of the compression zone is the reciprocal of its flexibility and is

$$K_c = 4{,}761{,}678.0 \text{ lb/in.} \tag{C.29}$$

The stiffness-based load introduction factor (SBLIF) is calculated in terms of the flexibilities of the relieving load path and the compression-zone stiffness using Equation (30), within K_a replaced with K_c and repeated here for convenience:

$$n = K_c \left(\sum_{i=1}^{N} \frac{1}{K_i} \right)_{relieving} = K_c \sum_{i=II}^{V} \frac{1}{K_i} \tag{30}$$

Substituting Equations (C.8), (C.11), (C.18), (C.27), and (C.29) into Equation (30) the SBLIF is

$$n = 4,761,678.0 \left(\frac{1}{26,060,911.71} + \frac{1}{161,571,728.38} + \frac{1}{69,552,630.26} + \frac{1}{314,376,726.53} \right) = 0.30 \tag{C.30}$$

C.2 Geometric LIF

The LIF, defined in Reference 9 as the ratio of the thickness of the relieving load path to the total thickness of the compression zone, is denoted herein as the geometric LIF (GLIF) n_G because it is defined entirely on geometric considerations, the ratio of two lengths or thicknesses.

Referring to Figure C.2, the thickness of the compression zone L_c is based on engineering judgment and is assumed to be the distance from the interface between the washer and nut, extending through the clamped members to half of the countersunk head depth, and is given in the denominator in Equation (C.31). The external tensile load enters the PBJ through the loading planes, which based on engineering judgment are assumed to be located at half of the effective thicknesses of clamped members 1 and 3. The effective thickness of clamped member 1 is assumed to be its baseline thickness less half the fastener countersunk head depth. The distance between the loading planes is given in the numerator of Equation (C.31). Therefore, based on engineering judgment, the GLIF is defined as

$$n_G = \frac{\frac{1}{2}\left(L_1 - \frac{L_h}{2} \right) + L_2 + \frac{L_3}{2}}{L_1 - \frac{L_h}{2} + L_2 + L_3 + L_4} \tag{C.31}$$

and calculated using the dimensions in Figure C.1 to be

$$n_G = \frac{\frac{1}{2}\left(0.5 - \frac{0.16}{2} \right) + 0.05 + \frac{1.5}{2}}{0.5 - \frac{0.16}{2} + 0.05 + 1.5 + 0.078} = 0.49 \tag{C.32}$$

It should be noted that the LIF is a direct multiplier of the external tension load in the bolt equation, and so the SBLIF imparts about 39 percent less external tensile load into the fastener than does the GLIF:

$$\frac{n_G - n}{n_G} \times 100 = \frac{0.49 - 0.30}{0.49} \times 100 = 39 \text{ percent} \tag{C.33}$$

Appendix D.—Location of Maximum Diameter of Nonsymmetric Back-to-Back Frusta

This appendix derives the equation for the location of maximum diameter for a nonsymmetric compression zone comprising two back-to-back frusta, each of half-apex angle θ, as shown in Figure D.1.

The maximum diameter of the upper frustum D_{max}, located a distance X_d from the top of the compression zone, may be determined using the following geometric relationship:

$$D_{max} = D_U + 2X_d \tan(\theta) \tag{D.1}$$

The maximum diameter of the lower frustum is located a distance $L_c - X_d$ from the bottom of the compression zone and may be determined using the following geometric relationship:

$$D_{max} = D_L + 2(L_c - X_d)\tan(\theta) \tag{D.2}$$

It can also be seen from Figure D.1 that the maximum diameter of the upper and lower frustum is the same. This is expressed mathematically by equating Equations (D.1) and (D.2):

$$D_U + 2X_d \tan(\theta) = D_L + 2(L_c - X_d)\tan(\theta) \tag{D.3}$$

Rearranging Equation (D.3),

$$2X_d \tan(\theta) = D_L - D_U + 2(L_c - X_d)\tan(\theta) \tag{D.4}$$

and combining terms gives

$$4X_d \tan(\theta) = D_L - D_U + 2L_c \tan(\theta) \tag{D.5}$$

and solving for X_d results in

$$X_d = \frac{L_c}{2} + \frac{D_L - D_U}{4\tan(\theta)} \tag{D.6}$$

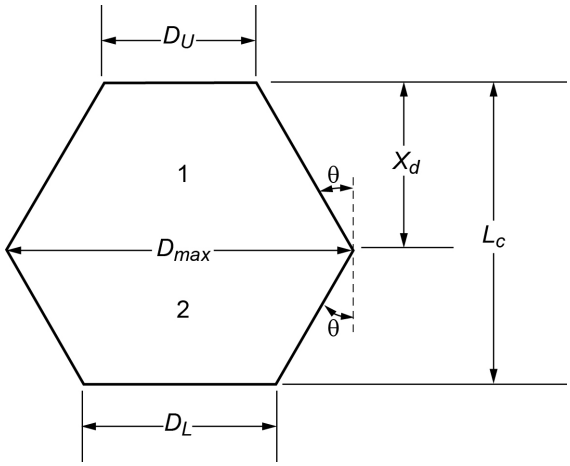

Figure D.1.—Nonsymmetric compression-zone dimensions.

Appendix E.—Bolt Thermal Load

The thermal load P_{th} is an internal tensile load resulting from a resistance to unconstrained thermal displacement of a body (Ref. 5, p. 110), as shown in Figure E.1. For the preloaded bolted joint (PBJ), the thermal load is created by a temperature change in conjunction with the differences in thermal expansion rates of the bolt and clamped members, α_b and α_m, respectively. The thermal load serves to restrain the thermal displacement of the bolt and the clamped members so that they are in equilibrium, and therefore the clamped' members' load path is solely that of the compression zone, just as is the load path under preload. In this work it is assumed that there is no gapping of faying surfaces because of a temperature change.

For the purposes of approximating the bolt stiffness, the effective bolt length L_b may be equal to the overall clamped-member thickness L, ignoring the flexibility of the bolt head and internally threaded component. If it is desired to include these flexibilities, some additional bolt length beyond the clamped-member thickness L may be considered (Ref. 10) as shown notionally in Figure E.2. The appropriate length of bolt used in determining the thermal effects is limited to that portion of the bolt shank included within L, as will be explained next.

Referring to Figure E.2, only the thermal displacement of the bolt shank and members within L can contribute to the thermal load P_{th} within the load paths of a PBJ, because members outside of this region are free to expand or contract and are thus unconstrained and therefore cannot result in the creation of an internal thermal load.

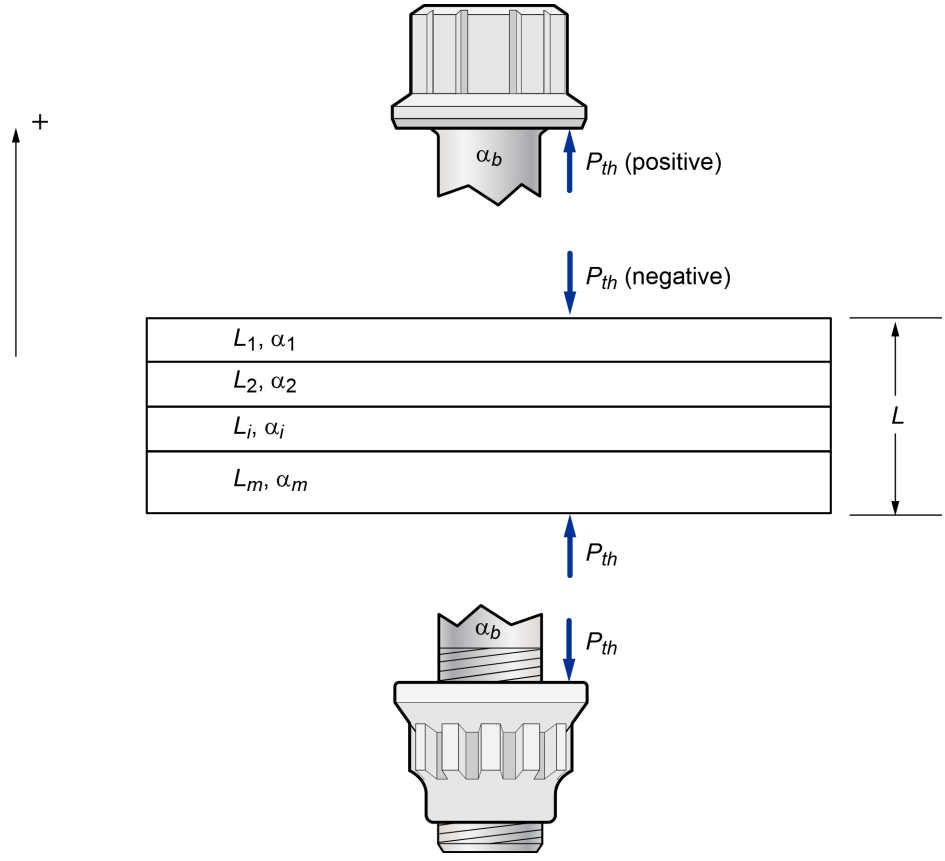

Figure E.1.—Free-body diagram of PBJ under thermal load. Shown is case of temperature increase where expansion rate of clamped members is larger than that of bolt, creating compressive thermal load in clamped members and equal and opposite tensile load in bolt.

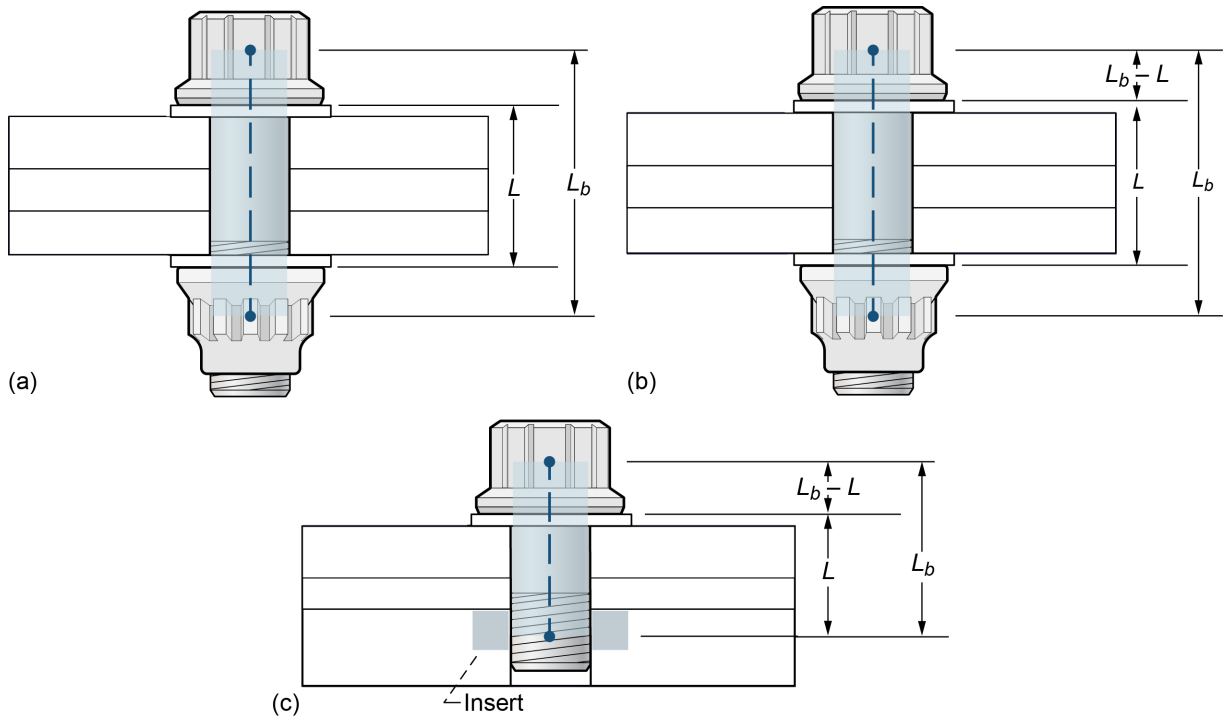

Figure E.2.—PBJ showing effective length of bolt L_b and thickness of clamped members L. (a) Bolt head and nut (internal threaded component) are not included as part of clamped members. (b) Part of nut (internal threaded component) is included as part of clamped members. (c) Part of insert (internal threaded component) is included as part of clamped members.

For each case in Figure E.2, the effective bolt length L_b, for purposes of bolt stiffness, is assumed to be larger than the clamped-member thickness L (Ref. 10), because of the inclusion of the partial thickness of the bolt head and internally threaded component in L_b. Also in these cases, the bolt head is not assumed to contribute to the thermal load and is therefore not included as part of the clamped members.

Figure E.2(a) represents the case where both the thermal expansion of the bolt head and nut are not assumed to affect the thermal load, being outside of the thickness L. The bolt head, being the same material as—and contiguous with—the bolt shank, is assumed to expand or contract freely, proud of the underside of the bolt head and therefore is assumed to not affect the thermal displacement of the bolt shank within the thickness L.

The internal threaded component, such as a nut or internally threaded clamped member, may be of different material than that of the bolt and may consequently expand or contract at a different rate than the bolt; thus, under a temperature change, it may contribute to the thermal load. If this effect is judged to be significant by the analyst, then a portion of the thickness of the internally threaded component should be included as part of the thickness L as shown in Figure E.2, parts (b) and (c).

One way to derive the equation for the thermal load is to write the equations for the displacement of the bolt shank and clamped members in terms of their original equivalent lengths L, their change in length due to the as-yet-to-be determined thermal load, and their unconstrained thermal displacement. Assuming there is no gapping of faying surfaces, the displacement of the bolt shank and clamped members must be equal. Therefore, the aforementioned bolt and clamped-member displacement equations can be set equal to each other and solved for the thermal load.

The original length of the bolt shank L is equivalent to the original clamped-members' thickness. The unconstrained thermal displacement of the bolt due to a temperature change ΔT, is expressed mathematically as $\alpha_b L \Delta T$, where α_b is the thermal expansion coefficient of the bolt.

Using Hooke's Law, the bolt shank displacement due to the thermal load is

$$\frac{P_{th}}{K_b}$$

where K_b is the bolt stiffness. The total displacement of the bolt shank due to a temperature change is equal to the sum of the bolt shank displacement from the thermal load and the unconstrained bolt shank thermal displacement. This is expressed mathematically as

$$\delta_{b_{th}} = \frac{P_{th}}{K_b} + \alpha_b L \Delta T \tag{E.1}$$

Likewise, under a temperature change ΔT, the unconstrained thermal displacement of the m clamped members, each of original individual thickness L_i and overall thickness L and having thermal expansion coefficient α_i, is expressed mathematically as

$$\left(\sum_{i=1}^{m} \alpha_i L_i \right) \Delta T$$

Using Hooke's Law, the displacement of the clamped members due to the thermal load is

$$\frac{-P_{th}}{K_a}$$

where K_a is the stiffness of the clamped-members' tension load path and where the thermal load is negative per Figure E.1. The question may arise as to which clamped-member stiffness to use, K_a or K_c. Under preload only, K_c seems more appropriate. Since the PBJ is to be evaluated under tensile load, and the thermal load is also acting simultaneously, the use of K_a seems more appropriate in this case. Therefore, the derivation of the thermal load will use K_a, even though K_c will likely be used in place of K_a following traditional practice.

The total displacement of the clamped members due to a temperature change δL_{th} is equal to the sum of the displacement from the thermal load and the unconstrained thermal displacement. This is expressed mathematically as

$$\delta L_{th} = -\frac{P_{th}}{K_a} + \left(\sum_{i=1}^{m} \alpha_i L_i \right) \Delta T \tag{E.2}$$

Because there is no gapping of faying surfaces, the displacements of the bolt and clamped members are equal. This is expressed mathematically by setting Equation (E.1) equal to Equation (E.2):

$$\frac{P_{th}}{K_b} + \alpha_b L \Delta T = -\frac{P_{th}}{K_a} + \left(\sum_{i=1}^{m} \alpha_i L_i \right) \Delta T \tag{E.3}$$

Rearranging and combining terms, and solving for the thermal load P_{th} results in

$$P_{th} = \left(\frac{K_b K_a}{K_b + K_a} \right) L \Delta T \left(\frac{\sum_{i=1}^{m} \alpha_i L_i}{L} - \alpha_b \right) \tag{E.4}$$

The effective thermal expansion coefficient of the clamped members is defined as

$$\alpha_a = \frac{\sum_{i=1}^{m} \alpha_i L_i}{L} \tag{E.5}$$

Upon substituting Equation (E.5) into Equation (E.4), the thermal load becomes

$$P_{th} = \left(\frac{K_b K_a}{K_b + K_a} \right) L \Delta T \left(\alpha_a - \alpha_b \right) \tag{E.6}$$

Substituting Equation (25) into Equation (E.6), the thermal load in terms of the stiffness factor becomes

$$P_{th} = \phi K_a L \Delta T \left(\alpha_a - \alpha_b \right) \tag{E.7}$$

Appendix F.—Derivation of Axial Stiffness of Frustum Element

Consider the bar of Figure F.1, of original length L aligned with the x-coordinate, with uniform cross-sectional area A and modulus of elasticity E. The displacement of the bar e in the x-direction is related to the loads P applied in the x-direction, according to the following equation that is derived in the literature, for example, in Reference 5:

$$e = \frac{PL}{AE} \tag{F.1}$$

Rearranging Equation (F.1) in the form of Hooke's Law, where force equals the product of the stiffness and displacement, $F = K\delta$, gives

$$F = K\,\delta \Rightarrow P = \left(\frac{AE}{L}\right)e \tag{F.2}$$

where it can be observed from Equation (F.2) that the stiffness of this bar of length L is

$$K = \frac{AE}{L} \tag{F.3}$$

and the flexibility, a reciprocal of the stiffness, is

$$\frac{1}{K} = \left(\frac{L}{AE}\right) \tag{F.4}$$

For bars of nonuniform cross section, where $A = A(x)$, and nonuniform modulus of elasticity $E = E(x)$, the flexibility of the bar can be determined by adding the flexibilities of individual segments of length Δx, comprising the total length L of the bar, as shown in Figure F.2.

This is expressed mathematically as

$$\left(\frac{1}{K}\right)_{total} = \sum_i \left(\frac{1}{K_i}\right) = \sum_i \frac{(\Delta x)_i}{A_i E_i} \tag{F.5}$$

where A_i and E_i are an average area and modulus of elasticity, respectively, corresponding to the segment of thickness $(\Delta x)_i$. From Reference 15, by taking the limit as $(\Delta x_i)_{max} \to 0$, the summation becomes an integral by definition:

$$\left(\frac{1}{K}\right)_{total} = \lim_{(\Delta x_i)_{max} \to 0} \sum_i \frac{(\Delta x)_i}{A_i E_i} = \int_0^L \frac{1}{A(x)E(x)}\,dx \tag{F.6}$$

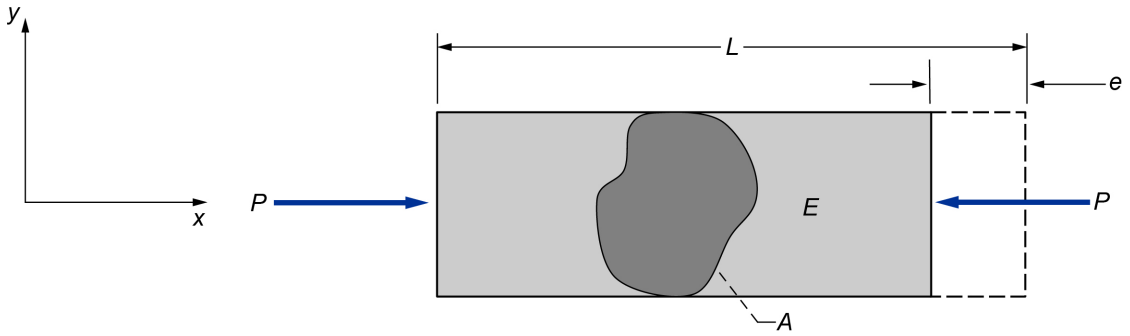

Figure F.1.—Axial compression of bar of constant area and modulus of elasticity.

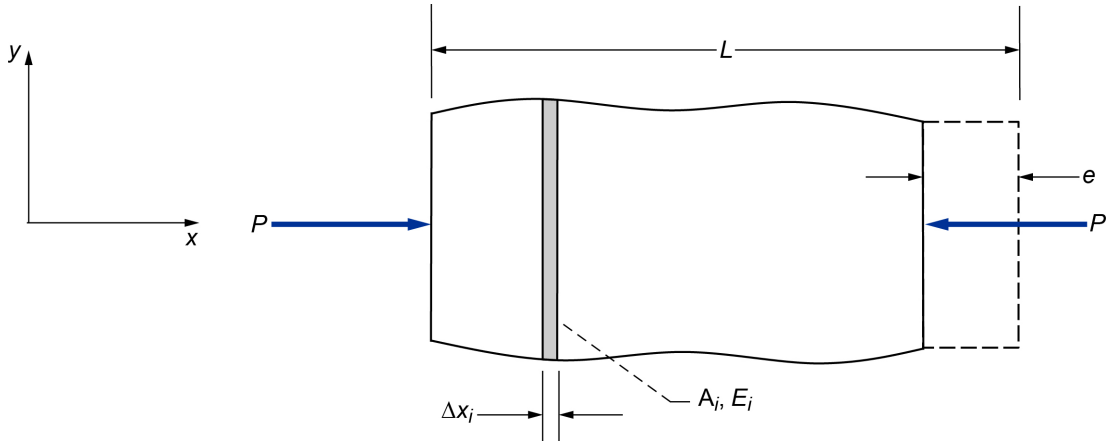

Figure F.2.—Axial compression of bar of variable area and modulus of elasticity.

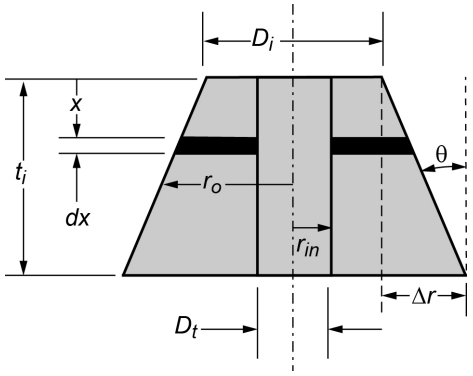

Figure F.3.—Frustum.

The flexibility of the frustum stiffness element shown in Figure F.3 may be obtained by using Equation (F.6), with the limits of integration chosen such that the integration covers a region of constant modulus of elasticity, as shown in Equation (F.7). The stiffness can be obtained through subsequent inversion of the flexibility.

$$\frac{1}{K_i} = \int_0^{t_i} \frac{dx}{E_i A(x)} \tag{F.7}$$

The cross-sectional area of the differential slice *i* of the frustum (Figure F.2) may be expressed as

$$A(x) = \pi\left[r_o(x)^2 - r_{in}^2 \right] \tag{F.8}$$

where r_{in} is frustrum inner radius. From Figure F.3 it can be seen that

$$r_{in} = \frac{D_t}{2} \tag{F.9}$$

and

$$r_o(x) = \Delta r(x) + \frac{D_i}{2} \tag{F.10}$$

where the corresponding radii *r* are defined in the figure, which also shows that

$$\frac{\Delta r(x)}{x} = \tan(\theta) \Rightarrow \Delta r(x) = x\tan(\theta) \tag{F.11}$$

Substituting Equation (F.11) into Equation (F.10),

$$r_o(x) = x\tan(\theta) + \frac{D_i}{2} \tag{F.12}$$

Substituting Equations (F.9) and (F.12) into Equation (F.8),

$$A(x) = \pi\left\{ \left[x\tan(\theta) + \frac{D_i}{2} \right]^2 - \left(\frac{D_t}{2} \right)^2 \right\} \tag{F.13}$$

Using the relationship

$$a^2 - b^2 = (a+b)(a-b) \tag{F.14}$$

Equation (F.13) becomes

$$A(x) = \pi\left\{ \left[x\tan(\theta) + \frac{D_i + D_t}{2} \right] \left[x\tan(\theta) + \frac{D_i - D_t}{2} \right] \right\} \tag{F.15}$$

Substituting Equation (F.15) into Equation (F.7) gives

$$\frac{1}{K_i} = \int_0^{t_i} \frac{dx}{E_i \pi\left\{ \left[x\tan(\theta) + \frac{D_i + D_t}{2} \right] \left[x\tan(\theta) + \frac{D_i - D_t}{2} \right] \right\}} \tag{F.16}$$

From integral tables,

$$\int \frac{dx}{(ax+b)(cx+e)} = \frac{1}{bc - ae} \ln\left(\frac{cx+e}{ax+b} \right) \tag{F.17}$$

Letting

$$a = c = \tan(\theta) \tag{F.18}$$

$$b = \frac{D_i + D_t}{2} \tag{F.19}$$

$$e = \frac{D_i - D_t}{2} \tag{F.20}$$

and upon substituting Equations (F.18) to (F.20) into Equation (F.17), the integral of Equation (F.16) becomes

$$\frac{1}{K_i} = \frac{1}{\pi E_i}\left\{\frac{1}{\left(\frac{D_i + D_t}{2}\right)\tan(\theta) - \left(\frac{D_i - D_t}{2}\right)\tan(\theta)} \ln\left[\frac{x\tan(\theta) + \left(\frac{D_i - D_t}{2}\right)}{x\tan(\theta) + \left(\frac{D_i + D_t}{2}\right)}\right]\right\}\Bigg|_0^{t_i} \tag{F.21}$$

Simplifying,

$$\frac{1}{K_i} = \frac{1}{\pi E_i}\left\{\frac{1}{\tan(\theta) D_t} \ln\left[\frac{x\tan(\theta) + \left(\frac{D_i - D_t}{2}\right)}{x\tan(\theta) + \left(\frac{D_i + D_t}{2}\right)}\right]\right\}\Bigg|_0^{t_i} \tag{F.22}$$

and evaluating at the limits gives

$$\frac{1}{K_i} = \frac{1}{\pi E_i D_t \tan(\theta)}\left\{\ln\left[\frac{t_i\tan(\theta) + \left(\frac{D_i - D_t}{2}\right)}{t_i\tan(\theta) + \left(\frac{D_i + D_t}{2}\right)}\right] - \ln\left[\frac{\left(\frac{D_i - D_t}{2}\right)}{\left(\frac{D_i + D_t}{2}\right)}\right]\right\} \tag{F.23}$$

Utilizing the relationship

$$\ln(a) - \ln(b) = \ln\left(\frac{a}{b}\right) \tag{F.24}$$

Equation (F.23) becomes

$$\frac{1}{K_i} = \frac{1}{\pi E_i D_t \tan(\theta)} \ln\left[\frac{\left(t_i\tan(\theta) + \frac{D_i - D_t}{2}\right)\left(\frac{D_i + D_t}{2}\right)}{\left(t_i\tan(\theta) + \frac{D_i + D_t}{2}\right)\left(\frac{D_i - D_t}{2}\right)}\right] \tag{F.25}$$

Reducing further and inverting, the stiffness of a single frustum as shown in Figure F.3 is

$$K_i = \frac{\pi E_i D_t \tan(\theta)}{\ln\left\{\frac{\left[t_i \tan(\theta) + \frac{D_i - D_t}{2}\right](D_i + D_t)}{\left[t_i \tan(\theta) + \frac{D_i + D_t}{2}\right](D_i - D_t)}\right\}} \tag{F.26}$$

Factoring out the ½ from the numerator and denominator of the natural log term leads to the familiar frustum stiffness formula:

$$K_i = \frac{\pi E_i D_t \tan(\theta)}{\ln\left\{\frac{[2t_i \tan(\theta) + D_i - D_t](D_i + D_t)}{[2t_i \tan(\theta) + D_i + D_t](D_i - D_t)}\right\}} \tag{F.27}$$

Appendix G.—Finite Element Prediction of $n\phi$ for Pure Tension Joint Biased Towards Cylindrical Compression Zone[4]

A finite element model of the preloaded bolted joint (PBJ), shown in the inset of Figure G.1, was created for analysis with the commercial software, ABAQUS® 6.10 (TECHNIA). Solid elements were used to model the bolt with A286 alloy material properties and each of the three joint members with generic aluminum alloy properties. The nut and the bolt are modeled as a single part rather than as an assembly. Surface contact is modeled between the mating aluminum joint members, between the bolt head and the upper joint member, and between the nut and the lower joint member. The lower joint member is constrained in the three translational degrees of freedom at the nodes on its aftmost surface. The upper joint member has additional displacement boundary conditions and is used to apply the tension load to the joint: the three translational degrees of freedom of the nodes on the forwardmost surface of the upper joint member are connected to an in-plane center node using a kinematic coupling constraint (rigid element connection). This center node is free to translate in the bolt axial direction and is constrained in the remaining two translational degrees of freedom and all three rotational degrees of freedom. Applied tension to the joint is modeled with an axial force applied at this center node. For numerical stability, select nodes on the middle joint member and on the bolt-nut part are constrained in the two lateral directions in a strategic manner to not invalidate the response. Preload in the bolt is modeled with the *PRE-TENSION SECTION feature in ABAQUS® at a bolt cross-sectional surface about midway along the shank. Additional features of the ABAQUS® Finite Element Model are

- The model is a 360° solid model.
- Linear elastic material properties are used.
- Preload was set at 7,600 lb.
- Elastic modulus for the bolt is 29×10^6 psi.
- Elastic modulus for the fittings and spacer is 10.5×10^6 psi.
- The head and nut fittings are symmetric. They are 1 in. tall, have a 1.6875-in. outside diameter (OD) with a 1.3125-in.-diameter counterbore that is 0.625 in. deep.
- The spacer is 3 in. long with a 1.125-in. OD and a 0.400-in. inside diameter (ID).
- The bolt head is 0.200 in. thick and 0.553 in. in diameter.
- The bolt shank is 0.375 in. in diameter, and the threaded portion of the shank was modeled as a cylinder that is 0.348 in. in diameter.
- The nut is 0.375 in. thick and 0.591 in. in diameter.

Figure G.1 shows a bolt-load trajectory with a secant-line load-deflection curve beginning from initial preload up to total joint separation with an average slope of $(n\phi)_{FEA} = 0.25$, indicating that on the average, 25 percent of the tension load is being reacted by the bolt. The initial slope of the bolt-load trajectory, $(n\phi)_{FEA}$, is 0.148, indicating that initially, 14.8 percent of the tension load is being reacted by the bolt.

Figure G.2 shows the contact pressure on the bottom of top tension fitting as function of applied load. Prying action is indicated prior to joint separation by nonuniform pressure.

Figure G.3 and Figure G.4 show the axial and von Mises stresses, respectively, in the top tension fitting as function of applied load.

Figure G.5 presents the effects of preload on the bolt-load trajectories.

[4]Finite element model and analysis courtesy of Robert J. Wingate and Dawn R. Phillips Price, NASA Marshall Space Flight Center.

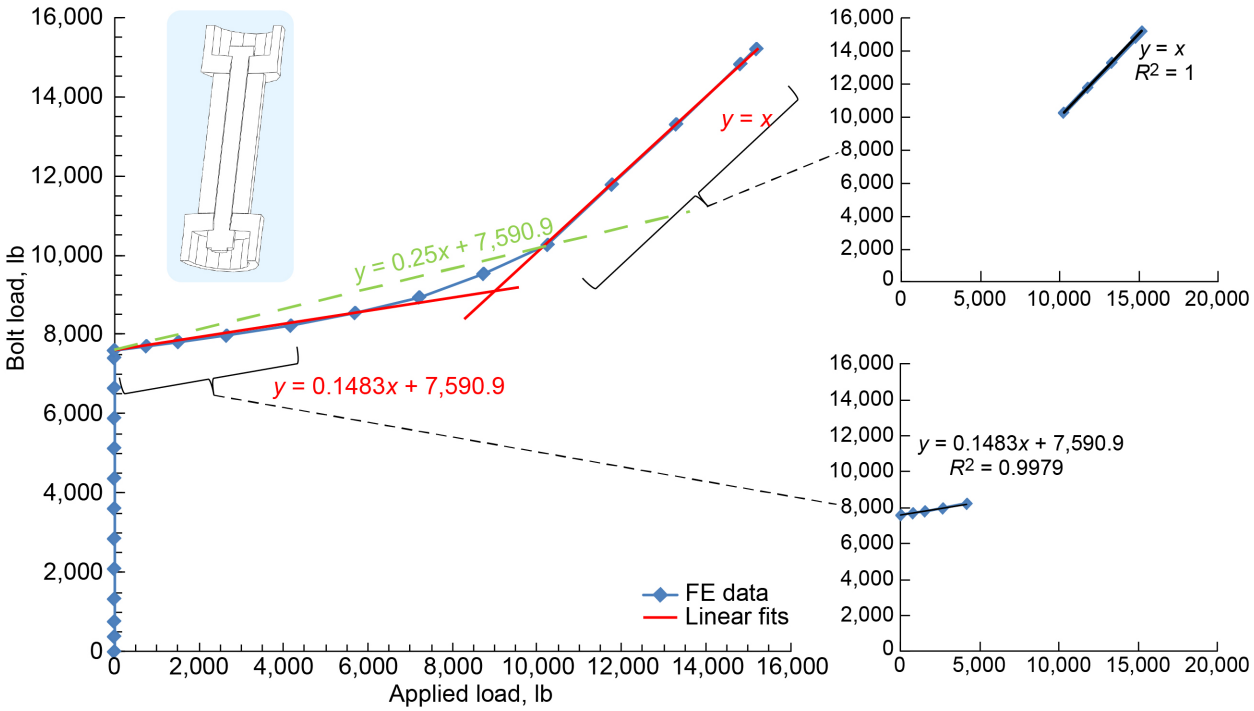

Figure G.1.—Bolt-load trajectory for PBJ assembly.

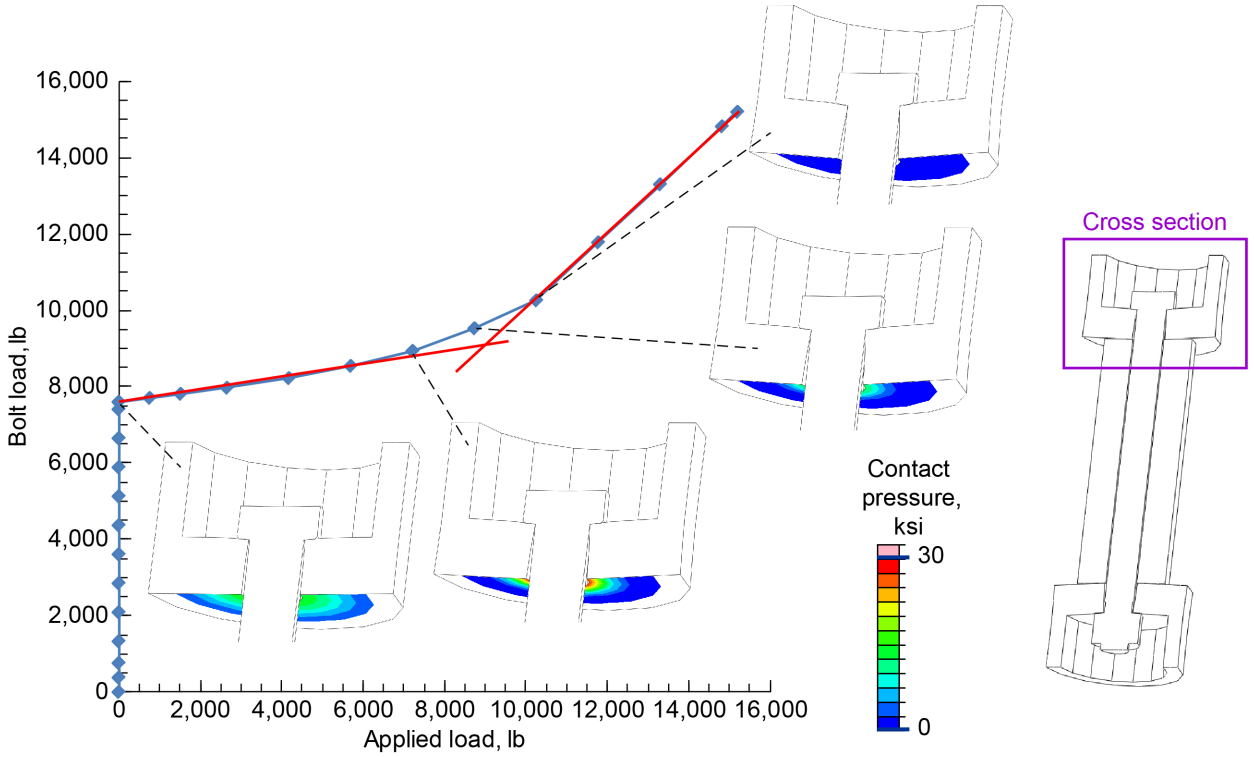

Figure G.2.—Contact pressure on bottom of top tension fitting of PBJ.

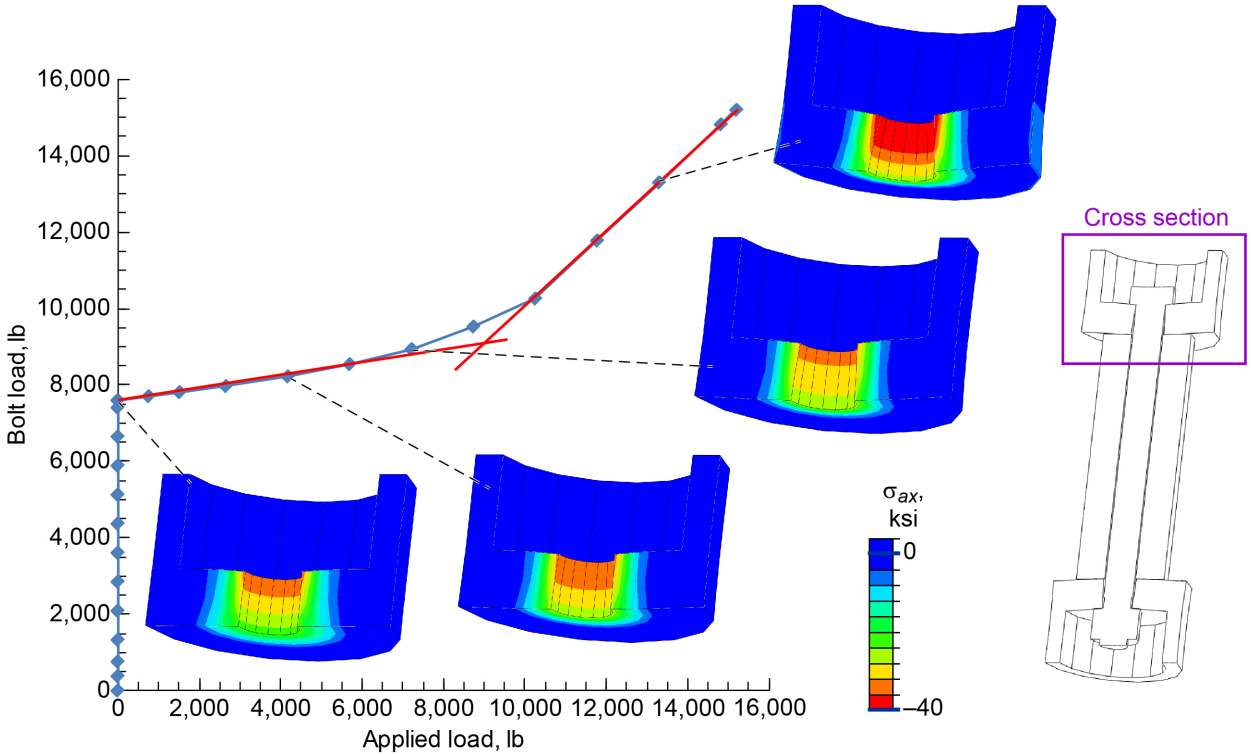

Figure G.3.—Axial stress σ_{ax} in top tension fitting of PBJ.

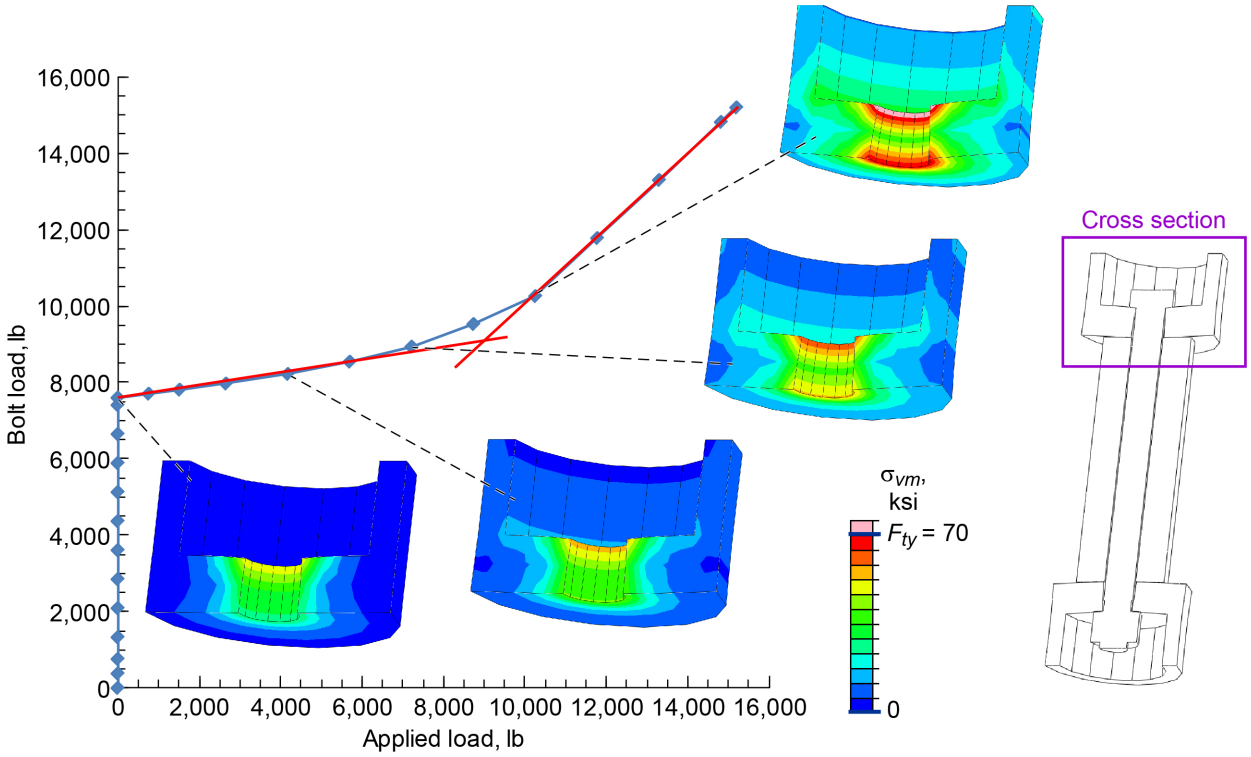

Figure G.4.—Von Mises stress σ_{vm} in top tension fitting of PBJ, where F_{ty} is tensile yield stress.

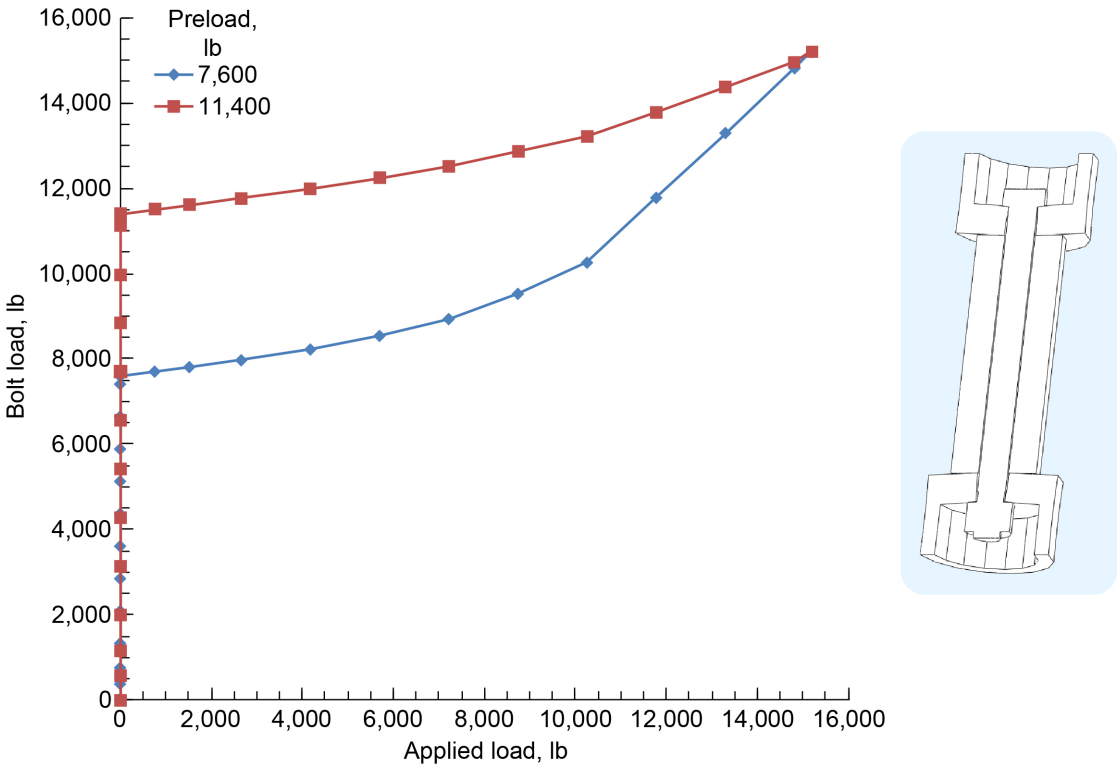

Figure G.5.—Bolt-load trajectories for PBJ as function of preload variation.

Appendix H.—Comparing Analytical Load Introduction Factors With Finite Element Analysis for Tension Joint of Appendix G

This appendix presents the calculation of the stiffness-based and geometric load introduction factors, SBLIF and GLIF, for the tension joint of Appendix G shown in Figure H.1 and compares them to the LIF extracted from finite element analysis (FEA).

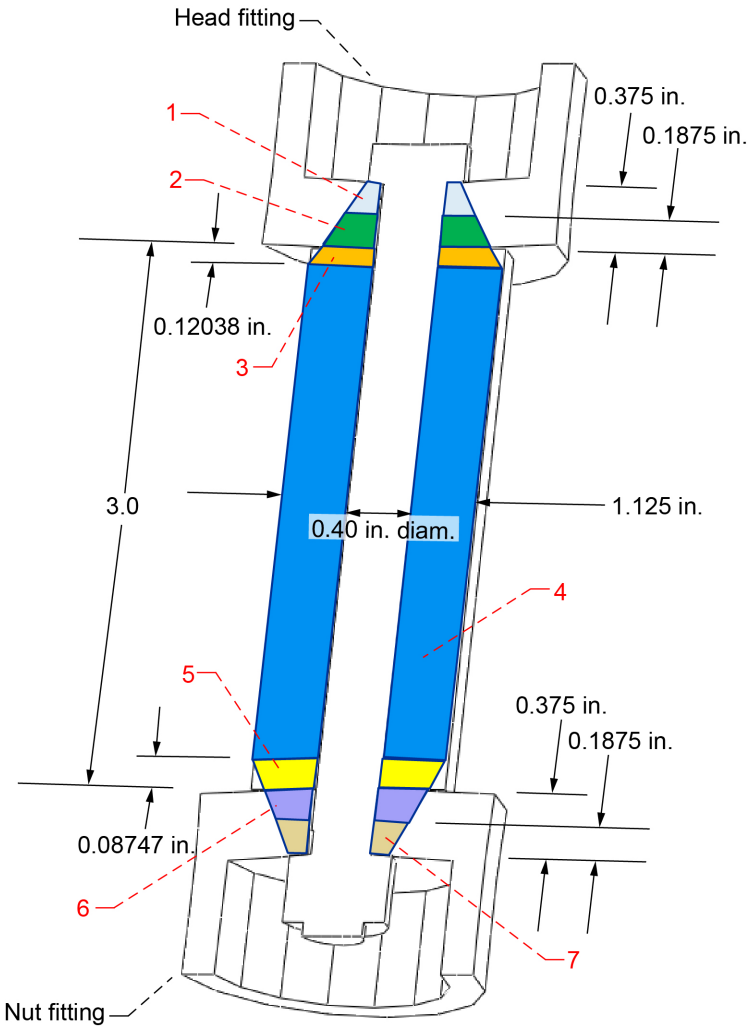

Figure H.1.—Preloaded bolted tension joint detail. Numbers in red indicate frustum or cylindrical stiffness elements constituting compression zone. Thickness of stiffness elements determined by author based on 30° frustrum half-apex angle. Joint geometry courtesy of Robert Wingate and Dawn Phillips Price, NASA Marshall Space Flight Center.

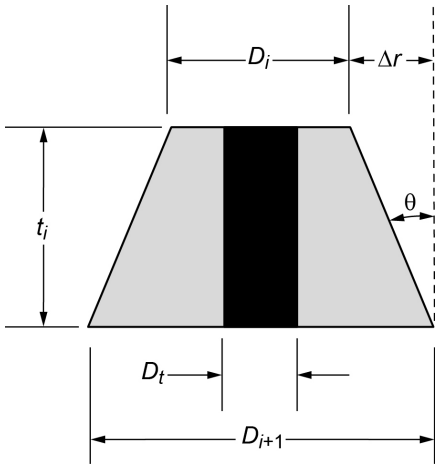

Figure C.3.—PBJ frustum element, *i*.

H.1 Joint Stiffness

The stiffness of the compression zone of the preloaded bolted tension joint of Figure H.1 may be represented by a series combination of individual cylindrical and frustum stiffness elements. The general frustum stiffness element configuration is shown in Figure C.3.

It should be mentioned that since the modulus of elasticity is the same for all frustum stiffness elements, for the purposes of calculating the compression-zone stiffness, K_c, elements 1 to 3 could have been treated as one element as could have elements 5 to 7. If the stiffness of the relieving load path is used to calculate the LIF, elements 2 and 3 as well as 5 and 6 could be combined into one stiffness element each for that purpose.

The stiffness of a single frustum element K_i as shown in Figure C.3 is derived in Appendix F Equation (F.27), repeated below for convenience:

$$K_i = \frac{\pi E_i D_t \tan(\theta)}{\ln\left[\frac{(2t_i \tan(\theta) + D_i - D_t)(D_i + D_t)}{(2t_i \tan(\theta) + D_i + D_t)(D_i - D_t)}\right]} \tag{F.27}$$

where E_i is the modulus of elasticity of the frustum element i, D_i is the minor diameter corresponding to the smaller end of frustum element i, D_t is the through-hole diameter, t_i is the element thickness, and θ is the frustum half-apex angle.

The following recursive relationship between the major and minor diameters of the frustum stiffness element is presented in Appendix C, Equation (C.2), and is repeated here for convenience:

$$D_{i+1} = D_i + 2\Delta r = D_i + 2t_i \tan(\theta) \tag{C.2}$$

Equation (C.2) will be useful in the calculations that follow.

The stiffness elements are numbered 1 through 7, starting at the bolt head.

The stiffness of elements 1 through 7 are calculated below using the geometry of Figure H.1 and the half-apex angles of θ = 21.8° and 30° for the frustum stiffness elements.

H.1.1 Stiffness Element 1

The bolt head diameter is given as 0.553 in., and this is assumed equal to the minor end diameter of stiffness element 1,

$$D_1 = 0.553 \text{ in.} \tag{H.1}$$

The effective thickness of the head fitting is 0.375 in. It is assumed that the tensile load enters this joint at the midplane of this effective thickness. Therefore, the thickness of stiffness element 1 is half of the effective thickness of the head fitting. This is expressed mathematically as

$$t_1 = \frac{0.375}{2} = 0.1875 \text{ in.} \tag{H.2}$$

Using Equation (F.27), the stiffness of element 1 is

$$K_1(\alpha = 30°) = \frac{\pi(1.05\times10^7)(0.4)\tan(\theta)}{\ln\left\{\frac{[2(0.1875)\tan(\theta)+0.553-0.4](0.553+0.4)}{[2(0.1875)\tan(\theta)+0.553+0.4](0.553-0.4)}\right\}} = 11,252,390.70 \text{ lb/in.} \tag{H.3a}$$

$$K_1(\theta = 21.8°) = 9,826,004.03 \text{ lb/in.} \tag{H.3b}$$

H.1.2 Stiffness Element 2

The thickness of stiffness element 2 is the distance from the top loading plane to the bottom of the head fitting. This is equivalent to the thickness of stiffness element 1, since the loading plane divides the effective thickness of the head fitting equally:

$$t_2 = t_1 = 0.1875 \text{ in.} \tag{H.4}$$

Using Equation (C.2), the minor diameter of element 2 is

$$D_2(\theta = 30°) = D_1 + 2(t_1)\tan(\theta) = 0.553 + 2(0.1875)\tan(\theta) = 0.7695 \text{ in.} \tag{H.5a}$$

$$D_2(\theta = 21.8°) = 0.7030 \text{ in.} \tag{H.5b}$$

and using Equation (F.27), the stiffness is

$$K_2(\theta = 30°) = \frac{\pi(1.05\times10^7)(0.4)\tan(\theta)}{\ln\left\{\frac{[2t_2\tan(\theta)+D_2(\theta)-0.4](D_2(\theta)+0.4)}{[2t_2\tan(\theta)+D_2(\theta)+0.4](D_2(\theta)-0.4)}\right\}} = 26,148,920.08 \text{ lb/in.} \tag{H.6a}$$

$$K_2(\theta = 21.8°) = 19,216,250.30 \text{ lb/in.} \tag{H.6b}$$

H.1.3 Stiffness Element 3

Using Equation (C.2), the minor diameter of stiffness element 3 is

$$D_3(\theta = 30°) = D_2(\theta) + 2(t_2)\tan(\theta) = 0.7695 + 2(0.1875)\tan(30) = 0.9860 \text{ in.} \tag{H.7a}$$

$$D_3(\theta = 21.8°) = D_2(\theta) + 2(t_2)\tan(\theta) = 0.7030 + 2(0.1875)\tan(21.8) = 0.8530 \text{ in.} \tag{H.7b}$$

The major diameter of stiffness element 3 is the same as the outside diameter of the cylindrical spacer, which is 1.125 in. Rearranging Equation (C.2) to solve for the thickness of element 3,

$$t_3(\theta = 30°) = \frac{D_4 - D_3(\theta)}{2\tan(\theta)} = \frac{1.125 - 0.9860}{2\tan(30)} = 0.1204 \text{ in.} \tag{H.8a}$$

$$t_3(\theta = 21.8°) = \frac{D_4 - D_3(\theta)}{2\tan(\theta)} = \frac{1.125 - 0.8530}{2\tan(21.8)} = 0.3400 \text{ in.} \tag{H.8b}$$

and using Equation (F.27), the stiffness is

$$K_3(\theta = 30°) = \frac{\pi(1.05\times10^7)(0.4)\tan(\theta)}{\ln\left[\frac{(2t_3(\theta)\tan(\theta) + D_3(\theta) - 0.4)(D_3(\theta) + 0.4)}{(2t_3(\theta)\tan(\theta) + D_3(\theta) + 0.4)(D_3(\theta) - 0.4)}\right]} = 64{,}945{,}258.98 \text{ lb/in.} \tag{H.9a}$$

$$K_3(\theta = 21.8°) = 19{,}274{,}187.65 \text{ lb/in.} \tag{H.9b}$$

Equation (F.27) provides the stiffness of a frustum element in terms of the minor diameter of the frustum. Because of this, it is more convenient to calculate the stiffness of element 7 next, followed by elements 6 and 5.

H.1.4 Stiffness Element 7

The minor diameter of this stiffness element is equal to the nut diameter, which is given as

$$D_7 = 0.591 \text{ in.} \tag{H.10}$$

The lower loading plane is assumed to be at midplane of the effective thickness of the nut fitting. The effective thickness of the nut fitting is 0.375 in., and therefore the thickness of stiffness element 7 extends from the underside of the nut to the loading plane, which is equal to half the effective thickness of the nut fitting and is

$$t_7 = \frac{0.375}{2} = 0.1875 \text{ in.} \tag{H.11}$$

and using Equation (F.27), the stiffness is

$$K_7(\theta = 30°) = \frac{\pi(1.05\times10^7)(0.4)\tan(\theta)}{\ln\left[\frac{(2(0.1875)\tan(\theta) + 0.591 - 0.4)(0.591 + 0.4)}{(2(0.1875)\tan(\theta) + 0.591 + 0.4)(0.591 - 0.4)}\right]} = 13{,}599{,}003.22 \text{ lb/in.} \tag{H.12a}$$

$$K_7(\theta = 21.8°) = 12{,}031{,}470.75 \text{ lb/in.} \tag{H.12b}$$

H.1.5 Stiffness Element 6

Using Equation (C.2) with a rearrangement of its indices to accommodate the current situation of working from stiffness element 6 backwards at this point,

$$D_6(\theta = 30°) = D_7 + 2(t_7)\tan(\theta) = 0.591 + 2(0.1875)\tan(30) = 0.8075 \text{ in.} \tag{H.13a}$$

$$D_6(\theta = 21.8°) = D_7 + 2(t_7)\tan(\theta) = 0.591 + 2(0.1875)\tan(21.8) = 0.7410 \text{ in.} \tag{H.13b}$$

Stiffness element 6 extends from the lower loading plane to the interface of the nut fitting and spacer, and therefore its thickness is equal to half of the effective thickness of the nut fitting and is

$$t_6 = \frac{0.375}{2} = 0.1875 \text{ in.} \tag{H.14}$$

and using Equation (F.27), the stiffness is

$$K_6(\theta = 30°) = \frac{\pi(1.05\times10^7)(0.4)\tan(\theta)}{\ln\left\{\frac{[2(0.1875)\tan(\theta) + D_6(\theta) - 0.4](D_6(\theta) + 0.4)}{[2(0.1875)\tan(\theta) + D_6(\theta) + 0.4](D_6(\theta) - 0.4)}\right\}} = 29{,}165{,}512.20 \text{ lb/in.} \tag{H.15a}$$

$$K_6(\theta = 21.8°) = 21{,}895{,}056.58 \text{ lb/in.} \tag{H.15b}$$

H.1.6 Stiffness Element 5

Using Equation (C.2) with a rearrangement of its indices to accommodate the current situation of working from stiffness element 6 backwards at this point, the minor diameter of stiffness element 5 becomes

$$D_5(\theta = 30°) = D_6(\theta) + 2(t_6)\tan(\theta) = 0.8075 + 2(0.1875)\tan(30) = 1.024 \text{ in.} \tag{H.16a}$$

$$D_5(\theta = 21.8°) = D_6(\theta) + 2(t_6)\tan(\theta) = 0.741 + 2(0.1875)\tan(21.8) = 0.8910 \text{ in.} \tag{H.16b}$$

The major diameter of stiffness element 5 is the same as the outside diameter of the cylindrical spacer, which is 1.125 in. Rearranging Equation (C.2) to solve for the thickness of element 5,

$$t_5(\theta = 30°) = \frac{D_4 - D_5(\theta)}{2\tan(\theta)} = \frac{1.125 - 1.024}{2\tan(30)} = 0.08747 \text{ in.} \tag{H.17a}$$

$$t_5(\alpha = 21.8°) = \frac{D_4 - D_5(\alpha)}{2\tan(\alpha)} = \frac{1.125 - 0.8910}{2\tan(21.8)} = 0.2925 \text{ in.} \tag{H.17b}$$

and using Equation (F.27) the stiffness is

$$K_5(\theta = 30°) = \frac{\pi(1.05\times10^7)(0.4)\tan(\theta)}{\ln\left\{\frac{[2t_5(\theta)\tan(\theta) + D_5(\theta) - 0.4](D_5(\theta) + 0.4)}{[2t_5(\theta)\tan(\theta) + D_5(\theta) + 0.4](D_5(\theta) - 0.4)}\right\}} = 93{,}474{,}291.71 \text{ lb/in.} \tag{H.18a}$$

$$K_5(\theta = 21.8°) = 23{,}651{,}263.32 \text{ lb/in.} \tag{H.18b}$$

H.1.7 Stiffness Element 4

The stiffness of the spacer may be calculated using Equation (F.3), repeated here for convenience:

$$K = \frac{AE}{L} \tag{F.3}$$

where A is the cross-sectional area of the spacer, L is its length, and E is its modulus of elasticity. The cross-sectional area is

$$A = \frac{\pi\left(D_{out}^2 - D_{in}^2\right)}{4} = \frac{\pi\left(1.125^2 - 0.4^2\right)}{4} = 0.8684 \text{ in.}^2 \tag{H.19}$$

where D_{out} and D_{in} are the outside and inside diameter, respectively. The spacer length is equal to its baseline length of 3.0 in., minus the thickness of stiffness elements 3 and 5, and is

$$L(\theta = 30°) = 3.0 - t_3(\theta) - t_5(\theta) = 3.0 - 0.1204 - 0.08747 = 2.792 \text{ in.} \tag{H.20a}$$

$$L(\theta = 21.8°) = 3.0 - t_3(\theta) - t_5(\theta) = 3.0 - 0.34 - 0.2925 = 2.368 \text{ in.} \tag{H.20b}$$

Using Equation (F.3), the stiffness of element 4 is

$$K_4(\theta = 30°) = \frac{AE}{L} = \frac{(0.8684)\left(1.05 \times 10^7\right)}{2.792} = 3{,}265{,}830.95 \text{ lb/in.} \tag{H.21a}$$

$$K_4(\theta = 21.8°) = \frac{AE}{L} = \frac{(0.8684)\left(1.05 \times 10^7\right)}{2.368} = 3{,}850{,}591.22 \text{ lb/in.} \tag{H.21b}$$

H.1.8 Compression-Zone Flexibility

The compression-zone flexibility is the sum of the flexibilities of all seven of the stiffness elements comprising it and is

$$\frac{1}{K_c}(\theta = 30°) = \sum_{i=1}^{7} \frac{1}{K_i} = 5.67231 \times 10^{-7} \text{ in./lb} \tag{H.22a}$$

$$\frac{1}{K_c}(\theta = 21.8°) = \sum_{i=1}^{7} \frac{1}{K_i} = 6.36462 \times 10^{-7} \text{ in./lb} \tag{H.22b}$$

H.1.9 Compression-Zone Stiffness

The stiffness of the compression zone is the reciprocal of its flexibility and is

$$K_c(\theta = 30°) = 1{,}762{,}950.2 \text{ lb/in.} \tag{H.23a}$$

$$K_c(\theta = 21.8°) = 1{,}571{,}185.7 \text{ lb/in.} \tag{H.23b}$$

The stiffness-based LIF (SBLIF) n is calculated in terms of the flexibilities of the relieving load path, and the compression-zone stiffness, using Equation (30):

$$n = K_c\left(\sum_{i=2}^{6} \frac{1}{K_i}\right)_{relieved} \tag{30}$$

Substituting Equations (H.6a), (H.9a), (H.15a), (H.18a), (H.21a), and (H.23a) into Equation (30) the SBLIF for θ = 30° is

$$n(\theta = 30°) = 1{,}762{,}950.2\left(\frac{1}{26{,}148{,}920.08} + \frac{1}{64{,}945{,}258.98} + \frac{1}{3{,}265{,}830.95} + \frac{1}{93{,}474{,}291.71} + \frac{1}{29{,}165{,}512.20}\right) = 0.71 \tag{H.24a}$$

Substituting Equations (H.6b), (H.9b), (H.15b), (H.18b), (H.21b), and (H.23b) into Equation (30) the SBLIF for θ = 21.8° is

$$n(\theta = 21.8°) = 1{,}571{,}185.7\left(\frac{1}{19{,}216{,}250.30} + \frac{1}{19{,}274{,}187.65} + \frac{1}{3{,}850{,}591.22} + \frac{1}{23{,}651{,}263.32} + \frac{1}{21{,}895{,}056.58}\right) = 0.71 \tag{H.24b}$$

It is not surprising that the SBLIF does not change significantly past the second decimal point for the two different half-apex angles considered. This is because the frustra make up a minor portion of the clamped-member stiffness.

H.2 Geometric LIF

As mentioned previously, the LIF defined in Reference 9 as the ratio of the thickness of the relieving load path to the total thickness of the clamped members is denoted herein as the geometric LIF (GLIF) n_G, because it is defined entirely on geometric considerations that being the ratio of two lengths or thicknesses.

Referring to Figure H.1, the thickness of the compression zone is assumed to be the distance from the interface between the nut and nut fitting, extending through the clamped members to the interface between the bolt head and head fitting, and is given in the denominator in Equation (H.25). The external tensile load is assumed to enter the PBJ through the loading planes, which based on engineering judgment are assumed to be located in the middle of the head and nut fittings. The distance between the loading planes is given in the numerator of Equation (H.25). Therefore, the GLIF is calculated as follows using the dimensions in Figure H.1,

$$n_G = \frac{3.0 + 0.1875 + 0.1875}{3.0 + 0.375 + 0.375} = 0.90 \tag{H.25}$$

It should be noted that the LIF is a direct multiplier of the external tension load in the bolt tensile load equation. As such, the SBLIF imparts about 21 percent less external tensile load into the fastener than does the GLIF:

$$\frac{n_G - n}{n_G} \times 100 = \frac{0.9 - 0.71}{0.9} \times 100 = 21 \text{ percent} \tag{H.26}$$

Appendix G showed that FEA of this tension joint predicts the product $(n\phi)_{FEA}$ to be an average value of 0.25, which is the slope of the line from the start of the application of external tensile load up to joint separation.

The product $(n\phi)_{FEA}$ includes any prying action captured by the FEA, whereas the analytical product of the LIF and stiffness factor in this example does not.

Calculating the stiffness factor ϕ_c for this tension joint and dividing the product $(n\phi)_{FEA}$ by this stiffness factor will give the LIF n_{FEA} from FEA. Then the LIF based on FEA will be compared with the GLIF and the SBLIF.

To calculate the stiffness factor ϕ_c, the bolt stiffness must first be calculated. This can be accomplished by omitting the bolt head and nut flexibility and only using the flexibility of the bolt shank or by including the bolt head and nut flexibility as additional lengths of 0.4∗(minimum external thread diameter) for each (Ref. 10).

In comparing the SBLIF and GLIF, the bolt flexibility excluding that of the bolt head and nut will be considered, followed by the bolt flexibility including that of the bolt head and nut. Based on the finite element model geometry, the bolt in this example has a grip length of 3.625 in. with a corresponding diameter 0.375 in., and it has a threaded length between bolt shank and nut of 0.125 in. with a corresponding effective threaded diameter of 0.348 in.

H.3 Comparison of n, n_G, and n_{FEA}, Excluding Bolt Head and Nut Flexibility

Using Equation (F.4) in series, the flexibility of the bolt shank is

$$\begin{aligned}\frac{1}{K_b} &= \left(\frac{L}{AE}\right)_{\text{GRIP}} + \left(\frac{L}{AE}\right)_{\text{THREADED}} \\ &= \frac{1}{2.9\times10^{7}\ \text{psi}}\left[\frac{3.625\ \text{in.}}{\frac{\pi(0.375\ \text{in.})^2}{4}} + \frac{0.125\ \text{in.}}{\frac{\pi(0.348\ \text{in.})^2}{4}}\right] = 1.17709\times10^{-6}\ \text{in./lb}\end{aligned} \tag{H.27}$$

Taking the reciprocal of Equation (H.27), the bolt stiffness is

$$K_b = 849{,}552.7\ \text{lb/in.} \tag{H.28}$$

Substituting Equations (H.23a), (H.23b), and (H.28) into the left-hand side of Equation (B.3) repeated here for convenience, showing functional dependence on θ,

$$\phi_c(\theta) = \left(\frac{K_b}{K_b + K_c(\theta)}\right) \tag{B.3}$$

the stiffness factors are

$$\phi_c(\theta = 30°) = \left(\frac{849{,}552.7}{1{,}762{,}950.2 + 849{,}552.7}\right) = 0.325 \tag{H.29a}$$

$$\phi_c(\theta = 21.8°) = \left(\frac{849{,}552.7}{1{,}571{,}185.7 + 849{,}552.7}\right) = 0.351 \tag{H.29b}$$

Dividing the average $(n\phi)_{FEA}$ by the stiffness factors of Equations (H.29a) and (H.29b), the LIFs predicted by FEA are

$$n_{FEA}(\theta = 30°) = \frac{(n\phi)_{FEA}}{\phi_c(\theta)} = \frac{0.25}{0.325} = 0.77 \tag{H.30a}$$

$$n_{FEA}(\theta = 21.8°) = \frac{(n\phi)_{FEA}}{\phi_c(\theta)} = \frac{0.25}{0.351} = 0.71 \tag{H.30b}$$

which is an upper bound, since $\phi_c < \phi$ as shown in Appendix B, and which results in a 27-percent worst-case difference between the GLIF and the FEA prediction for the two frustra angles used:

$$\frac{n_G - n_{FEA}}{n_{FEA}} \times 100 = \frac{0.9 - 0.77}{0.77} \times 100 = 17 \text{ percent} \tag{H.31a}$$

$$\frac{n_G - n_{FEA}}{n_{FEA}} \times 100 = \frac{0.9 - 0.71}{0.71} \times 100 = 27 \text{ percent} \tag{H.31b}$$

The difference between the SBLIF and that predicted by FEA results in an 8-percent worst-case difference as shown, while matching n_{FEA} for $\theta = 21.8°$:

$$\frac{n - n_{FEA}}{n_{FEA}} \times 100 = \frac{0.71 - 0.77}{0.77} \times 100 = -8 \text{ percent} \tag{H.32a}$$

$$\frac{n - n_{FEA}}{n_{FEA}} \times 100 = \frac{0.71 - 0.71}{0.71} \times 100 = 0 \text{ percent} \tag{H.32b}$$

Even in this pure tension joint, with physical geometry biased towards a cylindrical compression zone, the SBLIF using ϕ_c compared more favorably with FEA than did the GLIF.

H.4 Comparison of n, n_G, and n_{FEA} Including Bolt Head and Nut Flexibility

Now the SBLIF and the GLIF will be compared with the LIF predicted by FEA, including the additional flexibility of the bolt head and nut (Ref. 10). Including these additional terms, the total bolt flexibility becomes

$$\frac{1}{K_b} = \frac{1}{2.9 \times 10^7 \text{ psi}} \left[\frac{3.625 \text{ in.} + 0.4(0.348 \text{ in.})}{\frac{\pi(0.375 \text{ in.})^2}{4}} + \frac{0.125 \text{ in.} + 0.4(0.348 \text{ in.})}{\frac{\pi(0.348 \text{ in.})^2}{4}} \right] = 1.27101 \times 10^{-6} \text{ in./lb} \tag{H.33}$$

Taking the reciprocal of Equation (H.33), the bolt stiffness is

$$K_b = 786,775.9 \text{ lb/in.} \tag{H.34}$$

which is about a 7.4-percent stiffness decrease from the bolt stiffness without including the bolt head and nut flexibility as shown in Equation (H.28). Substituting Equations (H.23a), (H.23b), and (H.34) into Equation (25) the stiffness factors are

$$\phi_c(\theta = 30°) = \left(\frac{786,775.9}{1,762,953.3 + 786,775.9} \right) = 0.309 \tag{H.35a}$$

$$\phi_c(\theta = 21.8°) = \left(\frac{786,775.9}{1,571,185.7 + 786,775.9} \right) = 0.334 \tag{H.35b}$$

Dividing $(n\phi)_{FEA}$ by the stiffness factors, Equations (H.35a) and (H.35b), gives

$$n_{FEA}(\theta = 30°) = \frac{(n\phi)_{FEA}}{\phi_c(\theta)} = \frac{0.25}{0.309} = 0.81 \tag{H.36a}$$

$$n_{FEA}(\theta = 21.8°) = \frac{(n\phi)_{FEA}}{\phi_c(\theta)} = \frac{0.25}{0.334} = 0.75 \tag{H.36b}$$

which is an upper bound, since $\phi_c < \phi$ as shown in Appendix B (see Eq. (B.3)), and which results in a 20-percent worst-case difference between the FEA prediction and the GLIF for the two frustra angles used,

$$\frac{n_G - n_{FEA}}{n_{FEA}} \times 100 = \frac{0.9 - 0.81}{0.81} \times 100 = 11 \text{ percent} \tag{H.37a}$$

$$\frac{n_G - n_{FEA}}{n_{FEA}} \times 100 = \frac{0.9 - 0.75}{0.75} \times 100 = 20 \text{ percent} \tag{H.37b}$$

and a 12-percent worst-case difference with the SBLIF for $\theta = 30°$, while resulting in a 5-percent difference for $\theta = 21.8°$:

$$\frac{n - n_{FEA}}{n_{FEA}} \times 100 = \frac{0.71 - 0.81}{0.81} \times 100 = -12 \text{ percent} \tag{H.38a}$$

$$\frac{n - n_{FEA}}{n_{FEA}} \times 100 = \frac{0.71 - 0.75}{0.75} \times 100 = -5 \text{ percent} \tag{H.38b}$$

The comparisons between the GLIF, SBLIF, and FEA LIF are summarized in Table H.1.

TABLE H.1.—COMPARISON OF FINITE ELEMENT, GEOMETRIC, AND STIFFNESS-BASED LIF FOR PURE TENSION JOINT OF APPENDIX H WITH DIFFERENT HALF-APEX ANGLES[a]
[$n\phi = 0.25$.]

(a) $\theta = 30°$

LIF	Without bolt head and nut flexibility $\phi_c(\theta) = 0.325$	With bolt head and nut flexibility $\phi_c(\theta) = 0.309$
$n_{FEA}(\theta)$	0.77	0.81
n_G	0.9 (17%)	0.9 (11%)
$n(\theta)$	0.71 (–8%)	0.71 (–12%)

(b) $\theta = 21.8$

LIF	Without bolt head and nut flexibility $\phi_c(\theta) = 0.351$	With bolt head and nut flexibility $\phi_c(\theta) = 0.334$
$n_{FEA}(\theta)$	0.71	0.75
n_G	0.9 (27%)	0.9 (20%)
$n(\theta)$	0.71 (0%)	0.71 (–5%)

[a]Percent difference (rounded) between the predicted and FEA LIF (Appendix G) is shown in parentheses.

Appendix I.—Calculated SBLIF for Comparison With Experiment

The following sequence of calculations demonstrate how the SBLIF is calculated for the PBJ used in the experiments of Reference 3. The compression-zone stiffness is used instead of the clamped-members tensile stiffness. Using the information from Reference 3, the back-to-back frustra and cylindrical geometry are used to represent the compression zone corresponding to the various flange diameters. The compression-zone geometry corresponding to a 60-mm flange is shown in Figure I.1.

The compression zone is divided into six segments. Because of symmetry about the faying surface, segments 1 through 3 are geometrically the same as segments 6 through 4, respectively. The modulus of elasticity is the same for all six segments and is 200,000 N/mm^2.

Using the reciprocal of Equation (F.27), the flexibility $1/K$ of segments 1 and 6 is calculated to be

$$\frac{1}{K_1}=\frac{1}{K_6}=\frac{\ln\left\{\dfrac{[2(36)\tan(30)+17-10](17+10)}{[2(36)\tan(30)+17+10](17-10)}\right\}}{\pi(200{,}000\ \text{N/mm}^2)(10)\tan(30)}=2.77063\times10^{-7}\ \text{mm/N} \tag{I.1}$$

Likewise, the flexibility of segments 2 and 5 is calculated to be

$$\frac{1}{K_2}=\frac{1}{K_5}=\frac{\ln\left\{\dfrac{[2(1.239)\tan(30)+58.56921938-10](58.56921938+10)}{[2(1.239)\tan(30)+58.56921938+10](58.56921938-10)}\right\}}{\pi(200{,}000\ \text{N/mm}^2)(10)\tan(30)} \tag{I.2}$$

$$=2.31032\times10^{-9}\ \text{mm/N}$$

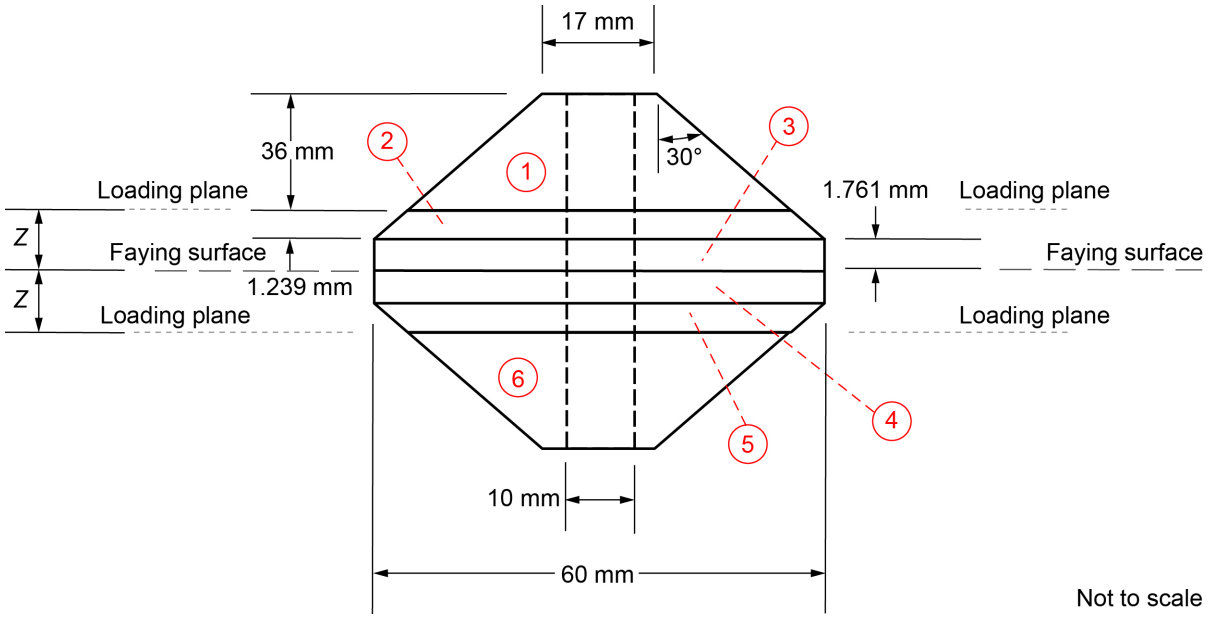

Figure I.1.—Geometric approximation of compression zone for 60-mm-diameter flange of experiments of Reference 3.

Using the reciprocal of Equation (F.3), the flexibility of segments 3 and 4 is

$$\frac{1}{K_3} = \frac{1}{K_4} = \frac{4(1.761)}{\pi\left(60.000^2 - 10^2\right)\left(200{,}000 \text{ N/mm}^2\right)} = 3.20311 \times 10^{-9} \text{ mm/N} \tag{I.3}$$

The flexibility of the compression zone becomes

$$\begin{aligned} \frac{1}{K_c} &= 2\left(\frac{1}{K_1} + \frac{1}{K_2} + \frac{1}{K_3}\right) = 2\left(2.77063 \times 10^{-7} + 2.31032 \times 10^{-9} + 3.20311 \times 10^{-9}\right) \\ &= 5.65153 \times 10^{-7} \text{ mm/N} \end{aligned} \tag{I.4}$$

and taking the inverse of Equation (I.4), the stiffness of the compression zone is

$$K_c = 1{,}769{,}432 \text{ N/mm} \tag{I.5}$$

Using the flexibilities of segments 2 and 3, the flexibility of the relieving load path is obtained:

$$\frac{1}{K_{2-4}} = 2\left(\frac{1}{K_2} + \frac{1}{K_3}\right) = 2\left(2.31032 \times 10^{-9} + 3.20311 \times 10^{-9}\right) = 1.10269 \times 10^{-8} \text{ mm/N} \tag{I.6}$$

Taking the reciprocal of Equation (I.6), the stiffness of the relieving load path is

$$K_{2-4} = 90{,}687{,}319 \text{ N/mm} \tag{I.7}$$

Using Equation (45), the SBLIF is calculated to be

$$n = \frac{K_c}{K_{2-4}} = \frac{1{,}769{,}432}{90{,}687{,}319} = 0.019511 \tag{I.8}$$

Detailed calculations for all flange diameters are shown in Table I.1.

TABLE I.1.—CALCULATION OF SBLIF *n* FOR EXPERIMENTAL CONFIGURATION OF FIGURE 19 AND PRESENTED IN FIGURE 20

[Tensile and relieving load-path stiffnesses were calculated using Equations (F.3) and (F.27).]

[Cells highlighted in gray are associated specifically with relieving load path.]

Flange diameter, mm							
80				60			
Element,[a] i	Thickness, t, mm	Diameter,[b] D_i, mm	Flexibility, mm/N	Element,[a] i	Thickness, t, mm	Diameter,[b] D_i, mm	Flexibility, mm/N
Distance of faying surface to loading plane, Z = 3 mm							
1	36	17	2.77063×10^{-7}	1	36	17	2.77063×10^{-7}
2	3	58.56921938	5.40557×10^{-9}	2	1.239	58.56921938	2.31032×10^{-9}
3	NA			3	1.761	59.99989335	3.20311×10^{-9}
4	NA			4	1.761	59.99989335	3.20311×10^{-9}
5	3	58.56921938	5.40557×10^{-9}	5	1.239	58.56921938	2.31032×10^{-9}
6	36	17	2.77063×10^{-7}	6	36	17	2.77063×10^{-7}
Total = 78		$1/K_c = 5.64937\times10^{-7}$		Total = 78		$1/K_c = 5.65153\times10^{-7}$	
K_c = 1,770,109.15 N/mm $K_{2\text{–}4}$ = 92,497,126.40 N/mm **n = 0.01913691**				K_c = 1,769,433.55 N/mm $K_{2\text{–}4}$ = 90,687,731.50 N/mm **n = 0.019511278**			
Z = 19.5 mm							
1	19.5	17	2.29511×10^{-7}	1	19.5	17	2.29511×10^{-7}
2	19.5	39.5166605	5.29578×10^{-8}	2	17.739	39.5166605	4.98626×10^{-8}
3	NA			3	1.761	60	3.20311×10^{-9}
4	NA			4	1.761	60	3.20311×10^{-9}
5	19.5	39.5166605	5.29578×10^{-8}	5	17.739	39.5166605	4.98626×10^{-8}
6	19.5	17	2.29511×10^{-7}	6	19.5	17	2.29511×10^{-7}
Total = 78		$1/K_c = 5.64937\times10^{-7}$		Total = 78		$1/K_c = 5.65153\times10^{-7}$	
K_c = 1,770,109.15 N/mm $K_{2\text{–}4}$ = 9,441,471.35 N/mm **n = 0.187482341**				K_c = 1,769,433.55 N/mm $K_{2\text{–}4}$ = 9,422,282.35 N/mm **n = 0.187792456**			
Z = 36 mm							
1	3	17	7.75522×10^{-8}	1	3	17	7.75522×10^{-8}
2	36	20.46410162	2.04916×10^{-7}	2	34.239	20.46410162	2.01821×10^{-7}
3	NA			3	1.761	60	3.20311×10^{-9}
4	NA			4	1.761	60	3.20311×10^{-9}
5	36	20.46410162	2.04916×10^{-7}	5	34.239	20.46410162	2.01821×10^{-7}
6	3	17	7.75522×10^{-8}	6	3	17	7.75522×10^{-8}
Total = 78		$1/K_c = 5.64937\times10^{-7}$		Total = 78		$1/K_c = 5.65153\times10^{-7}$	
K_c = 1,770,109.15 N/mm $K_{2\text{–}4}$ = 2,440,021.04 N/mm **n = 0.725448315**				K_c = 1,769,433.55 N/mm $K_{2\text{–}4}$ = 2,438,737.48 N/mm **n = 0.725553104**			

[a]Elements 1, 2, 5, and 6 are frustra; elements 3 and 4 are sleeves.

[b]Diameter of small end.

TABLE I.1.—CONCLUDED

Flange diameter, mm							
40				20			
Element,[a] i	Thickness, t, mm	Diameter,[b] D_i, mm	Flexibility, mm/N	Element,[a] i	Thickness, t, mm	Diameter,[b] D_i, mm	Flexibility, mm/N
Distance of faying surface to loading plane, Z = 3 mm							
1	19.919	17	2.31312×10^{-7}	1	2.598	17	6.92768×10^{-8}
2	16.081	40.00048002	6.82499×10^{-8}	2	33.402	19.999912	7.08812×10^{-7}
3	3	40	1.27324×10^{-8}	3	3	20	6.3662×10^{-8}
4	3	40	1.27324×10^{-8}	4	3	20	6.3662×10^{-8}
5	16.081	40.00048002	6.82499×10^{-8}	5	33.402	19.999912	7.08812×10^{-7}
6	19.919	17	2.31312×10^{-7}	6	2.598	17	6.92768×10^{-8}
Total = 78		$1/K_c = 6.24589\times10^{-7}$		Total = 78		$1/K_c = 1.6835\times10^{-6}$	
K_c = 1,601,053.45 N/mm $K_{2\text{–}4}$ = 39,269,908.17 N/mm **n = 0.040770491**				K_c = 593,999.70 N/mm $K_{2\text{–}4}$ = 7,853,981.63 N/mm **n = 0.075630391**			
Z = 19.5 mm							
1	19.5	17	2.29511×10^{-7}	1	2.598	17	6.92768×10^{-8}
2	0.419	39.5166605	1.80149×10^{-9}	2	16.902	19.999912	3.58672×10^{-7}
3	19.081	40	8.09823×10^{-8}	3	19.5	20	4.13803×10^{-7}
4	19.081	40	8.09823×10^{-8}	4	19.5	20	4.13803×10^{-7}
5	0.419	39.5166605	1.80149×10^{-9}	5	16.902	19.999912	3.58672×10^{-7}
6	19.5	17	2.29511×10^{-7}	6	2.598	17	6.92768×10^{-8}
Total = 78		$1/K_c = 6.24589\times10^{-7}$		Total = 78		$1/K_c = 1.6835\times10^{-6}$	
K_c = 1,601,053.45 N/mm $K_{2\text{–}4}$ = 6,039,830.98 N/mm **n = 0.265082493**				K_c = 593,999.70 N/mm $K_{2\text{–}4}$ = 1,208,304.87 N/mm **n = 0.49159754**			
Z = 36 mm							
1	3	17	7.75522×10^{-8}	1	2.598	17	6.92768×10^{-8}
2	16.919	20.46410162	1.5376×10^{-7}	2	0.402	19.999912	8.53070×10^{-9}
3	19.081	40	8.09823×10^{-8}	3	36	20	7.63944×10^{-7}
4	19.081	40	8.09823×10^{-8}	4	36	20	7.63944×10^{-7}
5	16.919	20.46410162	1.5376×10^{-7}	5	0.402	19.999912	8.53070×10^{-9}
6	3	17	7.75522×10^{-8}	6	2.598	17	6.92768×10^{-8}
Total = 78		$1/K_c = 6.24589\times10^{-7}$		Total = 78		$1/K_c = 1.6835\times10^{-6}$	
K_c = 1,601,053.45 N/mm $K_{2\text{–}4}$ = 2,129,996.30 N/mm **n = 0.751669595**				K_c = 593,999.70 N/mm $K_{2\text{–}4}$ = 654,498.47 N/mm **n = 0.907564688**			

[a]Elements 1, 2, 5, and 6 are frustra; elements 3 and 4 are sleeves.

[b]Diameter of small end.

Appendix J.—Detailed Derivation of Joint Diagram

The joint diagram is a plot of the load-displacement curves of the various preloaded bolted joint (PBJ) load paths and their associated regions. The joint diagram is constructed by presenting the load-displacement curves of interest on the same plot. The following sections will address the detailed construction of the joint diagram in terms of the stiffness-based load introduction factor (SBLIF), preload, and mechanical tensile and thermal loads, by first considering the preload phase.

J.1 Preload Phase

For the preload phase, only the bolt and compression-zone load paths are explicitly exercised, as shown in Figure 6.

J.1.1 Compression Zone

Using Hooke's Law, the preload P_0 may be expressed in terms of the stiffness of the compression zone K_c and its displacement at preload δ_{c_0} :

$$P_0 = K_c \delta_{c_0} \tag{J.1}$$

Solving for the compression-zone displacement,

$$\delta_{c_0} = \frac{P_0}{K_c} \tag{J.2}$$

J.1.2 Bolt Tension Load Path

The displacement of the bolt at preload equilibrium δ_{b_0} is determined using Hooke's Law as shown:

$$\delta_{b_0} = \frac{P_0}{K_b} \tag{J.3}$$

where K_b is the bolt stiffness. The load-displacement relationships for the bolt and compression zone have been determined for the preload phase and may be plotted in a Cartesian coordinate system.

Referring to Figure 11, and considering preload only by setting the external load f_c to 0, the preload applies a tension load to the fastener and an equal and opposite compressive load to the compressed region. Since the bolt has a positive displacement under a positive (tensile) external load, the load-displacement curve for the bolt lies in quadrant I of a typical Cartesian coordinate system with positive load on the positive ordinate and positive displacement on the positive abscissa.

This same preload that imparts a tensile load to the bolt also imparts an equal and opposite compressive load to the compression zone. This compressive load decreases the thickness of the compression zone. Since the compression zone decreases in thickness under a negative (compressive) load, its load-deflection curve naturally exists in quadrant III below the abscissa of the same Cartesian coordinate system used for the bolt. These load-displacement relationships may be plotted as curves above and below the abscissa, as depicted in Figure J.1. The load-deflection curves of the bolt and compression zone originate at the origin because their changes of displacement are plotted excluding their original thickness.

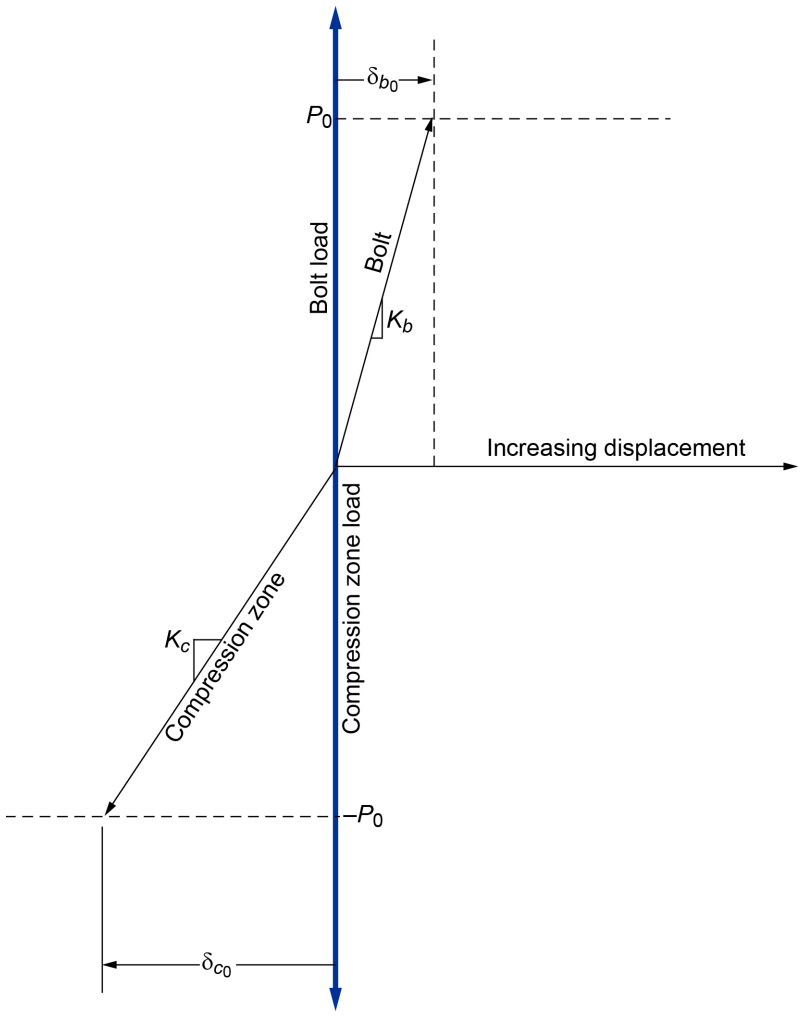

Figure J.1.—Load-displacement curves of PBJ and compression zone under preload only, in natural coordinates.

Traditionally, all the load-displacement curves of a joint diagram are plotted above the abscissa, which make it easier to see the interaction of the various load paths as the external tensile and thermal loads are varied. To accomplish this traditional joint diagram format, the load-displacement curve for the compression zone in its natural coordinates is mirrored about and translated along the abscissa, such that at preload the load-displacement curves of the bolt and compression zone join at the bolt preload coordinates $\left(P_0, \delta_{b_0}\right)$, as shown in Figure J.2.

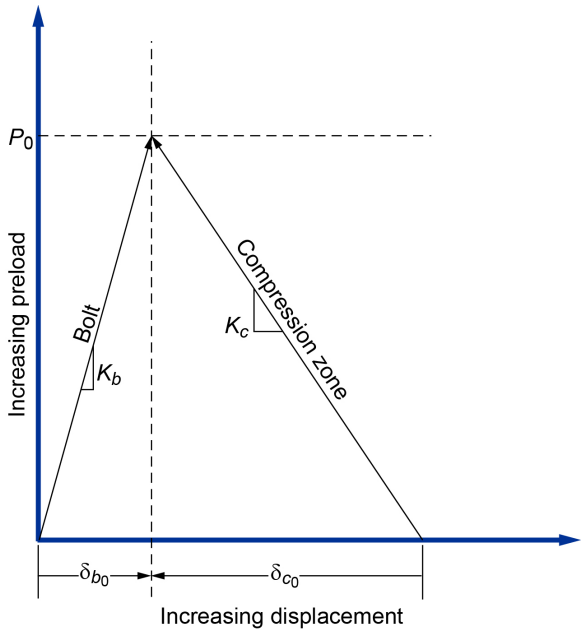

Figure J.2.—Load-path presentation of PBJ joint diagram up to preload.

J.2 Tensile Load Application After Preload

When tensile load is applied to the PBJ after preload, only the clamping and relieving load paths are explicitly exercised, with the clamping load path consisting of the bolt and compressed regions, as shown in Figure 5.

Consider the free-body diagram of Figure 8, represented by six individual free-body diagrams as depicted in Figure J.3. From Equation (36), the bolt load is equal to the sum of the preload P_0; the product of the LIF, stiffness factor, and external load, $n\phi P_{ext}$; and the thermal load P_{th}. It can be seen by summation of forces in the vertical direction of the topmost free-body diagram of Figure J.3 that

$$\sum F_x = 0 : F_c - (P_0 + n\phi P_{ext} + P_{th}) = 0 \tag{J.4}$$

The compressive force F_c in the clamping load path, and thus in the compressed region because it is part of this load path, is

$$F_c = P_0 + n\phi P_{ext} + P_{th} \tag{J.5}$$

which is equal in magnitude to the tensile bolt load P_b. Using this value of F_c, the remaining relieving load-path forces F_r in Figure J.3 may be determined and are shown in Figure J.4.

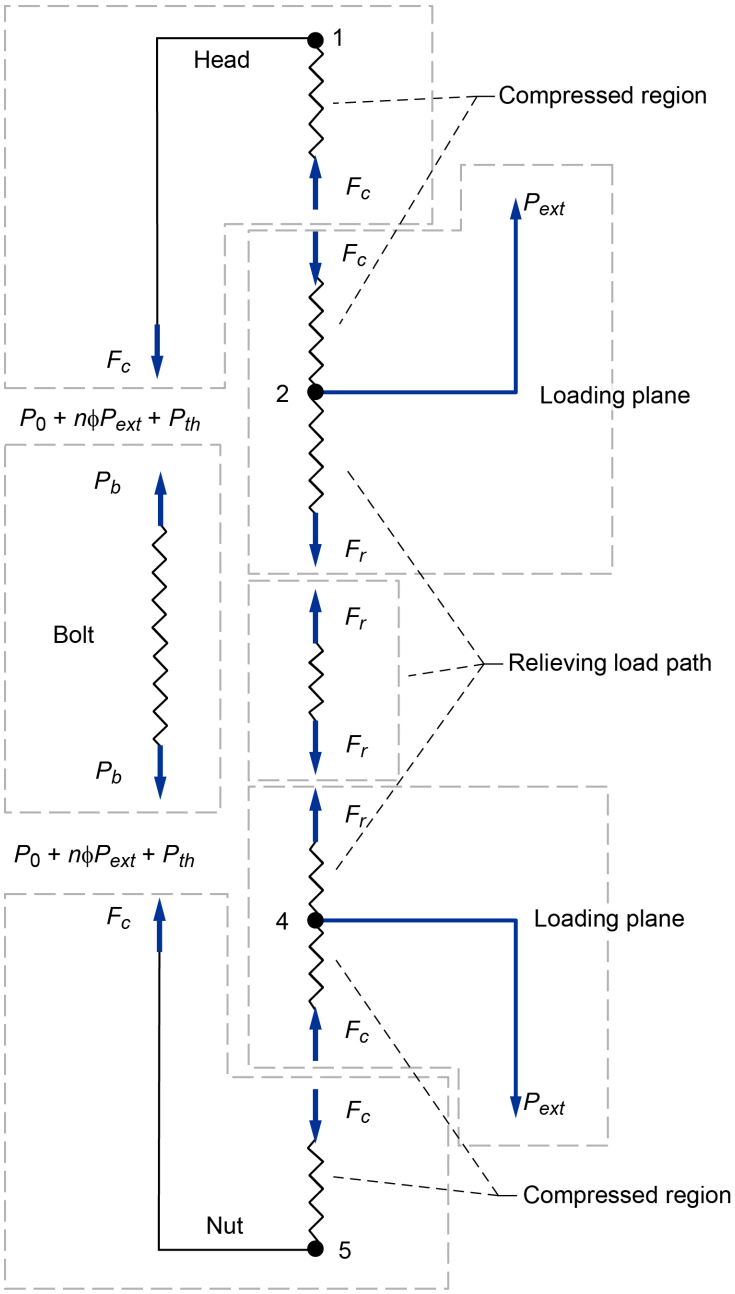

Figure J.3.—Free-body diagram of PBJ represented by springs under mechanical and thermal loading, showing assumed directions of forces.

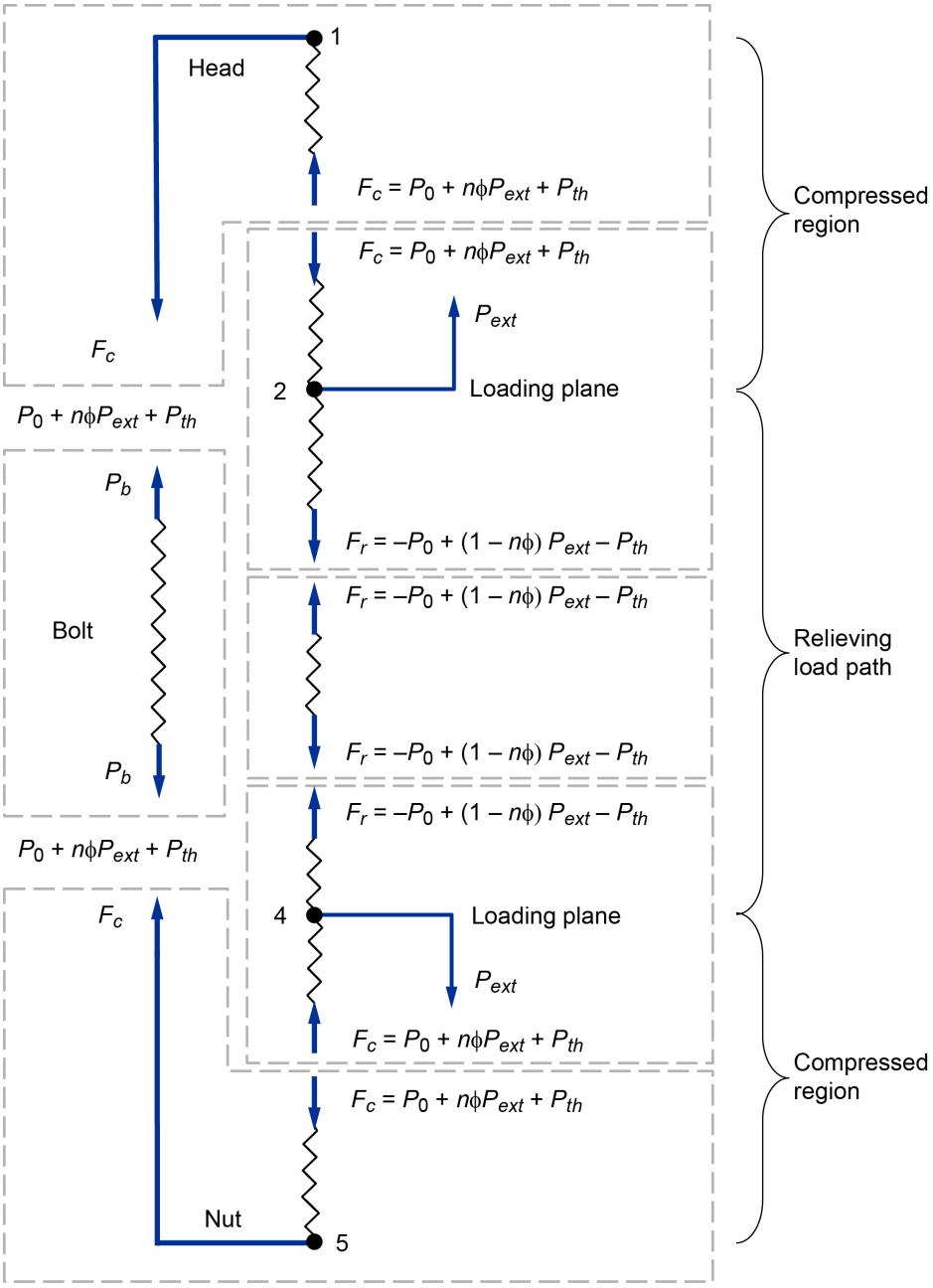

Figure J.4.—Free-body diagram of PBJ represented by springs, under combined mechanical and thermal loading, showing magnitude of forces.

J.2.1 Relieving Load Path

The stiffness of the relieving load path $K_{2\text{–}4}$, in terms of the SBLIF, is obtained by rearranging Equation (45):

$$K_{2-4} = \frac{K_a}{n} \tag{J.6}$$

where K_a is the stiffness of the clamped-members' tension load path. The displacement of the relieving load path δ_{2-4} may be expressed in terms of mechanical and thermal loads using Hooke's Law and the stiffness expressed in Equation (J.6):

$$\delta_{2-4} = \frac{F_r}{K_{2-4}} = \frac{F_r\, n}{K_a} \tag{J.7}$$

It can be seen by the free-body diagrams of Figure J.4 that the portion of the external load being reacted by the relieving load-path F_r is

$$F_r = P_{ext}(1 - n\phi) - P_0 - P_{th} \tag{J.8}$$

Substituting Equation (J.8) into Equation (J.7) and rearranging, δ_{2-4} becomes

$$\delta_{2-4} = \frac{-P_0 n + P_{ext}(1 - n\phi)n - nP_{th}}{K_a} \tag{J.9}$$

Upon substituting Equations (25) and (34) into Equation (J.9) and separating into terms associated with preload, mechanical tensile load, and thermal load,

$$\delta_{2-4} = -\frac{P_0\, n}{K_a} + \frac{P_{ext}\, n\left[K_a + (1-n)K_b\right]}{K_a\left(K_a + K_b\right)} - \frac{K_b L \Delta T\left(\alpha_a - \alpha_b\right)n}{\left(K_a + K_b\right)} \tag{J.10}$$

where L is the thickness of the clamped members, ΔT is the change in temperature, and α_a and α_b are the effective thermal expansion coefficients of the clamped members and thermal expansion coefficient of the bolt, respectively.

J.2.2 Compressed Region

The flexibility of the compressed region in terms of the SBLIF is obtained by substituting Equation (26) into Equation (31):

$$\frac{1}{K^*_{1-2,4-5}} = \frac{1}{QK_a} = \frac{1-n}{K_a} \tag{J.11}$$

Using Hooke's Law, the displacement of the compressed region $\delta^*_{1-2,4-5}$, may be expressed in terms of the SBLIF, mechanical and thermal loads of the clamping load path, and the flexibility given in Equation (J.11) as

$$\delta^*_{1-2,4-5} = -\frac{F_c}{K^*_{1-2,4-5}} = -\frac{F_c(1-n)}{K_a} \tag{J.12}$$

where the negative sign is introduced because the displacement is a contraction under the positive load F_c, violating the convention that the load and its corresponding displacement must be of the same sign.

Substituting Equation (J.5) into Equation (J.12), the displacement of the compressed region is

$$\delta^*_{1-2,4-5} = -\frac{\left[P_0 + n\phi P_{ext} + P_{th}\right](1-n)}{K_a} \tag{J.13}$$

Substituting Equations (25) and (34) into Equation (J.13) and separating into terms associated with preload, mechanical load, and thermal load gives

$$\delta^{*}_{1-2,4-5} = -\frac{P_0(1-n)}{K_a} - \frac{P_{ext}\, nK_b(1-n)}{K_a(K_a+K_b)} - \frac{K_b L\Delta T(\alpha_a-\alpha_b)(1-n)}{(K_a+K_b)} \tag{J.14}$$

J.2.3 Clamping Load Path

Substituting Equation (26) into Equation (12), the flexibility of the clamping load path is

$$\frac{1}{K_{1-2,4-5}} = \frac{1-n}{K_a} + \frac{1}{K_b} = \frac{(1-n)K_b + K_a}{K_a K_b} \tag{J.15}$$

The displacement of the clamping load-path $\delta_{1-2,4-5}$, may be expressed in terms of mechanical and thermal loads using Hooke's Law and the flexibility of the clamping load path:

$$\delta_{1-2,4-5} = \frac{F_c}{K_{1-2,4-5}} = \frac{F_c\left[(1-n)K_b + K_a\right]}{K_a K_b} \tag{J.16}$$

Substituting Equation (J.5) into Equation (J.16),

$$\delta_{1-2,4-5} = \frac{(P_0 + n\phi P_{ext} + P_{th})\left[(1-n)K_b + K_a\right]}{K_a K_b} \tag{J.17}$$

Substituting Equations (25) and (34) into Equation (J.17) and separating into terms associated with preload, mechanical tensile load, and thermal load, the displacement of the clamping load path becomes

$$\delta_{1-2,4-5} = \frac{P_0\left[(1-n)K_b + K_a\right]}{K_a K_b} + \frac{P_{ext}\, n\left[(1-n)K_b + K_a\right]}{K_a(K_a+K_b)} + \frac{L\Delta T(\alpha_a-\alpha_b)\left[(1-n)K_b + K_a\right]}{(K_a+K_b)} \tag{J.18}$$

J.2.4 Clamped-Members' Tension Load Path

By definition, assuming no gapping of faying surfaces, the displacement of the clamped-members' tension load path δ_a is equal to the sum of the displacements of the compressed region and relieving load path. This is expressed mathematically as

$$\delta_a = \delta^{*}_{1-2,4-5} + \delta_{2-4} \tag{J.19}$$

Substituting Equations (J.10) and (J.14) into Equation (J.19),

$$\begin{aligned}\delta_a = &-\frac{P_0(1-n)}{K_a} - \frac{P_{ext}\, nK_b(1-n)}{K_a(K_a+K_b)} - \frac{K_b L\Delta T(\alpha_a-\alpha_b)(1-n)}{(K_a+K_b)} \\ &-\frac{P_0 n}{K_a} + \frac{P_{ext}\, n\left[K_a + (1-n)K_b\right]}{K_a(K_a+K_b)} - \frac{K_b L\Delta T(\alpha_a-\alpha_b)n}{(K_a+K_b)}\end{aligned} \tag{J.20}$$

Combining terms,

$$\delta_a = -\frac{P_0}{K_a} + \frac{P_{ext}\, n}{K_a + K_b} - \frac{K_b L \Delta T (\alpha_a - \alpha_b)}{(K_a + K_b)} \tag{J.21}$$

J.2.5 Bolt

The displacement of the bolt δ_b may be expressed in terms of mechanical and thermal loads using Hooke's Law and the stiffness of the bolt:

$$\delta_b = \frac{F_c}{K_b} \tag{J.22}$$

Substituting Equation (J.5) into Equation (J.22),

$$\delta_b = \frac{P_0 + n\phi P_{ext} + P_{th}}{K_b} = \frac{P_0(K_a + K_b) + nK_b P_{ext} + P_{th}(K_a + K_b)}{K_b(K_a + K_b)} \tag{J.23}$$

Substituting Equations (25) and (34) into Equation (J.23) and separating into terms associated with preload, mechanical tensile load, and thermal load, the displacement of the bolt becomes

$$\delta_b = \frac{P_0}{K_b} + \frac{P_{ext}\, n}{K_a + K_b} + \frac{K_a L \Delta T (\alpha_a - \alpha_b)}{K_a + K_b} \tag{J.24}$$

It can be observed by comparing the mechanical tensile load term of Equations (J.10), (J.14), (J.18), and (J.23) that the corresponding displacement of the clamping load path is equal to the displacement of the relieving load path and also equal to the difference between the corresponding displacements of the bolt and compressed region, as represented mathematically in Equation (J.25) and shown here in Figure 21:

$$\delta_{1-2,4-5} = \delta_b - \delta^*_{1-2,4-5} = \delta_{2-4} \tag{J.25}$$

It can be observed by comparing the mechanical tensile load term of Equations (J.21) and (J.24) that the corresponding displacement of the clamped-members' tension load path is equal to the displacement of the bolt, as represented mathematically in Equation (J.26) and shown in Figure 21:

$$\delta_a = \delta_b \tag{J.26}$$

As mentioned previously, it is usually assumed that the compression-zone stiffness K_c is equivalent to K_a. In so doing, in joint diagrams the bolt displacement after preload is shown to be equivalent to the displacement of the preload load path; that is, the compression-zone load path, which is an approximation. Instead, it is theoretically correct to use K_a for this purpose, which is illustrated in Figure 21, where the displacement of the bolt is equal to that of the clamped-members' tension load path.

A traditional approach for showing the effects of the LIF on PBJs is to plot the load-displacement curve of both the clamping load path and relieving load path δ_{2-4}, on a joint diagram, as shown in Figure 21. Because we are assuming no gapping of faying surfaces, the displacement after preload of the clamping members $\delta_{1-2,4-5}$ due to mechanical loads equals that of the relieving members δ_{2-4}. This is shown by comparing the mechanical loading terms of Equations (J.10) and (J.18) and is indicated in Figure 21 by the vertical dashed line connecting the load-displacement curves of the clamping and relieving load paths.

Consider the free-body diagram of Figure 10 as shown in Figure J.5 with the displacements of the clamping and relieving load paths identified. The reaction loads shown here are those above preload and thermal load of the clamping and relieving load paths due to an external tension load, given in Equations (J.5) and (J.8), respectively, after setting P_0 and P_{th} equal to 0.

The loads reacted by the clamping and relieving load paths after preload are depicted in Figure 21. The loads reacted by the bolt and clamped-member tension load path are also depicted here. The loads acting on the clamping and relieving load paths are tension loads, serving to increase the load in the clamping load path and reduce the preload compression in the relieving load path.

Figure 21 only plots the portion of the clamping load path after preload. The load-deflection curve of the relieving load path and clamped-members' tension load path are represented with dashed lines that indicate the unrealized portion of their load paths under further increase of external tension load.

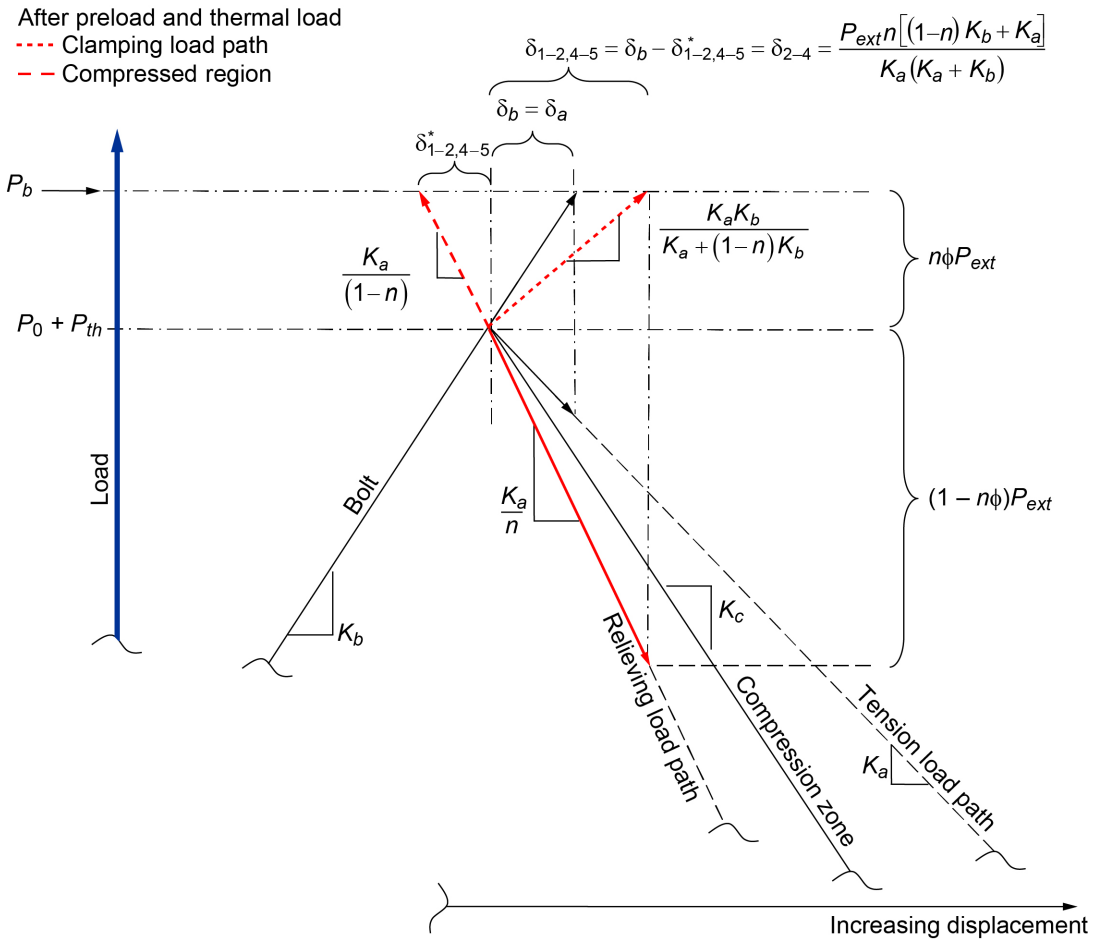

Figure 21.—Closeup view of PBJ joint diagram showing load-deflection curves for bolt, tension, clamping, and relieving load paths as well as compression zone. Load-deflection curves of compression zone and clamped-members' tension load paths are shown as being distinct but are usually assumed to be same.

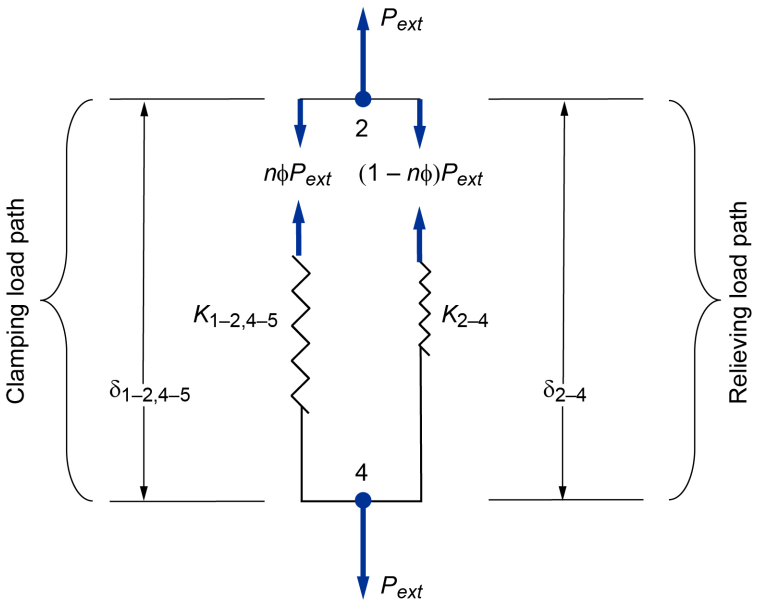

Figure J.5.—Stiffness representation of PBJ, indicating displacement and load being reacted by clamping and relieving load paths after preload.

J.3 Formulas for Key Features of Joint Diagram

The equations for the stiffness, displacement, and force for the bolt and the various load paths and associated regions of a PBJ under mechanical tensile and thermal loading have been derived in the previous sections of this appendix and are presented in Table J.1 in their natural coordinate systems. The corresponding force on the bolt and the various load paths and associated regions of the PBJ are obtained by the product of their stiffness and associated displacement; this force is also presented in Table J.1. Specifically, elements of column 4 may be obtained by multiplying elements of columns 2 and 3; elements of column 6 may be obtained by multiplying elements of columns 2 and 5; and lastly, elements of column 8 may be obtained by multiplying elements of columns 2 and 7.

The equations from Table J.1 are useful in creating joint diagrams. By applying the appropriate sign changes to the equations in Table J.1, the load-displacement curves may be plotted in quadrant I per tradition. In so doing, the load-displacement curves are mirrored from below to above the abscissa. By applying the appropriate displacement offsets, the load-displacement curves are translated along the abscissa, resulting in the formulas for the key coordinates of the traditional joint diagram for a PBJ under purely mechanical tensile load as shown in Table J.2, and for a PBJ under both thermal and mechanical tensile load as shown in Table J.3. The equations in Table J.2 and Table J.3 are based on the assumptions that the ordinate intersects the abscissa at the point of zero bolt load and that the load-displacement curves for all regions plotted intersect at the bolt preload coordinates $(P_{th}/K_b, P_0)$.

As an example, a joint diagram is created for the PBJ of Appendix C, as shown in Figure J.6. Coordinates of the points 1 to 6 in Figure J.6 are listed in Table J.2. They were calculated using the coordinate formulas also shown in the table with the input values from the table footnote and the SBLIF calculated in Appendix C. The coordinate formulas given in Table J.2 were determined from the formulas from Table J.1.

TABLE J.1.—CONTRIBUTION FROM PRELOAD, THERMAL LOAD, AND MECHANICAL TENSILE LOAD TO STIFFNESS, DISPLACEMENT, AND FORCE OF LOAD PATHS AND REGIONS OF PBJ

	Stiffness	Preload component		Thermal load component		Mechanical tensile load component	
		Displacement	Force	Displacement	Force[a]	Displacement	Force
Compressed region	$\frac{K_a}{(1-n)}$	$-\frac{P_0(1-n)}{K_a}$	$-P_0$	$-\frac{K_b L\Delta T(\alpha_a-\alpha_b)(1-n)}{(K_a+K_b)}$	$-P_{th}$	$-\frac{P_{ext}\,n(1-n)K_b}{K_a(K_a+K_b)}$	$-\frac{P_{ext}\,n\,K_b}{K_a+K_b}$
Relieving load path	$\frac{K_a}{n}$	$-\frac{P_0\,n}{K_a}$	$-P_0$	$-\frac{K_b L\Delta T(\alpha_a-\alpha_b)n}{(K_a+K_b)}$	$-P_{th}$	$P_{ext}\,n\left[\frac{(1-n)K_b+K_a}{K_a(K_a+K_b)}\right]$	$\frac{P_{ext}\left[(1-n)K_b+K_a\right]}{(K_a+K_b)}$
Clamping load path	$\frac{K_aK_b}{(1-n)K_b+K_a}$	$\frac{P_0\left[(1-n)K_b+K_a\right]}{K_aK_b}$	P_0	$\frac{L\Delta T(\alpha_a-\alpha_b)\left[K_a+(1-n)K_b\right]}{(K_a+K_b)}$	P_{th}	$P_{ext}\,n\left[\frac{(1-n)K_b+K_a}{K_a(K_a+K_b)}\right]$	$\frac{P_{ext}\,n\,K_b}{K_a+K_b}$
Clamped-members' tension load path	K_a	$-\frac{P_0}{K_a}$	$-P_0$	$-\frac{K_b L\Delta T(\alpha_a-\alpha_b)}{(K_a+K_b)}$	$-P_{th}$	$\frac{P_{ext}\,n}{K_a+K_b}$	$\frac{P_{ext}\,n\,K_a}{K_a+K_b}$
Bolt	K_b	$\frac{P_0}{K_b}$	P_0	$\frac{K_a L\Delta T(\alpha_a-\alpha_b)}{K_a+K_b}$	P_{th}	$\frac{P_{ext}\,n}{K_a+K_b}$	$\frac{P_{ext}\,n\,K_b}{K_a+K_b}$

[a] $P_{th}=\left(\frac{K_bK_a}{K_b+K_a}\right)L\Delta T(\alpha_a-\alpha_b)$, Equation (E.6).

A joint diagram for the PBJ of Appendix C with both mechanical and thermal loads is shown in Figure J.7. Coordinates of points 1, 2, and 7 to 11 of Figure J.7 are listed in Table J.3 and were calculated using the coordinate formulas shown in the table along with the data listed in the table caption and the SBLIF calculated in Appendix C. The coordinate formulas given in Table J.3 were determined from the formulas from Table J.1.

TABLE J.2—COORDINATE FORMULAS AND VALUES FOR KEY POINTS OF JOINT DIAGRAM FOR PBJ UNDER PURELY MECHANICAL LOAD AS SHOWN IN FIGURE J.6

Point	Coordinate formulas		Coordinate values[a]	
	Displacement	Force	Displacement, in.	Force, lb
1	Specified = 0	Specified = 0	0	0
2	$\frac{P_0}{K_b}$	P_0	1.926782×10^{-3}	3.000000×10^{3}
3	$\frac{P_0}{K_b}+\frac{P_{ext}\,n}{K_a+K_b}$	$P_0+\frac{P_{ext}\,n\,K_b}{K_a+K_b}$	2.043816×10^{-3}	3.182222×10^{3}
4	$P_0\left(\frac{1}{K_a}+\frac{1}{K_b}\right)$	Specified = 0	2.556812×10^{-3}	0
5	$\frac{P_0}{K_b}+P_{ext}\,n\left[\frac{(1-n)K_b+K_a}{K_a(K_a+K_b)}\right]$	$P_0-\frac{P_{ext}\left[(1-n)K_b+K_a\right]}{(K_a+K_b)}$	2.070765×10^{-3}	6.822219×10^{2}
6	$\frac{P_0}{K_b}+P_{ext}\,n\left[\frac{(1-n)K_b+K_a}{K_a(K_a+K_b)}\right]$	$P_0+\frac{P_{ext}\,n\,K_b}{K_a+K_b}$	2.070765×10^{-3}	3.182222×10^{3}

[a]Coordinate values were calculated using the following values: P_0 = 3,000 lb, $K_a = K_c$ = 4,761,678.0 lb/in., K_b = 1,557,000 lb/in., n = 0.2958, and P_{ext} = 2,500 lb.

TABLE J.3—COORDINATE FORMULAS AND VALUES FOR KEY POINTS OF JOINT DIAGRAM FOR PBJ UNDER COMBINED MECHANICAL AND THERMAL LOADING AS SHOWN IN FIGURE J.7

Point	Coordinate formulas[a]		Coordinate values[b] for Appendix C example	
	Displacement	Force	Displacement, in.	Force, lb
1	Specified = 0	Specified = 0	0	0
2	$\frac{P_0}{K_b}$	P_0	1.926782×10^{-3}	3.000000×10^{3}
7	$\frac{P_0+P_{th}}{K_b}$	P_0+P_{th}	1.647652×10^{-3}	2.565395×10^{3}
8	$\frac{P_0+P_{th}}{K_b}+\frac{P_{ext}\,n}{K_a+K_b}$	$P_0+P_{th}+\frac{P_{ext}nK_b}{K_a+K_b}$	1.764686×10^{-3}	2.747617×10^{3}
9	$\frac{P_0+P_{th}}{K_b}+\frac{P_0+P_{th}}{K_a}$	Specified = 0	2.186411×10^{-3}	0
10	$\frac{(P_0+P_{th})}{K_b}+P_{ext}\,n\left[\frac{(1-n)K_b+K_a}{K_a(K_a+K_b)}\right]$	$P_0+P_{th}-\frac{P_{ext}\left[(1-n)K_b+K_a\right]}{K_a+K_b}$	1.791635×10^{-3}	2.476167×10^{2}
11	$\frac{(P_0+P_{th})}{K_b}+P_{ext}\,n\left[\frac{(1-n)K_b+K_a}{K_a(K_a+K_b)}\right]$	$P_0+P_{th}+\frac{P_{ext}nK_b}{K_a+K_b}$	1.791635×10^{-3}	2.747617×10^{3}

[a] $P_{th}=\left(\frac{K_bK_a}{K_b+K_a}\right)L\Delta T(\alpha_a-\alpha_b)$, Equation (E.6).

[b]P_0 = 3,000 lb, $K_a = K_c$ = 4,761,678.0 lb/in., K_b = 1,557,000 lb/in., n = 0.2958, P_{ext} = 2,500 lb, L = 2.048 in., ΔT = 200 °F, $\alpha_a = 8.1957\times10^{-6}$ in./in./°F, and $\alpha_b = 9.1\times10^{-6}$ in./in./°F.

Figure J.8 plots the coordinates from Table J.2 and Table J.3 on the same plot, showing the effect that the thermal load has on the PBJ, and thus the joint diagram. It can be seen from Figure J.8 that the change in temperature results in a thermal load that effectively translates the preload equilibrium point 2 existing at the assembly temperature along the bolt load-deflection curve to a new equilibrium position at point 7 after preload, while preserving the stiffness of each load path that existed at the assembly temperature. The load-deflection curve for the compression zone runs from point 4 to point 2 during preload at assembly temperature, and then translates along the bolt load-deflection curve as a result of the temperature change, ending up as the load-deflection curve between points 9 and 7. As the joint experiences mechanical load at the new temperature, the relieving load path is traversed between points 7 and 10 as the clamping load path is traversed between points 7 and 11.

The clamping and relieving load paths are not explicitly exercised during the preload phase, and to be event consistent, are only plotted after preload, originating from the bolt preload coordinates $(P_0/K_b, P_0)$.

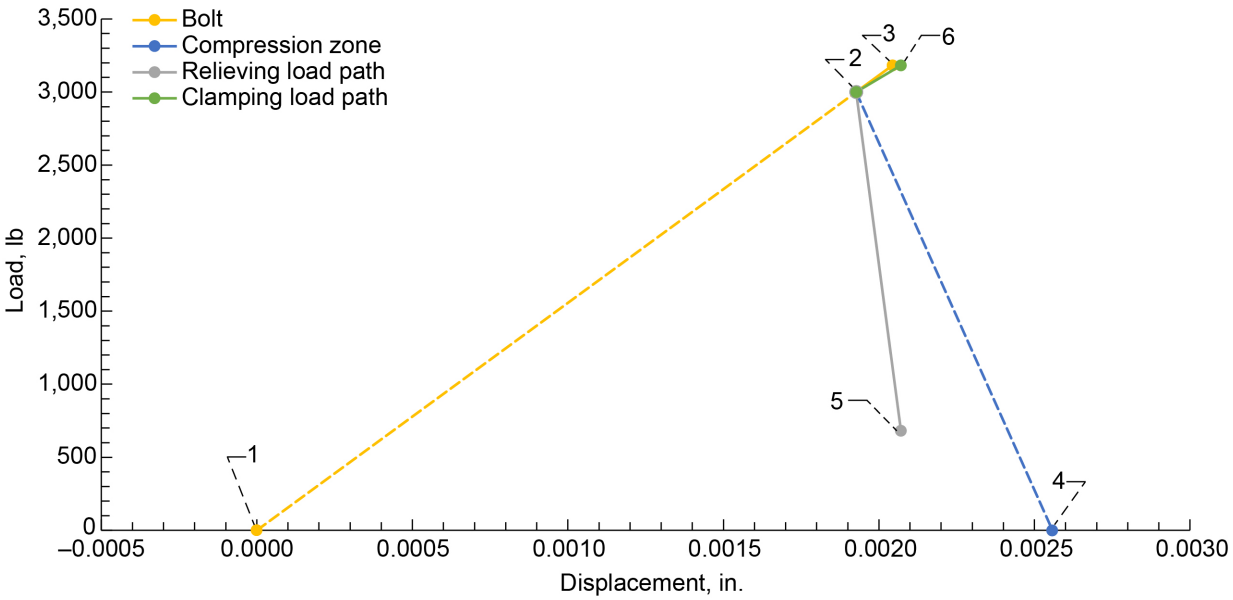

Figure J.6.—Coordinate point numbering of key points of bolted-joint diagram for example problem of Appendix C under pure mechanical tensile load (without thermal load). Point numbers correspond to points in Table J.2. Coordinates were calculated using P_0 = 3,000 lb, K_a = K_c = 4,761,574.8 lb/in., K_b = 1,557,000 lb/in., n = 0.2958, and P_{ext} = 2,500 lb.

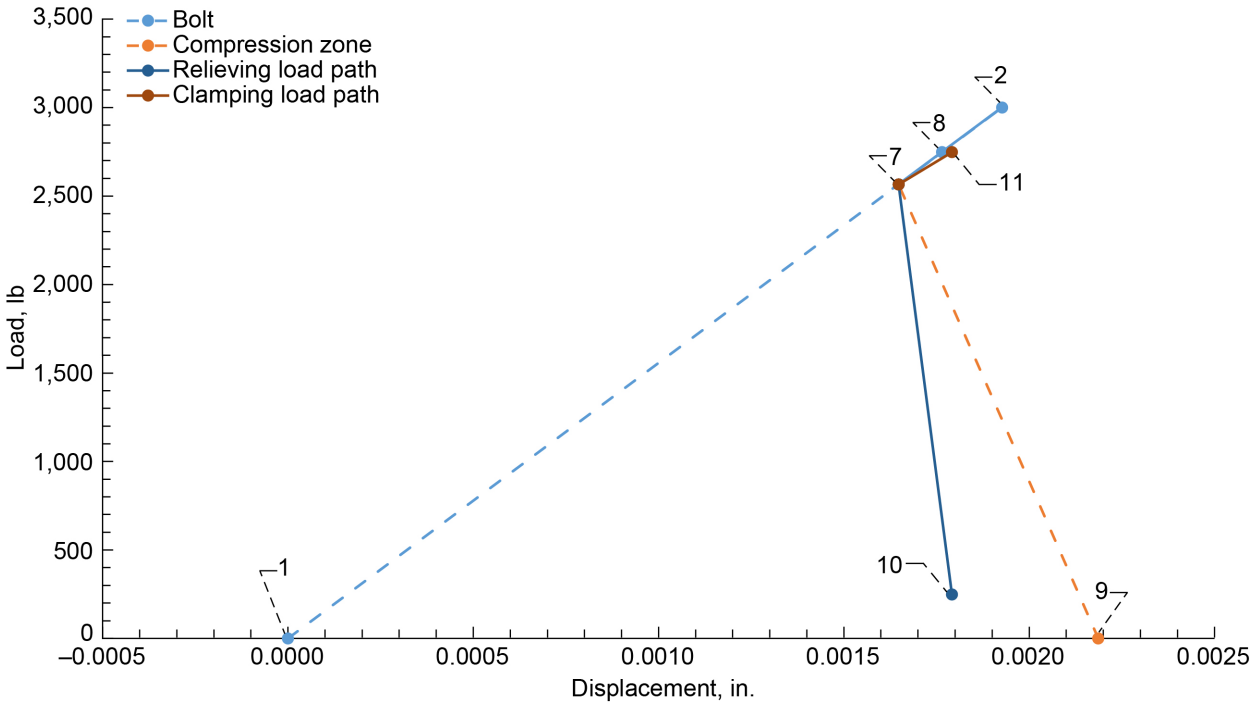

Figure J.7.—Coordinate point numbering of key points of bolted-joint diagram for example problem of Appendix C under mechanical tensile and thermal load. Point numbers correspond to points in Table J.3. Point 2 is preload equilibrium point without thermal load. Coordinates were calculated using following values: P_0 = 3,000 lb, K_a = K_c = 4,761,574.8 lb/in., K_b = 1,557,000 lb/in., n = 0.2958, P_{ext} = 2,500 lb, L = 2.048 in., ΔT = 200 °F, α_a = 8.1957×10^{-6} in./in./°F, and α_b = 9.1×10^{-6} in./in./°F.

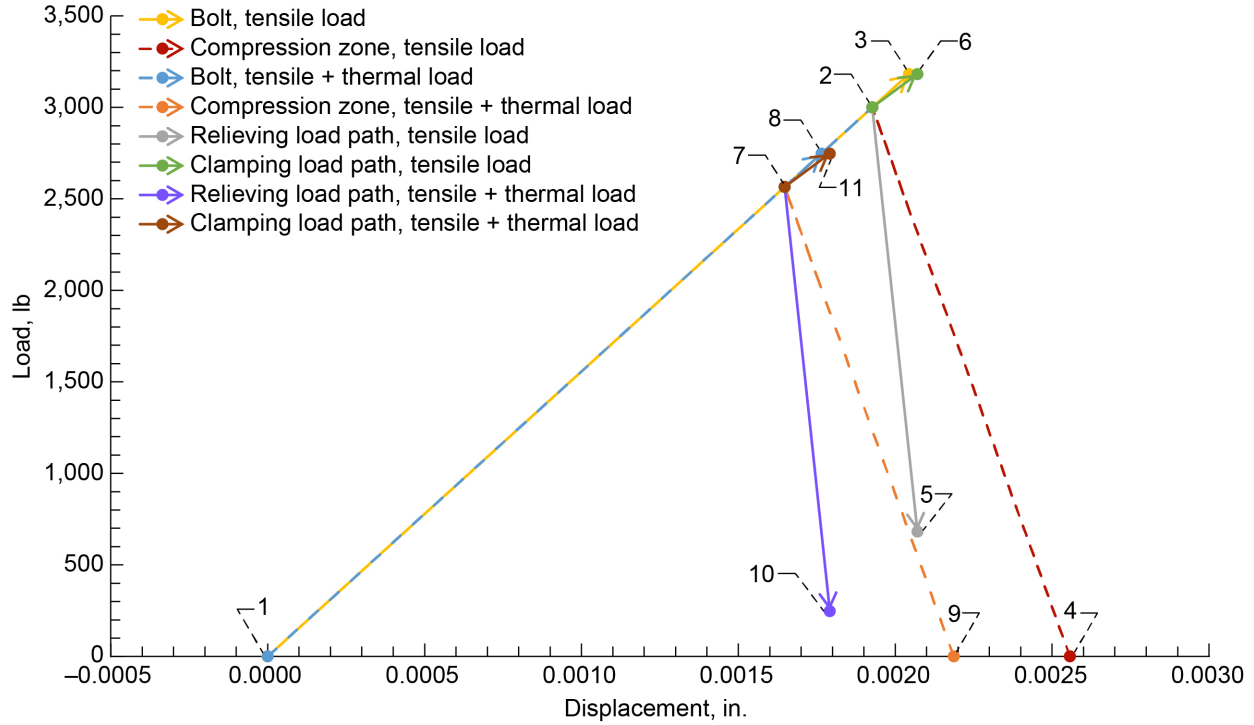

Figure J.8.—Joint diagram with tensile load, with and without thermal load for example problem of Appendix C.

References

1. Lee, H.M.: The Mechanism of Bolt Loading. NASA TM–108337, 1992. https://ntrs.nasa.gov
2. National Aeronautics and Space Administration: Requirements for Threaded Fastening Systems in Spaceflight Hardware. NASA–STD–5020A, 2019.
3. Boenick, Ulrich: Untersuchungen an Schraubenverbindungen. Dissertation, University of Berlin, 1966.
4. Smith, James: Preloaded Bolted Joint Stress Analysis. Performed Dec. 2020.
5. Byers, Edward Ford; and Snyder, Robert D.: Engineering Mechanics of Deformable Bodies. Third ed., Harper & Row, New York, NY, 1975, p. 110.
6. Nassar, Sayed A.; and Abboud, Antoine: An Improved Stiffness Model for Bolted Joints. J. Mech. Des., vol. 131, no. 12, 2009, pp. 121001-1–121001-11.
7. Wileman, J.; Choudhury, M.; and Green, I.: Computation of Member Stiffness in Bolted Connections. J. Mech. Des., vol. 113, 1991, pp. 432–437.
8. Lenhoff, T.F., et al.: Member Stiffness and Contact Pressure Distribution of Bolted Joints. J. Mech. Des., vol. 116, no. 2, 1994, pp. 550–557.
9. National Aeronautics and Space Administration: Criteria for Preloaded Bolts. NSTS 08307, Revision A, 1998.
10. Verein Deutscher Ingenieure: Systematic Calculation of High Duty Bolted Joints; Joints With One Cylindrical Bolt. VDI 2230, 2003.
11. Meyer, G.; and Strelow, D.: Simple Diagrams Aid in Analyzing Forces in Bolted Joints. Assembly Engineering, 1972, pp. 28–33.
12. Rohatgi, Ankit: Version 4.5 of WebPlotDigitizer. 2021.
13. Wikipedia contributors: Kilogram-force. Wikipedia, The Free Encyclopedia, 2023. https://en.wikipedia.org/wiki/Kilogram-force Accessed June 13, 2023.
14. Smith, James: National Aeronautics and Space Administration, email correspondence, Feb. 26, 2020.
15. Swokowski, Earl W.: Calculus With Analytic Geometry. Prindle, Weber, & Schmidt, Frederick, MD, 1975.